Design of Stewart Platform for Wave Compensation

Masters Thesis

EMSD4 - 2012

Anders Lohmann Madsen

Søren Giessing Kristensen

AALBORG UNIVERSITET

Aalborg University
Study Board of Industry and
Global Business Development
Fibigerstraede 16
DK - 9220 Aalborg East
Phone +45 99 40 93 09
http://www.industri.aau.dk/

Title:
Design of Stewart Platform for Wave Compensation

Semester:
4^{th} Electro-Mechanical System Design (EMSD)

Semester Theme:
Master's Thesis

Project Period:
1st of February 2012 - 1st of June 2012

Authors:

Anders Lohmann Madsen

Søren Giessing Kristensen

Supervisor:
Torben Ole Andersen

Number printed: 4

Pages: 82

Enclosed: CD

Synopsis:

Ship mounted cranes has a limited workability on the seas due to wave exited pendulation of the hoisted load. This poses a problem as crane operations are aborted and time is lost. The motion of ships and the pendulation of the hoisted load can be counteracted by a Stewart platform due to its 6 DOF motion capacity. The Stewart platform is a complex parallel manipulator which kinematics is difficult to design by hand. The design procedure involves selecting the type of Stewart platform, creating a design capable of generating forces and velocities in all direction, ensure the prescribed workspace can be reached, and many physical constraints on the design. To solve these problems a thorough theoretical review of kinematics and kinematic performance indices are included in this thesis. Mathematical optimization using Sequential Quadratic Programming (SQP) is used to create the best design for wave compensation. Methods of ensuring feasible actuator relations and avoidance of leg collision are developed and are incorporated into the optimization of kinematic performance indices. All methods described can equally be used for other applications than wave compensation. Two types of Stewart platforms are selected and optimized to find that the traditional type is inferior to a slightly more complex type. The more complex type is smaller and has 13.5 % better dexterity. The demands for a hydraulic actuation system are determined using optimization methods, and finally a complete simulation model of the hydraulic and mechanical system is derived.

Summary

Dette kandidat speciale er skrevet i foråret 2012 i forbindelse med afslutningen af civilingeniøruddannelsen inden for 'Elektro-Mekanisk System Design' på Aalborg Universitet. Specialet omhandler design metode, forståelse og optimering af en Stewart platform til kompensering af bølgebevægelsers påvirkning af skibskraner. Projektet er udarbejdet i samarbejde med HYDAC A/S, en større producent indenfor hydraulik komponenter, som har ønsket et dybere kendskab til Stewart platformen, dens kinematik og dimensionerende faktorer. HYDAC A/S har derfor stillet projektforslaget om Stewart platformens brug til bølgekompensering af skibskraner.

Skibskraner bruges ikke kun til at laste og losse i rolige havnemiljøer, men bruges også til offshore operationer og begrænses derved af de aktuelle havforhold, da bølgepåvirkninger af kranfartøjet kan forårsage store svingninger i kranlasten. Dette sker selv i forholdsvis roligt vejr med bølgehøjder ned til under 1 m [1], og søgangen kan dermed let udsætte arbejdsopgaver og koste operatøren penge. Det ønskes derfor at designe en Stewart platform som skal fungere som stabilt fundament for kranen, så svingningerne i kranen minimeres.

Det initierende problem for projektet er derfor defineret som:

Hvordan designes en Stewart platform optimalt til bølgekompensering?

En Stewart platform er en seksbenet parallel robot med 6 frihedsgrader. Dette er optimalt til bølgekompensering, da skibsbevægelser netop har 6 frihedsgrader og Stewart platformen har dermed potentiale til at kompensere for den totale skibsbevægelse. Yderligere har Stewart platformen den fordel, at den kan yde store kræfter, da der er 6 hydrauliske cylindere til at aktuere den samme platform. Dermed kan den også opnå stor positioneringsnøjagtighed, da en positionsfejl på en cylinder ikke akkumuleres i robotten som tilfældet er for serielle robotter.

Stewart platformen er et komplekst kinematisk system, hvor fordele og ulemper ved et givent design kan være svære at gennemskue. Derfor er en dybdegående teoretisk gennemgang af kinematikken og dens performance kriterier samlet i dette speciale. Ud fra gennemgangen kan relevante kriterier udvælges til det ønskede design. Det vælges, at designe Stewart platformen ud fra et krav om 'dexterity', hvilket beskriver robottens evne til at arbejde med ens kræfter og hastigheder i alle retninger og orienteringer.

Yderligere er der for at sikre et realiserbart design af Stewart platformen opstillet en række designkrav der skal tages højde for i designprocessen. Disse skal bl.a. sikre, at de hydrauliske cylindre ikke kolliderer indenfor arbejdsområdet og at aktuatorerne til systemet udnyttes optimalt. For at udregne et optimalt design ift. 'dexterity' og indenfor de givne designrammer, opstilles et optimeringsproblem som løses vha. en ' Sequential Quadratic Programming' (SQP) algoritme. Der bestemmes en optimal løsning for den almindelige Stewart Platform og et modificeret design kaldet den koncentriske cickel Stewart platform. Det viser sig, at der ved brug af det modificerede design kan opnås 13.55 % bedre 'dexterity', hvorfor dette design anses som det bedste til bølgekompensering. Oversigten over performance index er universel for både serielle og paralle robot-typer og kan dermed anvendes generelt for robot design. Desuden er hele den angivne designprocedure overførbar til Stewart platforme til andre applikationer.

Afslutningsvis dimensioneres udvalgte hydrauliske komponenter til det optimerede Stewart platform design, samt opstilles en fuld simuleringsmodel af det hydrauliske og mekaniske system. For at bestemme de maksimale kræfter, hastigheder, flow samt effekt i systemet, opstilles endnu flere optimeringsproblemer. Dette gøres da systemkræfterne og bevægelserne er funktioner af mange variable. En optimering har bl.a. beregnet at systemets maksimale effekt ved bølgekompensering er 155 kW.

Det kan fra det ovenstående konkluderes, at den endelige Stewart platform opfylder alle designkrav. Desuden kan der fra HYDACs Stewart platform prototype opnås en 59 % forbedring i 'dexterity' til single cirkle designet og yderligere 13.5 % til koncentrisk cirkle designet.

PREFACE

This master's thesis is written in the spring of 2012 by two graduate students enrolled in the Electro-Mechanical System Design (EMSD) study program in the Department of Mechanics and Production at Aalborg University.

The thesis is made in corporation with HYDAC A/S, a major manufacturing and design company of hydraulic components and systems. A special thanks to HYDAC for inspiration and guidance for the project, to Shaoping Bai and Torben Ole Andersen, professors at Aalborg University for their valuable help and advice.

The thesis is addressed to readers with knowledge of kinematics, optimization theory and mathematical modeling of mechanical- and hydraulic systems. To assist the reader, the applied notations for the different variables are outlined in the enclosed nomenclature list, which is placed before the introduction.

Referencing is made after the IEEE standard, where references to the bibliography, which is found in the end of the thesis, are encapsulated in square brackets as [x] or [x, pp. x]. If the reference is placed after a punctuation mark in a given paragraph, the reference relates to the whole paragraph, whereas the reference only relates to a specific sentence, if the reference is placed before the punctuation mark.

Figures, equations, and tables are numbered continuously throughout each chapter and the appendix, where e.g. figure 3.2 refers to the second figure in the third chapter.

Appended to the report is a supplement CD, which is found on the inside of the back cover, containing the report in pdf-format, simulation code and models, used in this report.

CONTENTS

NOMENCLATURE

Name	Explanation	Unit
A_p	Cylinder piston side area	$[\mathrm{m}^2]$
A_r	Cylinder ring side area	$[\mathrm{m}^2]$
B	Viscous damping coefficient	$[\frac{\mathrm{Nm \cdot s}}{\mathrm{rad}}]$
b_i	Leg mounting point on base	$[\mathrm{m}]$
d_{piston}	Cylinder Piston diameter	$[\mathrm{m}]$
d_{rod}	Cylinder Rod diameter	$[\mathrm{m}]$
e_i	Unit vector	$[-]$
F	Force	$[\mathrm{N}]$
f	Frequency	$[\mathrm{rad}]$
G	Gravitational force and moment vector	$[\mathrm{N}, \mathrm{Nm}]$
g	Leg forces	$[\mathrm{N}]$
h	Stewart platform height	$[\mathrm{m}]$
I	Moment of inertia Matrix	$[\mathrm{kg} \cdot \mathrm{m}^2]$
L	Characteristic length	$[\mathrm{m}]$
L_x	Length	$[\mathrm{m}]$
l	Length	$[\mathrm{m}]$
l_i	Length of leg i	$[\mathrm{m}]$
l_cant	Crane cantilever length	$[\mathrm{m}]$
l_max	Max. leg length	$[\mathrm{m}]$
l_min	Min. leg length	$[\mathrm{m}]$
l_stroke	Leg stroke length	$[\mathrm{m}]$
LB	Lower Bound	$[-]$
M	Mass and Inertia matrix	$[\mathrm{kg}, \mathrm{kgm}^2]$
m	Mass	$[\mathrm{kg}]$
P	Power	$[W]$
p	Pressure	$[bar]$
p_i	Leg mounting point on platform	$[m]$
Q_n	Valve rated flow	$[\frac{\mathrm{L}}{\mathrm{min}}]$
Q_x	Flow	$[\frac{\mathrm{L}}{\mathrm{min}}]$
q	End-effector pose	$[\mathrm{m}, \mathrm{rad}]$
R	Z-Y-X Rotational matrix	$[\mathrm{rad}]$
r_b	SP base radius	$[\mathrm{m}]$
r_p	SP platform radius	$[\mathrm{m}]$

Name	**Explanation**	**Unit**
T	Torque	$[\mathrm{Nm}]$
t	End-effector Cartesian coordinate	$[\mathrm{m}]$
TCP	Tool Center Point	$[-]$
UB	Design space Upper Bound	$[-]$
V_x	Volume	$[\mathrm{L}]$
α	Yaw	$[^\circ]$
β	Pitch	$[^\circ]$
β_F	Bulk modulus	$[\mathrm{bar}]$
γ	Roll	$[^\circ]$
κ	Condition number	$[-]$
λ_x	Design variable vector	$[-]$
θ	CC SP spacing angle	$[^\circ]$
θ	Crane lifting angle	$[^\circ]$
σ_i	Singular value	$[-]$
τ	TCP force and moments	$[\mathrm{N}, \mathrm{Nm}]$
ξ_i	Phase shift	$[\mathrm{rad}]$
Φ_x	Objevtive function	$[-]$
ϕ	CC SP spacing angle	$[^\circ]$
ϕ_b	SC SP base spacing angle	$[^\circ]$
ϕ_p	SC SP platform spacing angle	$[^\circ]$
ω	End-effector Rotational coordinate	$[\mathrm{m}]$
ω_n	System eigenfrequency	$[\frac{\mathrm{rad}}{\mathrm{s}}]$
ω_v	Valve eigenfrequency	$[\frac{\mathrm{rad}}{\mathrm{s}}]$

CHAPTER 1

INTRODUCTION

Ship mounted cranes have many applications and are used for several different operations, e.g. to unload ships in minor ports without regular unloading equipment, to offshore operations like transportation of cargo from one ship to another when deep water ports are not available, servicing offshore wind turbines, moving oil rig anchors etc. These operations are strictly scheduled and pose economic consequences if postponed. One of the reasons to suspend operations with ship mounted cranes is rough sea conditions, where wave-exited motion of the ship generates dangerous pendulation of the cargo hoisted by the crane.

To avoid wasted time and money due to unworkable sea conditions for loading/unloading of ships offshore, HYDAC A/S has made a prototype Stewart platform that is indented to counteract wave induced ship motion. The Stewart platform is intended as a mounting platform for the ship crane and to move opposite the ship to keep the crane steady in space, and not relative to the sea to minimize motion in the crane cargo. As great static and dynamics loads are applied to the Stewart platform by the ship crane a hydraulic actuation system is used for the Stewart platform.

This thesis deals with the design of a Stewart platform for wave compensation. The focus of the thesis is to design and optimize the kinematics of the Stewart platform. Secondly the thesis deals with the dimensioning of a hydraulic servo system to the optimized kinematic design.

CHAPTER 2

PROBLEM ANALYSIS

In this chapter the issues concerning pendulation of hoisted crane cargo due to wave induced ship motion is described. A Stewart platform is introduced as a solution to the problem. The kinematic design of a Stewart platform poses a number of problems which is described in this chapter. Finally the requirements to the solution are listed.

2.1 Crane Operation Problem

Ship mounted cranes are intensively used in the shipping industry to load and unload ships. As loading and unloading of cargo can take place at sea, the crane and cargo is exited by the motion of the ship. The excitation can cause the hoisted cargo to pendulate uncontrollably and coerce the crane operator to shut down the operation for safety reasons. Crane operations at sea are thus dependent on no or only small wave-exited motion of the ship to avoid uncontrollable pendulation of the hoisted cargo.

The US Army use Auxiliary Crane Ships for unloading of cargo ships offshore under the term Joint Logistics Over The Shore (JLOTS). Tests from JLOTS have shown that once seas build to a sea state as low sea state 3 on the Pierson-Moskowitz Sea Spectrum (defined as waves with significant wave height of 1 m to 1.5 m) crane operations must be aborted [2]. Additionally experience from operation Desert Storm show that sea conditions as low sea level 1 or 2 on the Pierson-Moskowitz Sea Spectrum (equal to wave heights up to approximately 1 m) caused frequent periods where crane operations was terminated due to dangerous pendulation of the cargo [1].

Also in civilian shipping the wave induced ship motion is a problem for crane operations. The assembly and maintenance of offshore wind turbines often require hoisting of parts from service ships onto the fixed foundation of the wind turbine. This poses a problem if the excitation of the ship is large as the parts or cargo hoisted by the crane potentially can collide with the wind turbine and cause damage.

Rawston and Blight [3] has presented data showing that typical crane ships in the North Sea has a available work time of approximately 10%-30% in winter and around 50% -60% in summer based on vertical displacement of the crane tip alone. Today the majority of crane operations at sea are only controlled by skilled crane operators and it is solely up to the operator and crew to decide wether or not, the operating conditions are safe or if operations should be suspended [4].

To increase the available work time of crane ships, HYDAC A/S wishes to design a hydraulic Stewart platform to work as a stable foundation for the ship crane and suppress the motion from the waves. The idea is to install the ship crane on the Stewart platform and then control the Stewart platform to counteract the ship motion to keep the crane steady in space. This should minimize excitation of the crane load and hereby reduce pendulation of the load and increase the available work time. The idea is illustrated in Fig. 2.1.

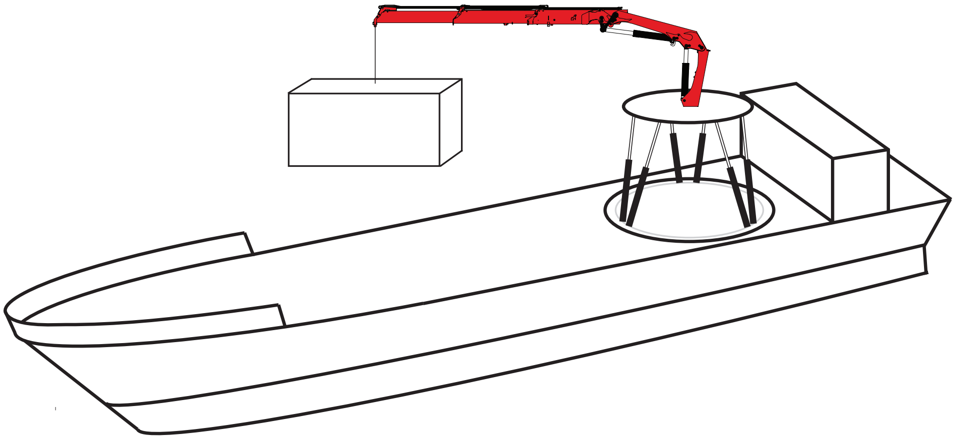

Figure 2.1: *Ship Crane mounted on Stewart platform. Crane by courtesy of HMF.*

To supply HYDAC A/S with knowledge about this solution, this thesis will investigate the design of a Stewart platform for ship motion suppression or simply: wave compensation.

2.2 Ship Motion

The motion exciting the hoisted crane cargo is equal to that of the installation ship and the motion notation used in this thesis is defined in this section. Waves can induce three types of linear and three types rotational motion and thus the ship motion has 6 degrees of freedom (DOF). The motions can be seen in Fig. 2.2.

As seen in Fig. 2.2 the linear motions are surge, sway and heave. Surge and sway is motion along the longitudinal and transverse axis respectively and heave is the motion along the vertical axis. The rotational motions are roll, pitch and yaw. Yaw is the rotation of the ship around its vertical axis. In pitching a ship is lifted at the bow and lowered at stern or vice versa, which is rotation around the transverse axis. Roll is the side to side rotational motion of the ship around the longitudinal axis.

In order to minimize the crane operation problem described in Section 2.1, the motion of the Stewart platform must be opposite of the ship, i.e if the ship heaves up 1 m (z-direction, Fig. 2.2) the platform is lowered 1 m.

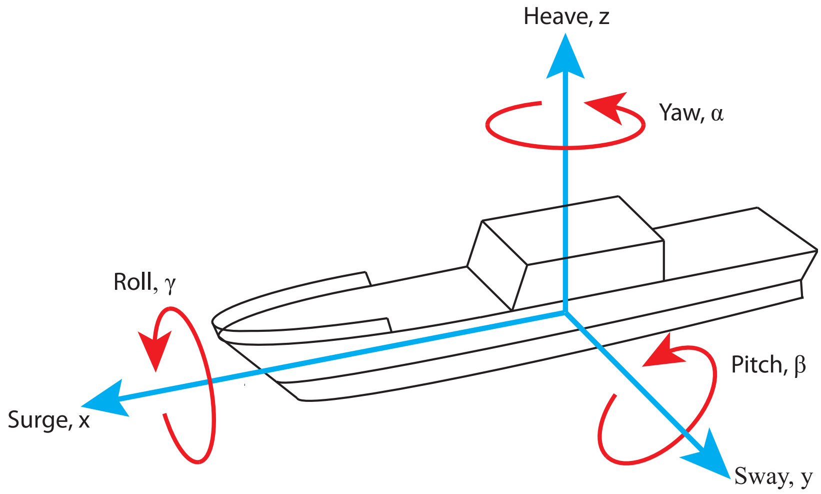

Figure 2.2: *Ship motion.*

2.3 The Stewart Platform Design

A Stewart platform is a 6 DOF parallel manipulator that incorporates six prismatic actuators connecting two rigid bodies. The Stewart platform originates from a universal tire testing machine designed by Gough [5] in 1956 for the Dunlop factories in England. Gough's design was later published by Stewart [6] in 1965 who suggested the use of the design for flight simulation. Though Gough invented the manipulator, the manipulator is commonly named a Stewart platform referring to Stewart's work. However the manipulator is sometimes also referred to as a Gough/Stewart platform. The term Stewart platform is used in this thesis. The Stewart platform has since the work of Gough and Stewart been studied extensively and is still used for flight simulation though the platform currently has many applications. A Stewart platform used for flight simulation is seen in Fig. 2.3.

Figure 2.3: *Flight simulator at the Baltic Aviation Academy.*

Stewart platforms consist of prismatic actuators connecting the bodies by a combination of universal and spherical joints. The bottom and top body is generally referred to as the base and platform respectively, and the base is usually the only stationary part of the manipulator as it typically is bolted to a stable surface. Stewart platforms are classified as parallel manipulators as multiple actuators are connecting and actuating the same rigid body (the platform), whereas serial manipulators uses series of rigid bodies connected by actuated joints to manipulate a tool point.

Parallel manipulator has several advantages compared to serial manipulators. Control accuracy of parallel manipulators is high as the positioning error of the actuators is not amplified as in serial manipulators. Additionally parallel manipulators are capable of handling heavier loads and have a greater weight to strength ratio than serial manipulators. However the workspace of parallel manipulators is considerably smaller.

There are a variety of different design possibilities of Stewart platforms regarding the type and position of the joints connecting the prismatic actuators to base and platform. The types of joints are universal and spherical which are denoted U and S in Fig. 4.4. Spherical joints are used in all manipulator designs to prevent the piston and rod from turning inside the cylinder.

The design variation of different Stewart platform types dependents only on the placements of the joint on base and platform. To classify these different design types three joint placement characteristics that describe the joint placements are used [7]. The joint placement characteristics are combinational, planarity, and arbitrarily:

1. **Combinational** define the number of prismatic actuators P that share the same spherical joint position. There are 35 different feasible combinations, cf. [7]. The combinations are denoted by two numbers separated by a dash, where the first number indicate the number of joint positions on the base and the second number indicate the number of joint positions on the platform, i.e the most ordinary combination is the 6-6 class (see Fig. 2.4a) which means that none of the prismatic actuators share the same spherical joint position. A 3-3 class manipulator as in Fig. 2.4d has three shared spherical joint positions on both base and platform and a 6-4 class has six joints on the base and four on the platform, see Fig. 2.4b. The 6-3 class is depicted in Fig. 2.4c. The remaining combinations can be seen in [7].

2. **Planarity** defines whether or not the joints is placed in the same plane on both base and platform respectively, as it is possible to create designs where some joints are elevated compared to others.

3. **Arbitrarity** defines on how many circular paths the manipulator joints are located on around the center point of base and platform respectively. The joints in the examples in Fig. 2.4 are all located on one single circular path on both the base and platform. The maximum number of paths is 6 due to the number of legs.

The joint placement characteristics can be combined to create a very large number of design possibilities. The combinational characteristic where the prismatic actuators are sharing the same joint require specially manufactured joints which eliminates the use of on-the-shelf components. The kinematics of the manipulators is dependent on the combination of the joint placement characteristics.

Stoughton and Arai [8] have worked with two types of Stewart platforms and have shown that the kinematics of a 6-6, planar, single circle manipulator can be improved by mounting the joints on two

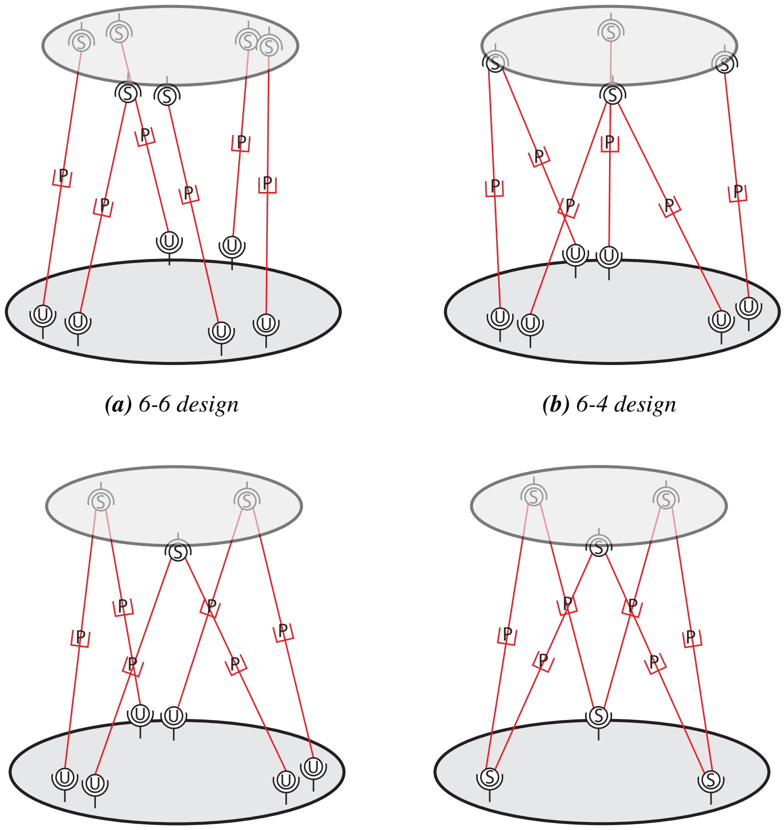

(a) 6-6 design *(b) 6-4 design*

(c) 6-3 design *(d) 3-3 design*

Figure 2.4: *Four different Stewart platform types.*

concentric circles on both base and platform, and thereby create a 6-6, planar, concentric circle Stewart platform. The 6-6 planar manipulator is the simplest and most popular type of manipulator and the 6-6 planar concentric circle manipulator is only slightly more complex. Both designs can be constructed from off-the-shelf components and for this reason and for simplicity, these designs are selected for analysis with regard to the wave compensation application. The designs are referred to as the Single Circle Stewart platform design and the Concentric Circle Stewart platform design respectively.

2.4 Kinematic Design Considerations

In the previous section the different design possibilities are discussed to indicate that a large number of different designs are possible. Two design types are chosen due their simplicity. The next step is to dimension the kinematic design; spacing angles between the mounting points, length properties of the prismatic actuators etc. When defining the dimensions of the Stewart platform, the following requirements must be taken into account:

1. The manipulator must be able to operate within the prescribed workspace required by the application.

2. The kinematic design must allow the prismatic actuators to produce the required forces and velocities in all directions needed for the specific application.

3. The prismatic actuation forces must be within the limit of what is possible and realistic from a structural point of view.

4. The length properties of the prismatic actuators must be physical realizable.

5. The usage of stroke length must be as large as possible in order to reduce the size of the prismatic actuators and the manipulator in general. (Provided that identical prismatic actuators are used.)

6. Avoid collisions of the prismatic actuators however this is only a concern for designs with arbitrary joint placements.

These six requirements can be fulfilled using trial and error and a CAD model in the design process, though this is an ineffective method as it relies on the engineer's intuition. However this may result in a feasible solution, it is questionable whether the solution is optimal. In literature no procedure for solving these problems exist for the given application, but methods for optimizing kinematic performance do exits which help to account for consideration 1 and 2. The absence of systematic methods for accounting for 4, 5 and 6 are a challenge to be addressed in the kinematic design process.

2.5 System Requirements

The problem analysis presents several factors that must be taken into consideration when designing a Stewart platform to stabilize the crane foundation and hence minimize pendulation in crane load. To design a Stewart platform that is suitable for wave compensation, this section specifies the requirements the final Stewart platform has to fulfill. These requirements are both to the overall system performance and the kinematic performance of the system.

The requirements for the wave compensating Stewart platform:

1. 95% workability up to sea state 5 to minimize downtime of crane operations due to sea conditions. 95% is set because very few waves in sea state 5 can have unusual wave heights that are unreasonable to counteract.

2. The Stewart platform kinematic design must fulfill all 6 kinematic requirements specified in Section 2.4. The design is improved depending on the degree of which the requirements are met. The kinematic design must fulfill the requirement as good as possible.

3. The maximum base diameter of the Stewart platform is defined by HYDAC to be 7 m due to limited deck space on ships. The platform is defined to have a minimum diameter of 4 m in order to ensure adequate space for the installation of the ship crane.

2.6 Problem Statement

From the previous analysis, the initial problem is stated:

How is a hydraulic Stewart platform optimally designed for wave compensation?

CHAPTER 3

Design Considerations

In this section the design procedure of the Stewart platform for wave compensation is described. The design procedure involves collecting information about the waves at the location of operation and how the operation ship responds the waves in order to determine the ship motion. These aspects are reviewed and a final design procedure is depicted in a flow chart.

3.1 Operation Location

The waves on the world's oceans are mainly generated by the wind. Many factors influence the formation of waves e.g. wind speed and its variation, wind direction, position and geometry of the coast line and water depth. The combination of these variables render many possible wave forms with different wave heights and frequencies [9]. Subsequent waves differ in height, frequency and shape with limited predictability. This indicates that an universal Stewart platform for waves compensation cannot be design for all locations around the world, because the frequencies and wave lengths the Stewart platform most counteract influence the actuation forces and velocities. To design the Stewart platform for a specific location, corresponding wave data in the form of a wave scatter diagram for this location must be used. Wave scatter diagrams depict the distribution of and relationship between wave height and period for a given number of samples.

3.2 Operation Ship

The contents in this section is inspired by Orcina [10]. The motions of ships are dependent on the waves and the design of the ship. In order to describe how a ship respond to wave displacement, Response Amplitude Operators (RAO's) can be used to determine the ship's response to waves for all six degrees of freedom. The RAO data for a ship describe the ship motion by a amplitudes and a phase for all degrees of freedom for each wave period and wave direction in relation to the ship. The RAO amplitude relates the wave amplitude to the amplitude of the ship motion. Likewise the phase relates the phase of the wave to the phase of the ship motion. This is described mathematically for an arbitrary degree of freedom as:

$$x_{DOF} = a_r a_w sin(\omega_w t + \phi_r) \tag{3.1}$$

where x_{DOF} is the displacement of the ship, a_w is the amplitude of the wave, ω_t is the frequency of the wave, and a_r and ϕ_r is the RAO amplitude and phase respectively. The RAO data is dependent on the type of ship in question, the direction and period of the waves, draught and speed. Accurate values for the RAO are important to ensure that the dynamics of the system are modeled accurately. RAO data can be obtained in model tests or in computer simulations.

RAO's for heave and pitch motions are typically such, that at low frequencies (long wave length) the ship follows the wave profile. This can be compared to a cork riding up and down on a wave; hence the RAO's tend to unity. In contrast at high frequencies (short wave length) the number of waves along the hull of the ship cancel out the wave motion and the RAO's tend to 0 [11]. This means that larger ships are less affected by the waves compared to smaller ships. Additionally the heave and pitch motions are relatively highly damped compared the roll motion.

3.3 Design Approach

Once the location of operation is selected the wave scatter diagram for this location must be collected using field measurements or library data if such exit. This step is denoted 1 and 2 in the flowchart in Fig. 3.1. The operation ship on which the Stewart platform is to be mounted is selected (3) and corresponding RAO data must be obtained (4). The scatter diagram for the waves and the RAO is used to calculate the response spectrum of the ship. Using inverse fast Fourier transformation yields 6 equations in the time domain describing the motion of the ship. This corresponds to step 5 in the flow chart. The 95% quantile of the amplitudes of each of the 6 motion equations prescribes the required workspace needed to achieve wave compensation with a workability of 95%, cf. Section 2.5. Note that the motion equations for the Stewart platform must be opposite that of the ship in order to cancel out the wave motion.

Unfortunately wave scatter data and especially RAO data for a conceivable ship suited for installation of a Stewart platform is unavailable for this thesis. However the Oak Ridge National Laboratory in Tennessee USA has constructed a ship motion simulation platform for testing purposes. The platform can simulate ship motion up to sea state 5 which is characterized as rough sea. The use of cranes are usually suspended in sea states above sea state 3, see Section 2.1, and for this reason any useful wave compensation system must allow crane operations at sea states above sea state 3. In this thesis an upper sea state limit is set to sea state 5, cf. Section 2.5. The Oak Ridge National Laboratory's ship motion simulation platform presume that ships in sea state 5 move with the magnitudes given in Table 3.1 within a frequency range of 0.1-1 Hz. In order to prescribe a realistic workspace the value in Table 3.1 is used in this thesis.

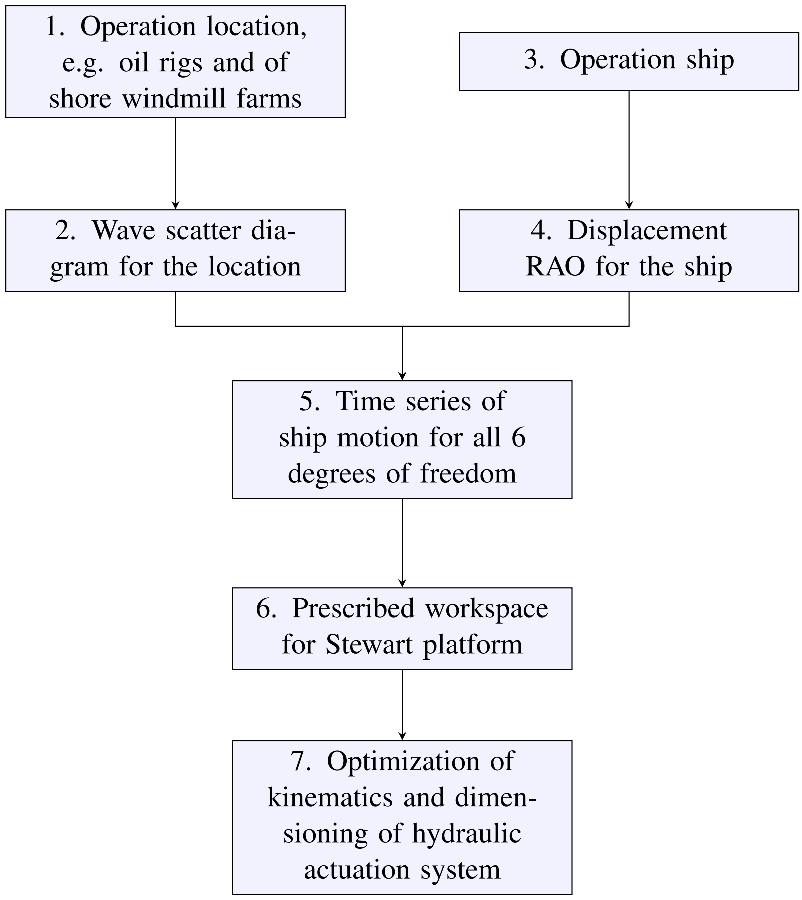

Figure 3.1: *Flowchart of design procedure.*

Table 3.1: *Ship motion in sea state 5.*

Motion:	Magnitude:
Surge	$\pm$ 0.23 m
Sway	$\pm$ 0.48 m
Heave	$\pm$ 1.22 m
Yaw	0°
Pitch	$\pm$3°
Roll	$\pm$ 10°

CHAPTER 4

KINEMATICS

In this chapter the kinematic equations describing the both the single circle design and concentric circle design, cf. Section 2.3, are derived and explained. As the kinematic equations for all Stewart platforms are identical the equations are derived using the single circle design. The singular values of the Jacobian matrix are used to explain and introduce kinematic performance indices and a simple kinematic example is shown to visualize these.

4.1 Kinematic Modeling

In this section the equations describing the kinematics of Stewart platforms is presented using the single circle design. The kinematic equations can be formulated by both forward and inverse kinematics. The forward kinematics of parallel manipulators describe the tool center point (TCP) position as a function of the leg length, and the inverse kinematics describe the leg lengths as a function of the TCP position. The inverse kinematics can be solved analytically, whereas the forward kinematics is a quite complex problem that has to be solved using numerical solvers. This is in contrast to serial manipulators where the inverse kinematics is complex and has to be solved numerically and the forward kinematics can be solved analytically [12]. The forward kinematics of the Stewart platform is not addressed further in this thesis.

4.1.1 Stewart Platform Kinematics

The Stewart platform consists of a base and an end-effector which are linked by six prismatic actuators with universal joints at the base and spherical joints at the end-effector. A diagram of the single circle Stewart platform can be seen in Fig. 4.1. The global coordinate system is placed in the center of the base plate. The end-effector coordinate system is attached to the center of the end-effector, which is also called the tool center point (TCP). The TCP pose has the global coordinates $q = [x, y, z, \alpha, \beta, \gamma]$ where the coordinates $[x, y, z]$ describe the Cartesian position of the end-effector and the coordinates $[\alpha, \beta, \gamma]$ (Z-Y-X

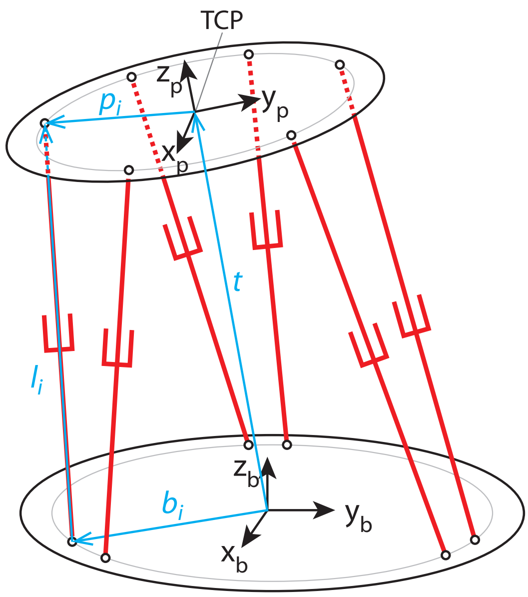

Figure 4.1: *Diagram of leg i.*

Euler angles) describe the orientation of the end-effector [13], which correspond to yaw, pitch and roll respectively as seen from Fig. 2.2 on page 5. The vectors p_i denotes the center positions of the spherical joints mounted on the end-effector plate and b_i denote positions of the universal joints on the base plate for $i = 1..6$. The geometrical relation between TCP and the mounting points of the legs can then be used to calculate the leg lengths in order derive the inverse kinematics, see Fig. 4.1. The inverse kinematics consists of six nonlinear equations that can be solved uniquely. The equations are:

$$l_i = t + Rp_i - b_i \qquad \text{for } i = 1..6 \tag{4.1}$$

where the vector t denotes the Cartesian coordinates of the TCP relative to the base and Rp_i is the rotation matrix R mapping the local coordinates of p_i into the global coordinate frame using the Z-Y-X convention. R is given by:

$$R = \begin{bmatrix} c\alpha c\beta & -s\alpha c\gamma + c\alpha s\beta s\gamma & s\alpha s\gamma + c\alpha s\beta c\gamma \\ s\alpha c\beta & c\alpha c\gamma + s\alpha s\beta s\gamma & -c\alpha s\gamma + s\alpha s\beta c\gamma \\ -s\beta & c\beta s\gamma & c\beta c\gamma \end{bmatrix} \tag{4.2}$$

where ”s” denotes sine- and ”c” denotes cosine functions. The angles $[\alpha, \beta, \gamma]$ in eq. (4.2) refer to the Euler angles of q.

4.1.2 Jacobian Matrix

The Jacobian matrix defines a mapping from joint space velocities to workspace velocities. As the Jacobi matrix is defined from the inverse kinematic analysis it is formally referred to as the inverse Jacobian matrix, but will in this thesis be referred to as the Jacobian or Jacobian matrix.

Equation (4.1) relates the leg lengths l_i to the pose q, as t in Eq. (4.1) is the Cartesian coordinates $[x,y,z]$ and the rotation matrix R contains the orientational angles $[\alpha,\beta,\gamma]$ of pose q. To derive the relation between the leg velocities and the end-effector velocities to derive the Jacobian matrix J, Eq. (4.1) is differentiated with respect to the differential time element ∂t, using the chain rule:

$$\frac{\partial l}{\partial t} = \frac{\partial l}{\partial q}\frac{\partial q}{\partial t} \tag{4.3}$$

The Jacobian J is then defined from Eq. (4.3) as $J = \frac{\partial l}{\partial q}$ which yield:

$$\begin{aligned} \frac{\partial l}{\partial t} &= J\frac{\partial q}{\partial t} \\ &\Downarrow \\ \dot{l} &= J\dot{q} \end{aligned} \tag{4.4}$$

where $\dot{l}$ is the vector containing the leg velocities and $\dot{q} = \left[\begin{smallmatrix}\dot{t}\\ \omega\end{smallmatrix}\right]$ contains the velocities $\dot{t}$ and angular velocities ω of the end-effector. To ease the derivation of the Jacobian for Stewart platform, eq. (4.1) is rewritten to eq. (4.5) where l_i denotes the magnitude of the i'th prismatic actuator length and e_i is the unit vector in the direction of the i'th prismatic actuator with respect to the global coordinate frame.

$$l_i e_i = t + Rp_i - b_i \qquad \text{for } i = 1..6 \tag{4.5}$$

In order to derive the Jacobian matrix as described, eq. (4.5) is differentiated with respect to time:

$$\dot{l}_i e_i + l_i \dot{e}_i = \dot{t} + (\omega \times Rp_i) \tag{4.6}$$

Rearranging Eq. (4.6), taking into account that e_i is a unit vector and hence $e_i \cdot e_i = 1$ and $e_i \cdot \dot{e}_i = 0$, yields:

$$\dot{l}_i = e_i \dot{t} + (Rp_i \times e_i) \cdot \omega \tag{4.7}$$

from which the 6 x 6 Jacobian matrix J is given by:

$$J(q) = \begin{bmatrix} e_1^T & (Rp_1 \times e_1)^T \\ \cdots & \cdots \\ e_6^T & (Rp_6 \times e_6)^T \end{bmatrix} \tag{4.8}$$

The Jacobian matrix J is function of the pose q. Given the Jacobian has full rank, it can be confirmed from the dimensions of the Jacobian that the Stewart platform has 6 DOF and 6 prismatic joints, as the row dimension are equal to the number of DOF and the number of columns are equal to the number of prismatic joints [13]. Also note, that the first three columns of J relate to the translational movements and that the last three relate to rotational movements of the manipulator.

4.1.3 Static Forces

The static model can also be rewritten to calculate forces in the actuators g:

$$\tau = J^T(q)g \tag{4.9}$$

where $\tau = [f \;\; m]^T$ are the total force and moment applied to the end-effector at the TCP. Rearranging the equation to calculate the leg forces:

$$g = J^T(q)^{-1}\tau \tag{4.10}$$

4.2 Kinematic Performance Indices

In this section the kinematic performance indices are described. A kinematic performance index is a scalar quantity that measures how well a manipulator behaves to motion transmission and force. Dexterity and manipulability are two typical performance indices to be considered when designing manipulators. The section concludes with a simple example that visualizes the performance indices presented to aid the comprehension of the theory.

4.2.1 Singular Value Decomposition

The Jacobian matrix J for parallel manipulators represents the linear mapping of velocities from the workspace to joint space. The singular value decomposition (SVD) of the Jacobian matrix procures useful information of this mapping relevant to the kinematic performance of the manipulator. This section is based on Lay [14] and Khalil and Dombre [15].

A linear transformation or mapping $x \mapsto Jx$ describe how a vector is transformed by the matrix J. It can be shown that the values of the mapping $x \mapsto Jx$ are maximized in the direction of the eigenvectors, and hence SVD is used to find the singular values of J, as the eigenvectors of the matrix are a function of these.

To find the singular values of matrix J, consider a $m \times n$ matrix J where J^TJ is symmetric and can be orthogonally diagonalized. Let $\{U_1, \ldots, U_n\}$ be an orthonormal basis for $\mathbb{R}^n$ consisting of the eigenvectors of J^TJ, and let $\lambda_1, ..., \lambda_n$ be the associated eigenvalues of J^TJ. Then consider the following statement for $1 \leq i \leq n$:

$$\begin{aligned} \|JU_i\|^2 &= (JU_i)^T JU_i = U_i^T J^T JU_i \\ &= U_i^T(\lambda_i U_i) && \text{Since } U_i \text{ is an eigenvector of } J^TJ \\ &= \lambda_i && \text{Since } U_i \text{ is a unit vector} \end{aligned} \tag{4.11}$$

Note that the quantity of the transformation $\|JU_i\|^2$ studied in eq. (4.11), is maximized at the same U_i that maximizes $\|JU_i\|$, and is easier to study. The singular values of J are equal to the square root of the eigenvalues of J^TJ given in eq. (4.11), which are also equal to the length of the vectors $JU_i, ..., JU_n$, giving:

$$\sigma_i = \sqrt{\lambda_i} = \|JU_i\|, ..., \|JU_n\| \qquad \text{for } 1 \leq i \leq n \tag{4.12}$$

The singular value decomposition theorem states that for a $m \times n$ matrix J with rank r exits:

- an $m \times n$ matrix Σ, eq. (4.14), for which the diagonal entries in D are the singular values σ of J, where $\sigma_1 \geq \sigma_2 \geq ... \geq \sigma_r > 0$,
- an $m \times m$ orthogonal matrix U containing the eigenvectors of $J^T J$
- and an $n \times n$ orthogonal matrix V containing the eigenvectors of J,

such that:

$$J = U \Sigma V^T \tag{4.13}$$

The $(m \times n)$ matrix Σ has the following form:

$$\Sigma = \begin{bmatrix} D_{r \times r} & 0_{r \times (n-r)} \\ 0_{(m-r) \times r} & 0_{(m-r) \times (n-r)} \end{bmatrix} \tag{4.14}$$

The columns of U and V are called left singular values of J and right singular vectors of J respectively. Substituting the singular value decomposition of J into the kinematic model:

$$\dot{q} = U \Sigma V^T \dot{l} \tag{4.15}$$

The matrix Σ contains zeros on the diagonal where $i > r$, meaning $\sigma_i = 0$ for $i > r$. Equation 4.15 can be rewritten:

$$\dot{q} = \sum_{i=1}^{r} \sigma_i U_i V_i^T \dot{l} \tag{4.16}$$

The eigenvectors $V_1, ..., V_r$ from the singular value decomposition of J, form an orthonormal basis for the subspace of $\dot{l}$ and hence is generating an end-effector velocity for the Stewart platform. An orthonormal basis for the achievable end-effector velocities is formed by $U_1, ..., U_r$ and the singular values σ_i represent the velocity transmission ratio from the joint space to the workspace. This can also be seen from eq. (4.17).

$$U_i^T \dot{q} = \sigma_i V_i^T \dot{l} \qquad \text{for } i \leq r \tag{4.17}$$

The Stewart platform velocities are described by eq. (4.4) on page 17. For the Stewart platform it is desired to know if the Jacobian matrix is invertible, since this allows calculations from workspace to joint space and vice versa. If the matrix is invertible, it is non-singular, but as the Jacobian changes over time it is important to know if the Jacobian is invertible for all values of q or for which values it is not. If the Jacobian is not invertible at a given position, it has become singular and hence the manipulator has lost one or more DOF in the Cartesian space in this position. This means that there in the Cartesian space is some direction in which it is impossible to move the end-effector, no matter what joints are actuated or at which rates. This also means that the manipulator has singularities on the boundary of it's workspace, since the manipulator is either fully stretched or folded at these positions and hence are limited from moving further out of the workspace.[13]

4.2.2 Velocity-Force Duality

The velocity transmission from the end-effector to the actuators and vice versa can be mapped using the Jacobian matrix of the Stewart platform, as described in Section 4.1.2. Figure 4.2 shows the mapping of a velocity ellipse for the TCP of a 2 DOF manipulator. From the figure it is seen that the vectors U_i (eigenvectors of $J^T J$) described in the SVD analysis in Section 4.2.1, form the principal axis for the ellipse and that the singular values σ_i are the lengths of the axis. The largest velocities can be transmitted along the major principal axis where the transmission ratio is largest, and the smallest velocities can be transmitted along the minor principal axis. Analog to the velocity transmission is the force transmission

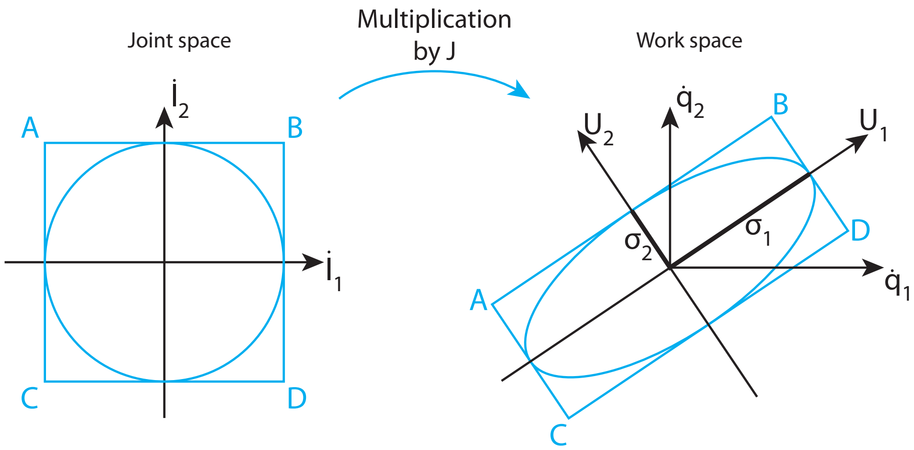

Figure 4.2: *Velocity transformation between spaces for a 2 DOF system [15].*

also expressed by the singular values of the Jacobian matrix. The force ellipse has the same principal axis as the velocity ellipse, with the difference that the lengths of the axis are reciprocal. This means that the largest force can be generated in the direction where the velocity transmission is smallest and vice versa. The relation between the velocity and force transmission can be seen in Fig. 4.3.

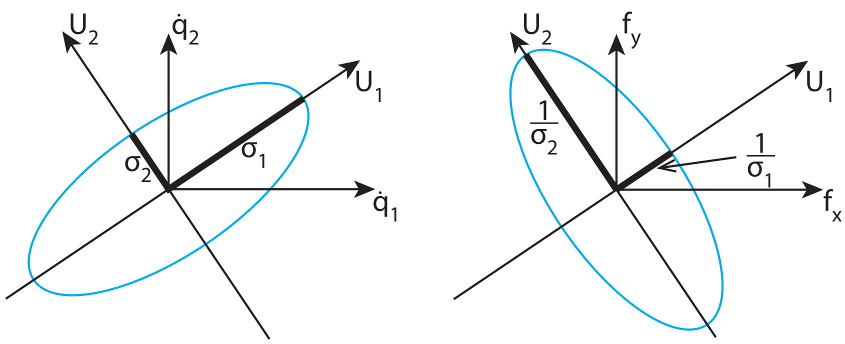

Figure 4.3: *Velocity (left) and force (right) ellipses. Note that the ellipses are scaled.*

4.2.3 Isotropy

A kinematic system is said to be isotropic when it in at least one point within the prescribed workspace exhibits homogeneous behavior in all directions for some kinetostatic property [16]. Isotropy is a property of the Jacobian matrix, and hence the Jacobian must be investigated. Angeles [12] formulates isotropy mathematically as follow:

$$J^T J = \lambda I_{6x6} \tag{4.18}$$

From eq. (4.18) it is seen that the eigenvalues λ must be equal for the system to be isotropic. This means that the singular values σ also must be identical, because the singular values are the square root of the eigenvalues. A kinematic system can be isotropic for velocity, force and stiffness. A manipulator is isotropic with respect to velocity and force if it can obtain the same velocities and forces in all directions.

4.2.4 Normalization of the Jacobian Matrix

The Jacobian matrix J Eq. (4.8) needs to be normalized as its columns have mixed dimensions. As stated in Section 4.1.2 the first three columns of the matrix relate to translational motion and the last three to rotational motion of the manipulator. As seen from Eq. (4.8) the first three columns of the matrix are dimensionless as they only contain directions in the form of the unit vectors e_i. Additionally the last three columns relate to rotational motion of the manipulator and have units of length. To analyze the Jacobian all columns need to be dimensionless to make a non-dimensional analysis of the system possible and thus the last three columns need to be normalized.

To normalize the last three columns and make them dimensionless, different methods have been proposed in literature. Angeles [12] defines that a "scaling factor" or characteristic length should be chosen and that the entries with the length units should be divided by this characteristic length to create a dimensionless Jacobian. Stoughton and Arai [8] chose the characteristic length as the length from the TCP to the center of the spherical joints between the platform and the actuators. This length is chosen as the last three columns of the Jacobian are related to the moment transmitted from the actuator to the TCP and as the charasteristic length is the moment arm for the force transmitted by the actuator to the end-effector. An other characteristic length L to normalize the Jacobian is proposed by Fattah and Ghasemi [17]. This length has been used by Mollnari et al. [18] in the design of a five-axis parallel manipulator *Celerius* which has shown isotropic kinematic performance. As the characteristic length proposed by Fattah and Ghasemi has shown good performance results on *Celerius*, Fassi et al. [16] have adapted this characteristic length to normalize the Jacobian for a 6 DOF parallel manipulator, which is the method that will be used in this thesis.

To calculate the characteristic length L as proposed by Fassi et al., the Jacobian is split up into two 6×3 matrices; J_F related to forces and J_T related to torques [16]:

$$J = [J_F \vdots J_T] \tag{4.19}$$

In order to eliminate the units of length, the entries in J_T is then divided by the characteristic length L:

$$J = \left[J_F \vdots \frac{1}{L} J_T \right] \tag{4.20}$$

The condition for isotropy is given by [12]:

$$J^T J = \lambda I_{6x6} \tag{4.21}$$

Using the condition for isotropy the left side of Eq. (4.21) becomes:

$$J^T J = \begin{bmatrix} J_F^T J_F & \frac{1}{L} J_F^T J_T \\ \frac{1}{L} J_T^T J_F & \frac{1}{L^2} J_T^T J_T \end{bmatrix} \tag{4.22}$$

To make the system isotropic and fulfill eq. (4.21), it is seen from eq. (4.22) that the diagonal entries must be equal, and hence:

$$J_F^T J_F = \frac{1}{L^2} J_T^T J_T \tag{4.23}$$

The characteristic length L is then derived to be:

$$L = \sqrt{\frac{\mathrm{trace}(J_T^T J_T)}{\mathrm{trace}(J_F^T J_F)}} \tag{4.24}$$

Using this characteristic length L it is now possible to normalize the Jacobian matrix to investigate the kinematic performance of the Stewart platform configuration.

4.2.5 Dexterity

Dexterity is the degree of isotropy in the force and velocity transmission in a given point for the manipulator, where the best possible dexterity is achieved when the dexterity is isotropic. This section is based on [19] and [20].

The dexterity of a manipulator is derived from the Jacobian matrix and as the Jacobian changes for every pose within the workspace, so does the dexterity. In order for a manipulator to exhibits isotropic dexterity in a point, the Jacobian must map a unit hypersphere into another precise hypersphere of arbitrary size, where the singular values of the Jacobian represent the value on the axis that span the sphere, cf. Fig. 4.3. This implies that all singular values of the Jacobian must be identical for the values to form a sphere. If the singular values are not identical, the variation in size can be considered a measure of how much the unit sphere is distorted by the mapping. If any of the singular values approaches zero the hyperellipsoid loses its volume and the end-effector becomes stationary with respect to the related DOF. Good dexterity is obtained when the singular values are identical or close to identical. It should be noted that the shape of the mapped hyperellipsoid is independent of whether the Jacobian is defined from forward or inverse kinematics. The degree of dexterity is determined by studying the condition number of the Jacobian matrix. The condition number of a matrix J equals the ratio between the maximum and minimum singular values:

$$\kappa(J) = \frac{\sigma_{max}(J)}{\sigma_{min}(J)} \tag{4.25}$$

To evaluate the dexterity at a specific point in the workspace the reciprocal of the condition number is used: $\kappa(J)^{-1}$. The value ranges from 0 (singular condition) to 1 (isotropic condition). To not only have a measure for a specific point, it is of greater interest to evaluate the dexterity with respect to a defined workspace w for the manipulator. To measure the dexterity over a defined workspace w the Global Conditioning Index (GCI) is used:

$$GCI(q) = \frac{\int_w 1/\kappa(J)dw}{\int_w dw} \tag{4.26}$$

To obtain the greatest dexterity throughout the entire workspace the GCI must be maximized. The manipulator is fully isotropic if the GCI is unity for all points in the workspace.

It is highly unlikely to obtain a dexterity value of unity throughout the entire workspace for any kinematic design configuration. This indicates that variations in dexterity must occur within a defined workspace. Maximizing GCI is therefore not enough to ensure the best design, as this index provide no information of the uniformity of dexterity within the workspace. A measure of uniformity is proposed by R. Kurtz and V. Hayward [21] where uniformity is checked by evaluating the gradient of the dexterity function in Eq. (4.26). The index is called the Global Gradient Index and is defined in Eq. (4.27).

$$\Delta GGI(q) = \max_w \left\| \Delta \frac{1}{\kappa(J)} \right\| \tag{4.27}$$

4.2.6 Manipulability

The manipulability is a measure of the amplification of actuator velocities into end-effector velocities in a given point. The manipulability is the determinant of the Jacobian matrix:

$$M = \prod_{i=1}^{6} \sigma_i(J^{-1}) = det(J^{-1}) \tag{4.28}$$

The determinant can be geometrically interpreted as the volume expanded by the columns of the matrix. This can be visualized as the singular values represent the lengths of the axis that constitutes the velocity ellipsoid. The greater the singular values, the greater manipulability are obtained. To evaluate the manipulability of a manipulator over a defined workspace w, the Global Manipulability Index (GMI) is derived by integration of Eq. (4.28) over the workspace. The GMI is formulation as:

$$GMI(q) = \frac{\int det(J^{-1})dw}{\int_w dw} \tag{4.29}$$

4.3 Visualization of Kinematic Performance

In this section the kinematic concepts and performance indices are visualized to ease the comprehension of the theory presented in this chapter. The Stewart platform consists of complicated closed kinematic chains which makes visualization very difficult, why a simple elbow mechanism is used instead. The elbow mechanism is a serial manipulator whereas the Stewart platform is a parallel manipulator, which is irrelevant as the kinematic concepts and performance indices are the same regardless of manipulator type.

In Fig. 4.4 the elbow mechanism, which has two actuated revolute joints and two degrees of freedom, is presented in 4 different poses. In the figure the elbow mechanism is performing a translational movement in the x-direction requiring actuation of both revolute joints.

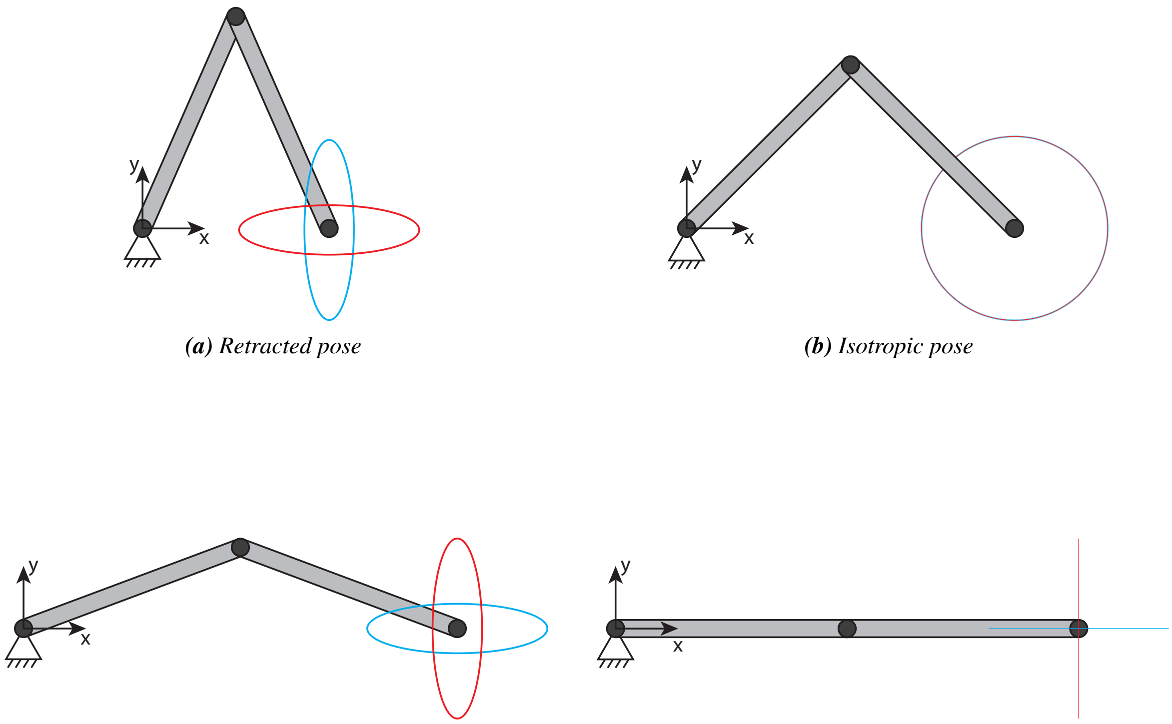

(a) Retracted pose *(b) Isotropic pose* *(c) Extented pose* *(d) Singular pose*

Figure 4.4: *Elbow mechanism with scaled force (blue) and velocity (red) ellipse.*

A retracted pose of the elbow mechanism can be seen in Fig. 4.4a. In this pose the minor semi-axis of the force ellipse is in the x-direction and the major semi-axis is in the y-direction. This means that the elbow mechanism is able to produce the greatest force in the y-direction and the smallest force in the x-direction in this pose. The velocity ellipse is reciprocal of the force ellipse and analogously the mechanism is able to produce the greatest velocity in the x-direction and the smallest velocity in the y-direction. Recall from Section 4.2.2 that the lengths of the semi-axis are the singular values for the velocity ellipsoid and the reciprocal for the force ellipsoid. Note that both ellipses in Fig. 4.4 are scaled (by the largest value) so that the longest axis is always 1.

In an isotropic pose all singular values are equal, and hence both the force and velocity ellipses become perfect circles, cf. Section 4.2.3. An isotropic pose of the elbow mechanism is depicted in Fig. 4.4b. The elbow mechanism is only isotropic in this exact pose and poses that are reflections of this pose over the axis. Some kinematic systems can be isotropic or close to isotropic in all poses within a defined workspace. The elbow mechanism is only close to isotropic in a small region around the perfect isotropic pose in Fig 4.4b. In this region the dexterity of the mechanism is said to be good, see Section 4.2.5. The most important characteristics of an isotropic pose of the elbow mechanism or any other isotropic kinematic system is, that the mechanism is able to yield equal tool center point forces and velocities in all directions (x- and y-direction for the elbow mechanism). This is illustrated in Fig. 4.5 where the magnitude of ω_1 and ω_2 are equal with the directions shown in the figure, which results in translational motion in the x-direction of the tool center point. In the figure the red vectors denotes the tangential velocity of the links, the black vectors denotes the x and y velocities and the curved arrow indicates the direction of rotation. Adding the black components of the red velocity vectors show, that the end-effector velocity in the y-direction becomes zero and the velocity in the x-direction is twice the contribution of each link. Likewise, the manipulator can exhibit twice the velocity contribution in the y-direction and zero in the x-direction, if ω_1 is negative in the isotropic pose.

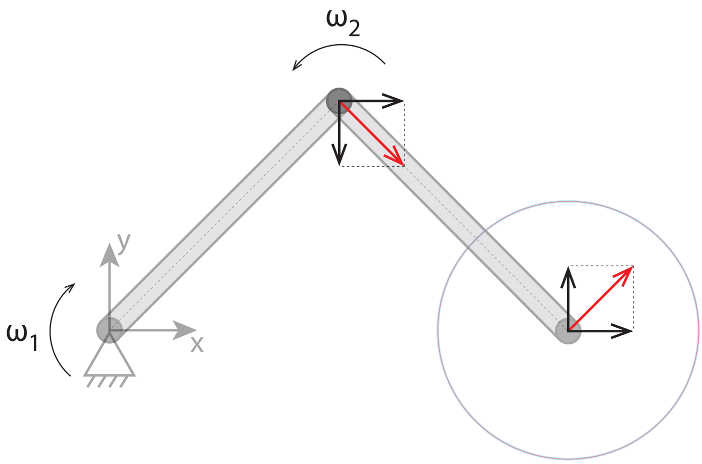

Figure 4.5: *Velocity in the isotropic pose.*

The velocity and force ellipses in the extended pose in Fig. 4.4c are inverted compared to the retracted pose. In Fig. 4.6 the velocity and force vectors are added to Fig. 4.4c to illustrate the duality between velocity and force. As mentioned earlier in this section the force ellipse is reciprocal of the velocity ellipse. The velocity components in the x-direction approach zero as the angle between horizontal approach zero. This means that the force ellipse and hence the end-effector force becomes infinitely large.

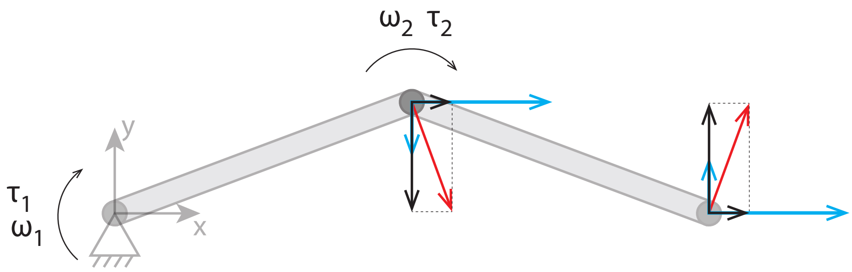

Figure 4.6: *Force and velocity duality with (red) velocity and (blue) force vectors.*

When the mechanism reaches the boundary, as depicted in Fig. 4.4d, it is said to be in singular pose. This is also the case when the elbow mechanism is fully retracted. A singularity occurs because the mechanism loses one or more degrees of freedom. Clearly the elbow mechanism cannot move in the y-direction in the pose in Fig. 4.4c, and hence this degree of freedom is lost. The same is true in the fully retracted pose.

CHAPTER 5

KINEMATIC OPTIMIZATION AND DESIGN

Traditional design has always been limited by the design engineer's experience, knowledge and intuition. Regardless of the engineering skills using the traditional approach to design does not necessarily ensure the best solution. This can be overcome today by using optimization methods. In this chapter the kinematic performance, as described in Section 4.2, is optimized for the two different types of Stewart platform designs selected in Section 2.3. The design variables and geometrical constraints are formulated and methods to ensure that the demands in Section 2.4 regarding avoidance of leg collisions and physical realizable prismatic actuators are developed. This is done formulating a multi objective optimization problem using the performance indices relevant for wave compensation and penalty functions. All steps in the formulation process are documented and the final solution is presented.

5.1 Prescribed Workspace

The Stewart platform in this thesis is intended to work on the ocean with a ship crane mounted on the platform as described in Section 2.1 to counteract the motion of the mounting ship. To counteract the ship motion the Stewart platform must move with the same relative motion as the ship but in the opposite direction.

It is desired to utilize the Stewart platform to compensate for ship motions up to sea state 5, meaning that the maximum relative motion of the ship in sea state 5 defines the prescribed workspace boundaries, see Table 3.1 on page 13. The prescribed workspace w is then defined by Table 5.1 and illustrated in Fig. 5.1. Note that the prescribed workspace in Fig. 5.1 only illustrate the Cartesian part of the workspace (x,y,z), but that every point also has an Eulerian part (α,β,γ) which is impossible to illustrate by points. The center of the prescribed workspace is placed in $(0,0,h)$, where h is equal to the height of the Stewart platform in its neutral pose.

In Fig. 5.1 the prescribed workspace w is marked by a cuboid, which holds n uniformly distributed random blue points. The random points are generated to create a finite number of representative poses

Table 5.1: *Prescribed Workspace limits.*

w:	Limits:
x	$\pm$ 0.23 m
y	$\pm$ 0.48 m
z	$\pm$ 1.22 m
α	0°
β	$\pm$3°
γ	$\pm$ 10°

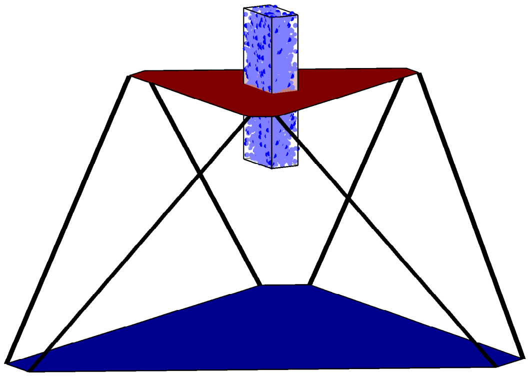

Figure 5.1: *Stewart platform with prescribed workspace w.*

of the prescribed workspace, using the random function in MATLAB. The matrix of poses within the prescribed workspace for the end-effector is calculated by Eq. (5.1).

$$q = \begin{bmatrix} x \\ y \\ z \\ \alpha \\ \beta \\ \gamma \end{bmatrix} = \begin{bmatrix} 0.23\, f_{rand}(n) \\ 0.48\, f_{rand}(n) \\ h + 1.22\, f_{rand}(n) \\ 0^\circ \\ 3^\circ\, f_{rand}(n) \\ 10^\circ\, f_{rand}(n) \end{bmatrix} \quad \text{where} \quad f_{rand}(n) \in [-1;1] \tag{5.1}$$

where h is the global z-coordinate of the center of the workspace (which equal the neutral height of the Stewart platform) and the function $f_{rand}(n)$ creates n random values between -1 and 1, and hence the dimension of the matrix becomes 6 by n with n random poses for the end-effector.

To find a sufficient number of points n that ensures adequate precision of the calculated performance indicies, the deviation in *GCI* (ΔGCI) as a function of n is evaluated for a given design with 30 different simulations. Figure 5.2 shows the difference between the maximum and minimum *GCI* for n points and a second order exponential approximation of these. As the points are uniformly distributed over the prescribed workspace independently of the number of points n, the value of the *GCI* for these points is an approximation of the actual *GCI*.

The precision of the *GCI* for a prescribed workspace is improved if more points n are used in the representation. If $n \rightarrow \infty$ the deviation $\Delta GCI \rightarrow 0$ and the exact value of *GCI* is obtained. The deviation

$\Delta GCI(n)$ for a given number n is approximated by 30 different simulations with 30 different sets of uniformly distributed random generated poses. The difference between the maximum and minimum result for a specific number of poses n represent the deviation $\Delta GCI(n)$. The deviation in GCI as a function of n is plotted in Fig. 5.2. From the figure it can be seen that the deviation in GCI is less than 0.25 % for 30 different simulations of $n \geq 2000$ points. As accuracy are desired within reasonable computational limits (as computation time increase with n), $n = 2000$ is chosen.

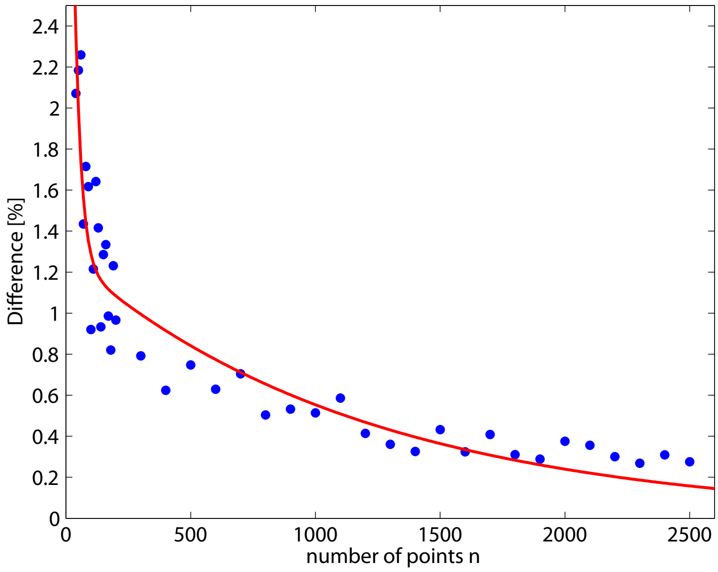

Figure 5.2: *ΔGCI versus number of poses in the prescribed workspace.*

5.2 Kinematic Performance Indices for Wave Compensation

In this section it is discussed why optimization of kinematic performance indices are relevant for the wave compensation application. No degree of freedom may be lost in any pose within the prescribed workspace as this inhibits the Stewart platform from performing the desired task. A degree of freedom is lost if one of the singular values becomes zero. A specific kinematic design may have singular values close to zero within the workspace meaning that the actuation speed must be very fast to move the end-effector in the directions were the singular values are close to zero. Another kinematic design may have large singular values which meaning that only small forces can be generate in these directions. The forces may be insufficient to perform the desired task.

Optimization of the Global Condition Index GCI (dexterity) is desired to ensure that the Stewart platform is able to obtain usable and equal forces and velocities in all directions and orientations. Recall from Section 4.2.5 that the dexterity is increased as the magnitude of the largest and smallest singular value of the Jacobian matrix approach the same value. Optimizing dexterity indirectly minimizes the possibility for singular values that are close to zero or large for all poses within the prescribed workspace.

Maximizing the Global Manipulability index (GMI) creates a kinematic design solution where the velocity transmission from actuator to end-effector is maximized. Recall from Section 4.2.6 that manipulability is the product the of all singular values and that the singular values are the force/velocity transmission ratio from actuator to end-effector:

$$J^{-1}\dot{l} = \dot{q}$$

Hence maximizing the manipulability yields a kinematic configuration where small actuator velocities results in large end-effector velocities which reduce the actuation speed. In correlation with the discussion above, optimization with respect to *GCI* and *GMI* is performed to obtain good kinematic performance of the wave compensation application.

5.3 Performance Analysis of the HYDAC Stewart Platform

HYDAC A/S has developed a Stewart platform prototype in order to increase their knowledge of all aspects within Stewart platform design. To evaluate this Stewart platform design the kinematic performance is calculated using the indices described in Section 4.2. The evaluation of the kinematic performance is performed to evaluate whether improvements can be made.

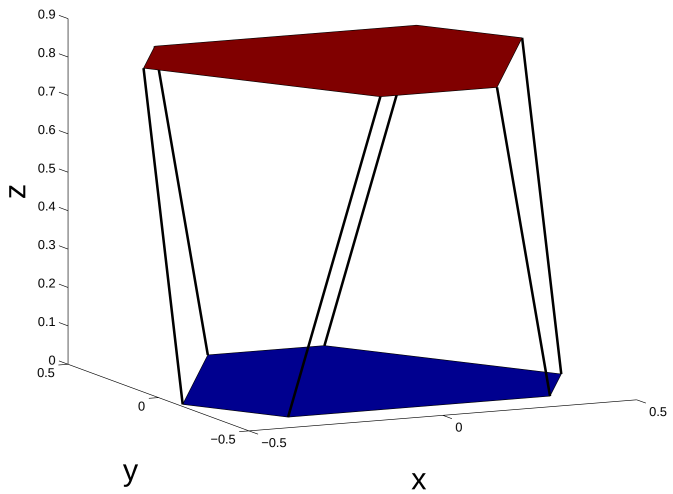

Figure 5.3: *Kinematic configuration of HYDAC's Stewart platform.*

The HYDAC Stewart platform is depicted in Fig. 5.3 and the geometrical data of the system is tabulated in Table 5.2. The design angles ϕ_b and ϕ_p are the leg spacing angles, and the radii R_b and R_p are the radii of the circular paths the legs are mounted on. An illustration of the geometrical data can be seen in Fig. 5.4 on page 32.

The original configuration of HYDAC's Stewart platform is unable to work within the prescribed workspace required for wave compensation, see Section 5.1, due to its the physical size. This means that the global performance indices cannot be calculated directly, as the global performance indices are dependent on the wave compensation workspace. To resolve this problem the HYDAC Stewart platform design is scaled by a factor of 5 to match the required workspace and still fulfill the physical size constraints for the system, see Section 2.5.

The kinematic performance indices are not dependent of the physical size of the system but of the geometric relations in the design. However, for the Global Conditioning Index (*GCI*) and the Global

Table 5.2: *Geometrical data*

Design variables:	Magnitude:
Base radius R_b	500 mm
Platform radius R_p	500 mm
Angle between legs on base ϕ_b	35°
Angle between legs on platform ϕ_p	85°
Minimum leg length	638 mm
Maximum leg length	1038 mm

Manipulability Index (*GMI*) the physical size of the system is important, as they are calculated for the given workspace. *GCI* and *GMI* are determined using the method described in Section 4.2.5 and 4.2.6 respectively. The results of the kinematic performance is tabulated in Table 5.3.

Table 5.3: *Kinematic Performance*

Performance index:	Magnitude:
Global Conditioning Index (*GCI*)	0.1739
Global Manipulability Index (*GMI*)	1.5571

The results indicate that the HYDAC Stewart platform is far from isotropic as a *GCI* of 0.1739 is far from the isotropy utopia point defined by *GCI*=1. Additionally the *GMI* is fairly large, which is good for velocity transmission from the actuators to the tool center point. The low *GCI* indicate that the HYDAC Stewart platform can only resist large forces in a few directions, which is supported by the high *GMI* allowing large velocity transmissions. Evaluating the HYDAC Stewart platform design visually, consolidate this assumption as the legs are fairly vertical. This allow the Stewart platform to resist large forces in z and perform large velocities in the xy-plane.

5.4 Design Configurations and Variables

To formulate an optimization problem that can optimize the kinematic performance indices chosen in Section 5.2, appropriate design variables for the Stewart platform design must be selected. The design variables must influence the objective function directly or indirectly for the design variables and objective function to be valid. Design variables can be regarded as free variables, as they can be assigned any value within a given range or subset by the optimization algorithm. This range or subset is mathematically formulated as constraints. The design variables should be independent of each other as far as possible, and the number of these specifies the degrees of freedom for the optimization problem. Optimization complexity is increased by the degree of freedom of the problem [22]. This section describes the two different types of Stewart platform designs selected in Section 2.3 and the associated design variables.

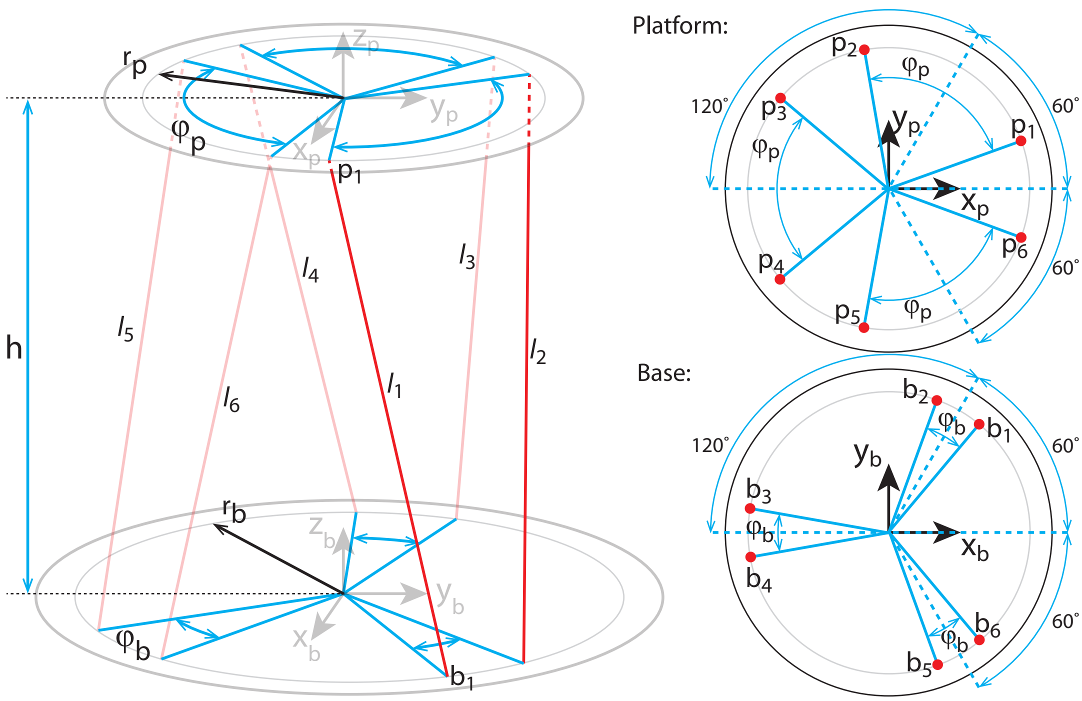

Figure 5.4: Single circle design of Stewart platform.

5.4.1 Single Circle Stewart Platform

The single circle (SC) design of the Stewart platform is the simplest and most common configuration of the Stewart platform, see Fig. 5.4. In the single circle design the actuators are located on the same planar circular path on both the base and platform respectively. The radii of the circular paths of the base and platform are denoted r_b and r_p respectively, and the spacing angles between the actuator mounting points are denoted ϕ_b and ϕ_p. The height of the platform is denoted h and describe the distance from the center of the base to the center of the end-effector in its neutral pose. This is also the center point for the prescribed workspace. These design variables are free to change independently of each other. In order to describe the SC Stewart platform design mathematically using the design variables shown in Fig. 5.4, the following equations are used.

A symmetric design of the single circle Stewart platform is chosen in order to distribute the load from the ship crane evenly as the crane may turned the load 360° around the center of the platform. To create a symmetric design, the actuator joints are distributed evenly with respect to the spacing angles ϕ_b and ϕ_p, as shown in Fig. 5.4. The position angles ψ_i and Ψ_i for the i'th actuator joints on the base and platform respectively, is calculated in Eq. (5.2) which ensures symmetry for the design and equal angle spacing between the actuator joints. The position angles ψ_i and Ψ_i is given by:

$$\begin{aligned} \psi_i &= \frac{i\pi}{3} - \frac{\phi_b}{2} \qquad \Psi_i = \frac{i\pi}{3} - \frac{\phi_p}{2} \qquad \text{for} \quad i = 1,3,5 \\ \psi_i &= \psi_{i-1} + \phi_b \qquad \Psi_i = \Psi_{i-1} + \phi_p \qquad \text{for} \quad i = 2,4,5 \end{aligned} \tag{5.2}$$

The local coordinate vector for the $i'th$ actuator position b_i and p_i, on the base and platform plate respectively, is then described by the following equations:

$$
\begin{aligned}
b_i &= \begin{bmatrix} r_b cos(\psi_i) \\ r_b sin(\psi_i) \\ 0 \end{bmatrix} = \begin{bmatrix} b_{ix} \\ b_{iy} \\ b_{iz} \end{bmatrix} \quad \text{for} \quad i = 1..6 \\
p_i &= \begin{bmatrix} r_p cos(\Psi_i) \\ r_p sin(\Psi_i) \\ 0 \end{bmatrix} = \begin{bmatrix} p_{ix} \\ p_{iy} \\ p_{iz} \end{bmatrix} \quad \text{for} \quad i = 1..6
\end{aligned}
\tag{5.3}
$$

In the equations above, five design variables are defined and consequently a design parameter vector λ_{SC} for the single circle design is defined:

$$\lambda_{SC} = \begin{bmatrix} \phi_b & \phi_p & r_b & r_p & h \end{bmatrix}^T \tag{5.4}$$

The value of the entries in the design vector is changed by the optimization algorithm in order to find the optimum solution for the single circle Stewart platform design configuration.

Single Circle Design Space

To constrain the optimization algorithm to search in the feasible domain of the design points, constraints are imposed on the design variables to model the physical limitations for the design. The system requirements in Section 2.5 defines that the platform must have a minimum diameter of 4 m to ensure adequate space for crane installation. This defines the lower bound (LB) for the radius of the platform r_p to be 2 m, and for simplicity 2 m is also chosen as the LB on the base plate radius r_b. The maximum of both radii are constrained as the maximum available deck space is 7 m in diameter, hence the upper bound (UB) on the maximum radii are 3.5 m.

The height h of the Stewart platform is constrained by the actuators because the actuators must be able to generate any pose within the prescribed workspace. The lengths of the actuators are closely related to the height of the Stewart platform due to the geometry of the Stewart platform. From the prescribed workspace definition in Table 5.1 on page 28, it is can be seen that the platform must move ± 1.22 m in the z-direction, which indicates that the minimum stroke length $l_{stroke,min}$ of the actuators must be approximately 2.44 m. As the length of a fully retracted actuator, l_{min}, has to be longer than the minimum required stroke length $l_{stroke,min}$, l_{min} is defined as $1.2\, l_{stroke,min} = 1.2(2.44\text{m}) \approx 3$ m. The lower bound on the height h is therefore 3 m. The upper bound is set at 7 m as this yields equal width and height of the Stewart platform.

The outer diameter of the actuators is estimated to be a maximum diameter of 0.3 m. To avoid that two adjacent actuators collide at their joints the minimum distance between the actuator joints must be at least equal to the actuator diameter to ensure adequate space between the joints. This defines the spacing angles ϕ_b and ϕ_p, where the angles between the actuator joints must be greater than $9°$ if the lower bound on the radius is active, according to Eq. (5.5), and greater than $5°$ if the upper bound on the radius is active, according to Eq. (5.6). Note that the calculations in Eq. (5.5) and Eq. (5.6) is based on the length of the circular arc between the points and not the exact distance.

$$\phi_b \vee \phi_p \geq 360^\circ \frac{d_{act}}{LB(r)2\pi} \approx 9^\circ \quad \text{for} \quad r_b \vee r_p \ = \ 2 \text{ m} \tag{5.5}$$

$$\phi_b \vee \phi_p \geq 360^\circ \frac{d_{act}}{UB(r)2\pi} \approx 5^\circ \quad \text{for} \quad r_b \vee r_p \ = \ 3.5 \text{ m} \tag{5.6}$$

As each actuator pair is symmetric around one of three symmetry lines 120° apart, see Fig. 5.4, the upper bound on the spacing angles ϕ_b and ϕ_p are equal to (120°-LB). Initial optimizations indicate that $r_b \rightarrow UB$ and $r_p \rightarrow LB$ why the spacing angle design space is chosen accordingly. The final optimizations in Section 5.7 confirm this assumption. The design space for the design variables is defined as:

Table 5.4: *SC Design space.*

LB		λ_{SC}		UB	unit
5	$\leq$	ϕ_b	$\leq$	115	[°]
9	$\leq$	ϕ_p	$\leq$	111	[°]
2	$\leq$	r_b	$\leq$	3.5	[m]
2	$\leq$	r_p	$\leq$	3.5	[m]
3	$\leq$	h	$\leq$	7	[m]

5.4.2 Concentric Circle Stewart Platform

In the concentric circle (CC) design the actuators are placed on two concentric circular paths on the base and platform with the radii r_b and $(r_b - \Delta r_b)$ on the base and r_p and $(r_p - \Delta r_p)$ on the plate, see Fig. 5.5. The actuator mounting points on the base are placed in pairs 120° apart with one mounting point on each circular path. On the platform plate the actuator mounting points are spaced with different angles ϕ and θ, as the spacing angles not are required to be equal which allows symmetric and asymmetric designs. The CC design configuration and the respective design variables are illustrated in Fig. 5.5 with one highlighted actuator pair. Note that the design variables are equal for all tree actuator pairs.

The concentric circle design is created to improve dexterity compared to the single circle design, as the actuators are placed in concentric circles. This allows the actuators to cross over one another and let the actuator orientation come closer to the xy-plane. This should in theory render the concentric circle design superior in terms of dexterity compared to the single circle design [8].

In the concentric circle design, the actuators are placed in pairs 120° apart on the base plate and with the spacing angles ϕ and θ on the platform, as described earlier. The position angles ψ_i and Ψ_i mathematically defines the position for the $i'th$ actuator from the x-axis on the base and platform respectively. The positioning angles are described by:

$$\begin{aligned} \psi_i &= \frac{i\pi}{3} \qquad \Psi_i = \frac{i\pi}{3} - \phi \qquad \text{for} \quad i = 1,3,5 \\ \psi_i &= \psi_{i-1} \quad \Psi_i = \frac{i\pi}{3} + \theta \qquad \text{for} \quad i = 2,4,5 \end{aligned} \tag{5.7}$$

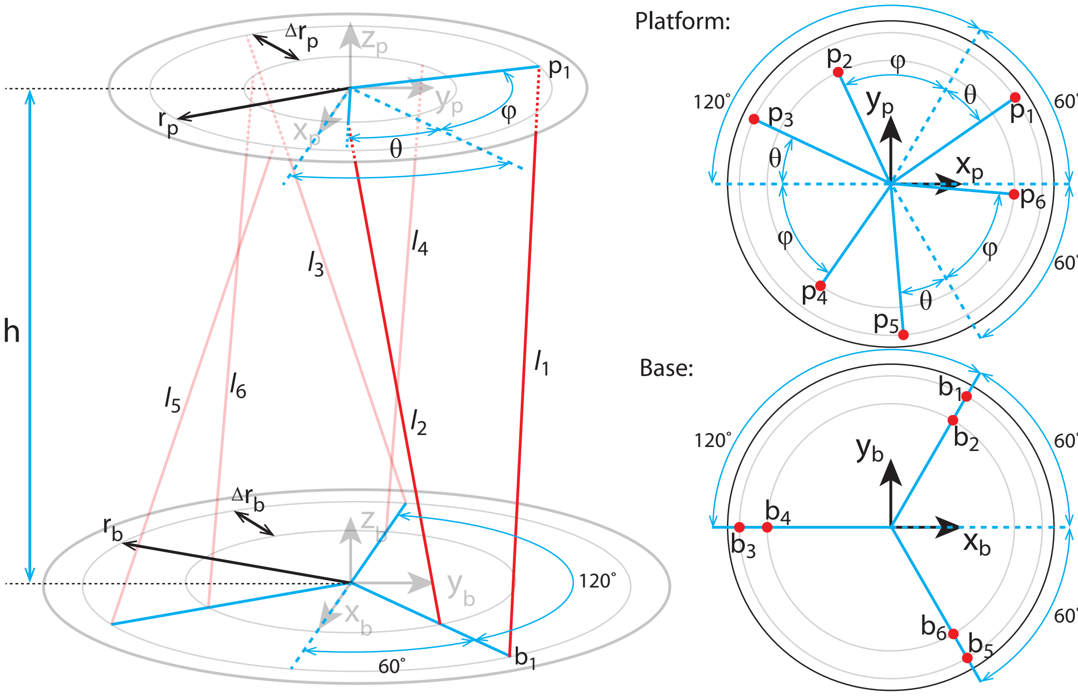

Figure 5.5: *Concentric circle design of Stewart platform.*

Utilizing the positioning angles in Eq. (5.7) the actuator positions vectors b_i and p_i for $i = 1$ is defined by:

$$b_i = \begin{bmatrix} r_b cos(\psi_i) \\ r_b sin(\psi_i) \\ 0 \end{bmatrix} = \begin{bmatrix} b_{ix} \\ b_{iy} \\ b_{iz} \end{bmatrix} \quad p_i = \begin{bmatrix} r_p cos(\Psi_i) \\ r_p sin(\Psi_i) \\ 0 \end{bmatrix} = \begin{bmatrix} p_{ix} \\ p_{iy} \\ p_{iz} \end{bmatrix} \quad \text{for} \quad i = 1,3,5 \tag{5.8}$$

and for $i = 2,4,6$ the actuator positions vectors b_i and p_i is defined as:

$$b_i = \begin{bmatrix} (r_b - \Delta r_b) cos(\psi_i) \\ (r_b - \Delta r_b) sin(\psi_i) \\ 0 \end{bmatrix} = \begin{bmatrix} b_{ix} \\ b_{iy} \\ b_{iz} \end{bmatrix} \quad p_i = \begin{bmatrix} (r_p - \Delta r_p) cos(\Psi_i) \\ (r_p - \Delta r_p) sin(\Psi_i) \\ 0 \end{bmatrix} = \begin{bmatrix} p_{ix} \\ p_{iy} \\ p_{iz} \end{bmatrix} \quad \text{for} \quad i = 2,4,6 \tag{5.9}$$

The kinematic design of the concentric circle Stewart platform can then be described by the seven design variables in λ_{CC}, Eq. (5.10), where h is the distance from the base plate to the middle of the end-effector in its neutral pose.

$$\lambda_{CC} = \begin{bmatrix} \phi & \theta & r_b & \Delta r_b & r_p & \Delta r_p & h \end{bmatrix}^T \tag{5.10}$$

Concentric Circle Design Space

Analog to the single circle Stewart platform design, the design variables for the concentric circle design are constrained to ensure a feasible design. Like the SC design, the upper and lower bound of the radii r_b and r_p are defined by the crane mounting width and available deck space, see 5.4.1. The radii differences

Δr_b and Δr_p is defined by the requirement of a minimum distance between the mounting points for the actuators. Similar to the SC design, the maximum actuator diameter is estimated to be 0.3 m, and hence Δr_b and Δr_p has a lower bound of 0.3 m. The upper bounds on the radii differences are chosen as the maximum radius of base or platform respectively minus the lower bound of 0.3 m. The upper and lower bound on the height h for the concentric circle design is also defined smiliar to the single circle design. The spacing angles ϕ and θ are constrained not to exceed 180° from the starting point. This means that ϕ and θ has a lower bound of 0° and and upper bound of 180°. The design space for the concentric circle Stewart platform design variables are defined as:

Table 5.5: *CC Design space.*

LB		λ_{CC}		UB	unit
0	$\leq$	ϕ	$\leq$	180	[°]
0	$\leq$	θ	$\leq$	180	[°]
1.25	$\leq$	r_b	$\leq$	3.5	[m]
0.3	$\leq$	Δr_b	$\leq$	3.2	[m]
1.25	$\leq$	r_p	$\leq$	3.5	[m]
0.3	$\leq$	Δr_p	$\leq$	3.2	[m]
3	$\leq$	h	$\leq$	7	[m]

5.5 Penalty Functions

The constrained design space for both the SC design and CC design, described in Section 5.4, ensures that the optimization algorithm finds feasible design variables concerning the physical size of the Stewart platform and distance between mounting points for the actuators. However, the constrained design spaces does not eliminate design configurations where non-feasible actuator length proportions are required, i.e. the actuators are impossible to produce physically because of the ratio between maximum and minimum actuator length. Neither does the constrained design space for the CC design account for the possibility of actuators colliding while moving within the prescribed workspace. To solve this problem penalty functions are used.

The idea is to expand the objective function from the its original form $\Phi(q_i,\lambda)$ to also contain a penalty function $P(q_i,\lambda)$ that inhibits either non-feasible actuator lengths or the actuators from colliding. The new objective function then yields:

$$\Phi_P(q_i,\lambda_i,r) = \Phi(q_i,\lambda) + P(q_i,\lambda)r \tag{5.11}$$

The factor r is an adjustment weight parameter that can be adjusted to control the magnitude of the penalty value, making violations more or less expensive. The objective of a penalty function is to penalize designs that are undesirable in order to focus the optimization process towards more desirable solutions. The purpose of geometrical constraints and the penalty functions are basically the same; that is to obtain real feasible solutions to the optimization problem. This section describes the penalty functions made to ensure feasible actuator length proportions for both the SC and CC design and to avoid actuator collision in the CC design. Note that the penalty functions used are soft constraints, meaning violations are possible however expensive in the objective function.

5.5.1 Actuator Penalty

The penalty function for the actuator length ratio is derived to prevent the optimization algorithm from choosing a design that require actuators where the ratio between the maximum and minimum lengths are impossible to recreate with a hydraulic cylinder, i.e. the stroke length is larger than the minimum required length. The ratio between the minimum and maximum actuator length for a given design is defined in Eq. (5.12), where a margin of 18 % is chosen to account for the difference between the minimum and stroke length of the cylinder.

$$L_{ratio,i} = \frac{L_{min,i}}{L_{max,i}} \geq 0.55 \qquad \text{for } i = 1..6 \tag{5.12}$$

To fullfil this criteria a penalty function P_{act} is derived. The penalty function value is zero or close to zero for feasible designs, i.e. $L_{ratio} \geq 0.55$, and goes to infinity for non-feasible designs, i.e. $L_{ratio} < 0.55$. The penalty function is defined in Eq. (5.13) and plotted in Fig. 5.6. Note that L_{ratio} is calculated for each cylinder separately, but that P_{cyl} only accounts for the smallest of these, $L_{ratio,min}$.

$$P_{cyl}(q_i, \lambda) = 1.079 \cdot 10^9 e^{-42.45 L_{ratio,min}(q_i,\lambda)} \tag{5.13}$$

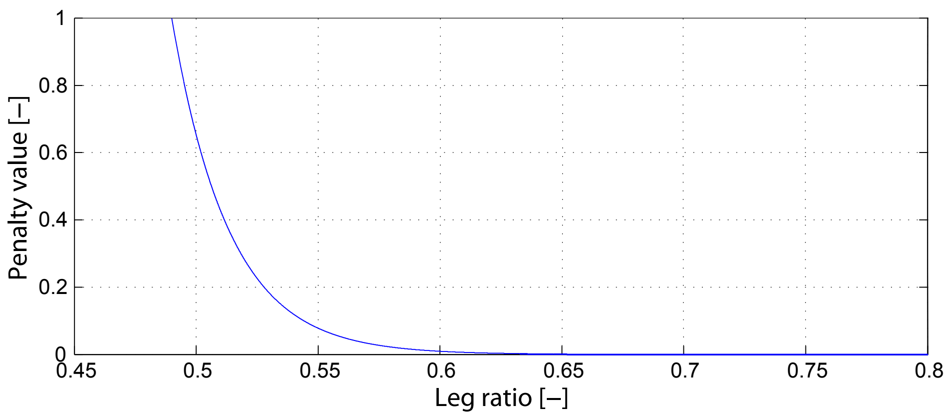

Figure 5.6: *Penalty function for actuator lengths.*

5.5.2 Leg Collision Penalty

A major concern in any kinematic design process is to avoid collisions of moving parts within the mechanism. In the single circle design the actuators cannot collide due to the even angular spacing of the actuators on one circular path. Opposed to this, the actuators in the concentric circle design may collide because the design allows them to cross each other. In order to design a feasible concentric circle design the distance between the legs must be incorporated in the solution process.

It is complex to define geometrical constraints of the type formulated in Section 5.4 that inhibit the kinematics of the optimized design from colliding the actuators. To calculate the shortest euclidean distance d_{leg} between the actuators, Eq. (5.14) is used. This distance is calculated to determine whether collision will occur in the designs.

$$d_{leg,j}(q_i,\lambda) = \frac{\left|\overrightarrow{B_jB_{j+1}} \cdot \overrightarrow{(e_j \times e_{j+1})}\right|}{\left\|\overrightarrow{e_j \times e_{j+1}}\right\|} \qquad for \ \ j = 1..6 \tag{5.14}$$

where B_j and B_{j+1} are the positions where the actuators j and $j+1$ are mounted on the base plate and e_j and e_{j+1} are the corresponding directions of the actuators. The distance $d_{leg,j}$ must be larger than the outer diameter of the actuators. To ensure that the distance is greater than the outer diameter of the actuators, the following penalty function is added to the objective function.

$$P_{col}(q_i,\lambda) = 26500e^{-42.44 d_{leg}(q_i,\lambda)} \tag{5.15}$$

The penalty function is plotted in Fig. 5.7. In order to ensure adequate space for the actuators, the minimum distance must be in excess of 0.3 meters in all poses within the workspace. As seen in Fig. 5.7 the penalty value P increases exponentially when the leg distance is below 0.3 meters. This property make designs with leg distances below 0.3 meters very expensive in the objective function and are thereby actively avoided.

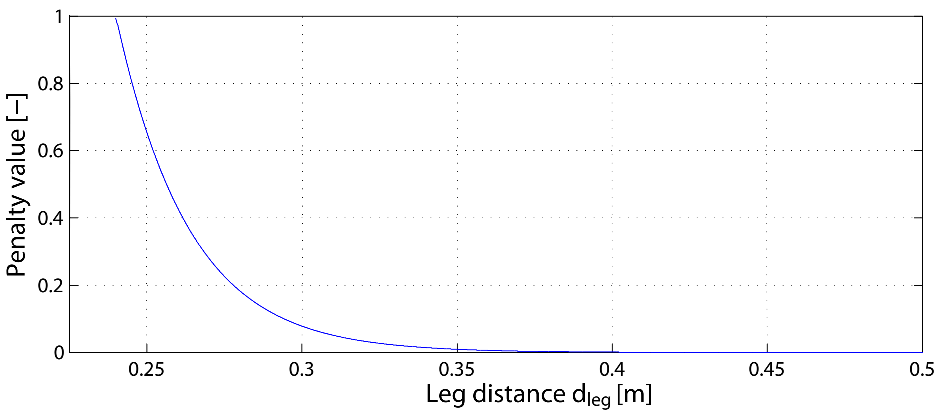

Figure 5.7: *Penalty function for leg distance.*

5.6 Formulation of Optimization Problem

In this section the formulation of the optimization problem is described. The multi objective optimization function is presented and a brief introduction to the optimization algorithm is included in this section. The overall outline of the optimization process is documented in a flow chart along with explanations.

5.6.1 Multiobjective Cost Function

In this section the objective function is derived and explained. The objective function in a minimization problem which is also called a cost function. The multiobjective optimization method used in this thesis is the weighted sum method, which according to Arora [22] is the most commonly used method. Mathematically the multiobjective cost function is formulated using the weighted sum method and is given by:

$$\Phi = \sum_{i=1}^{k} w_i f_i(x) \tag{5.16}$$

Optimization with regard to multiple objectives often require normalization of the individual objective functions to obtain similar order of magnitudes. Normalization of the objective functions make comparison of the results between different weightings possible provided the sum of weights equal 1. This is especially true if the magnitudes and units of the individual objective functions deviate significantly. In the optimization of the Stewart platform intended for wave compensation the relevant objectives are dexterity (GCI) and manipulability (GMI), see 5.2. The weighted sum method is therefore used as it is desired to optimize the two objectives GCI and GMI simultaneously. As the magnitudes of these performance indices are similar, normalization is not needed [22].

The multi objective optimization functions for single circle design and concentric circle design are different due to the possibility of leg interference in the concentric design configuration, see Section 5.5.2. To ensure feasibility of the concentric circle design the possibility of leg interference is eliminated by the penalty function Eq. (5.15) described in Section 5.5.2.

In order to ensure a feasible design for both design configurations, it is paramount that it is physically possible to design hydraulic cylinders capable of obtaining the maximum and minimum leg length required by the Stewart platform to work within the prescribed workspace. This design objective is obtained by the penalty function in Eq. (5.13) described in Section 5.5.1. The single circle objective function, including the penalty function, is given as:

$$\Phi_{SC} = \frac{1}{GCI} \cdot w + \frac{1}{GMI} \cdot (1-w) + P_{cyl} \cdot r_{SC1} \tag{5.17}$$

and the objective function for the concentric circle design including both penalty functions is derived to be:

$$\Phi_{CC} = \frac{1}{GCI} \cdot w + \frac{1}{GMI} \cdot (1-w) + P_{cyl} \cdot r_{CC1} + P_{col} \cdot r_{CC2} \tag{5.18}$$

Note that the objective functions are minimized and thus *GCI* and *GMI* are inverted in the functions to maximize their value. In the objective functions w is the weight factor and r_{SC1}, r_{CC1} and r_{CC2} are the penalty adjustment factors which can be used to increase the penalty value. The weight factors reflect the relative importance of the objectives. The penalty adjustment factor for the single circle design objective function r_1 is also set to 1 as this value yields acceptable results. Good results are obtained for the concentric circle design when the penalty adjustment factor r_{CC1} is set to 0.7 to decrease the magnitude of P_{cyl} and r_{CC2} is set to 1.

5.6.2 Optimization Algorithm

In this section the optimization method used to solve the objective function is briefly described. The algorithm used for the optimization is the Sequential Quadratic Programming (SQP) method. SQP is one of the most powerful algorithms to solve smooth constrained nonlinear optimization methods and is used in academia and industry to solve highly complex problems [23]. The section is inspired by Arora [22].

SQP is an iterative method that utilize a line search approach to obtain optimum of the objective function. The iterative procedure is given by:

$$\lambda_{(i+1,j)} = \lambda_{(i)} + t_j d_{(i)} \tag{5.19}$$

where i is the iteration number, λ_i is the current design, t_j is the step size and d_i is the search direction. In iteration $i+1$ the design is optimized by calculating the search direction d_i from design λ_i and adjusting the step size j until the descent condition is satisfied. The design in iteration $i+1$ is then defined as the sum of these. The search direction d_i is calculated using a quadratic subproblem which is strictly convex and thus have a unique solution from an arbitrary point, making the SQP method robust. The subproblem is obtained by linearizing the constraints and approximating the Lagrangian function quadratically. The quadratic subproblem is given by following equation:

$$minimize \quad \bar{f} = c^T d + \frac{1}{2} d^T H d \tag{5.20}$$

subject to linearized constraints:

$$\begin{aligned} N^T d &= e \\ A^T d &\leq b \end{aligned} \tag{5.21}$$

In Eq. (5.20) c^T is the gradient of the objective function f, d is the search direction and H is the approximation of the Hessian matrix. The rate of convergence is improved as second order information about the problem is incorporated into the solution process, however the approximation of Hessian require some computational effort.

5.6.3 Optimization Flow

To describe the optimization as a whole a flowchart of the optimization procedure is shown in Fig. 5.8. In the flowchart every box is enumerated and a corresponding explanation is given below.

1. In the first iteration (iteration 0) the design is created from the initial guess λ_0. The initial guess is used as a starting point from where the optimization algorithm starts the search procedure as described in Section 5.6.2. After the first iteration a new better design λ_i is used and in this manner the design is continuously improved.

2. The performance indices are dependent on the pose of the Stewart platform. To discretize the prescribed workspace into a finite number of poses, 2000 random uniformly distributed poses are generated. The poses are only generated once and are reused for all iterations. 2000 poses are chosen as this produce results that only deviate approximately 0.25% from the exact solution, see Section 5.1.

3. The design variables in vector λ_i is used to generate the kinematic design, using the design equations for single and concentric circle design in Section 5.4.1 and 5.4.2 respectively and Section 4.1.1. The Jacobian matrix is derived from the kinematic equations.

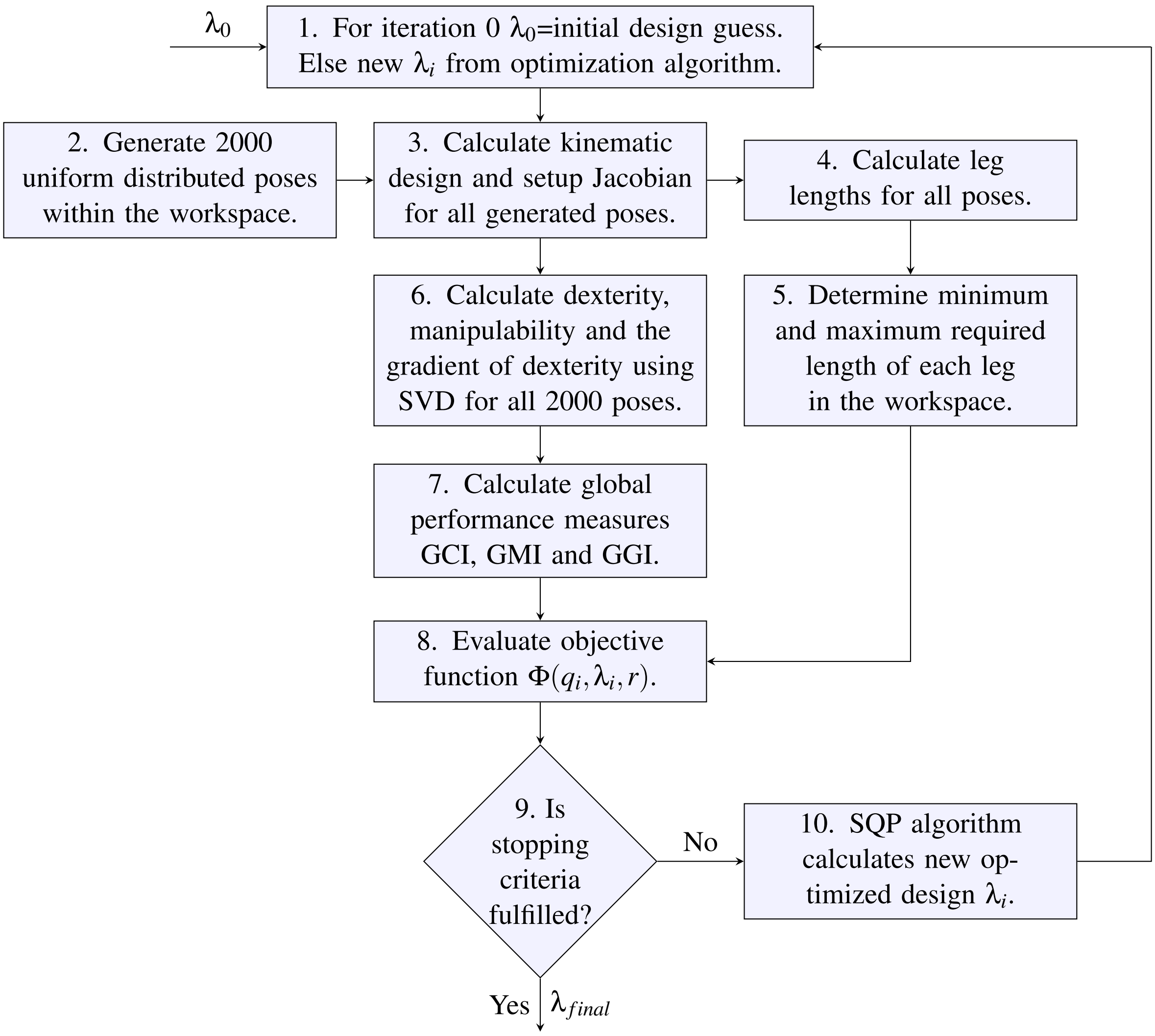

Figure 5.8: *Flowchart for the kinematic design optimization procedure.*

4. The leg lengths are calculated for each leg in all 2000 poses, representing the required leg lengths to cover the whole workspace.

5. In order to determine whether the actuators can physically be designed for the design λ_i, the absolute maximum and minimum length of all individual legs is determined within the workspace. The absolute maximum and minimum lengths are inputs to the penalty term P_{cyl} of the objective function, see Section 5.5.1.

6. Singular value decomposition is used to determine the singular values of the Jacobian matrix, cf. Section 4.2.1. The dexterity, manipulability and the dexterity gradient of all 2000 poses is calculated.

7. The dexterity, manipulability and dexterity gradients are averaged for all 2000 poses, i.e. the entire workspace, to obtain the global measures GCI, GMI and GGI, which are the performance indices to be optimized.

8. The performance indices (point 7) and the minimum and maximum length of the legs are inputs to the objective function. For the concentric circle design the leg collision penalty function P_{col} is also an input to the objective function. This is not shown in Fig. 5.8 but is done parallel to points 4 and 5. The objective function is evaluated to determine the objective function value.

9. If the change of objective function value from one iteration to the next is below $1 \cdot 10^{-4}$ the stopping criteria satisfied and the optimization algorithm is terminated and the final result λ_{final} is printed. If not the algorithm continues to point 10.

10. The SQP algorithm searches for an improved design λ_{i+1}, that is send to point 1 in order for the next iteration $i+1$ to begin.

5.7 Results of the Kinematic Optimization

In this section the results of the kinematic optimization is presented. The optimizations are made with regard to the Global Conditioning Index (GCI) and the Global Manipulability Index (GMI) of both the single and concentric circle Stewart platform design. Graphical presentations of the optimum kinematic designs are shown along with the results of respective performance indices.

5.7.1 Single Circle Design

The optimization is performed using different weights in the multi objective cost function (5.7.1). For the sake of convenience the multi objective cost function is repeated here:

$$\Phi_{SC} = \frac{1}{GCI} \cdot w + \frac{1}{GMI} \cdot (1-w) + P_{cyl} \cdot r_{SC1}$$

From the equation it can be seen that a weight w equal to 0 yields an optimization problem only dependent on the *GMI* and likewise if the weight equal 1 the optimization problem is only dependent on the *GCI*. Weights between 0 and 1 reflects the relative importance of both design objectives (*GMI* and *GCI*). Optimizations with weights ranging from 0 to 1 with 0.1 increments are performed and the results are listed in Table 5.6.

The optimization objectives are plotted as a Pareto front in Fig. 5.10. As seen in the figure the *GCI* and *GMI* are conflicting objectives and a comprise must be made between them. In Table 5.6 it can be seen that the height h is decreased as the weight w favors *GCI*. A lower height is desirable as low designs require less deck space and shorter actuators where full stroke capacity is used. Whereas in designs where the weight favors *GMI* the Stewart platform becomes taller, the cylinders longer and the stroke capability is unutilized, as the ratio between minimum and maximum length are large. Additionally the shear size due the height of these designs render these design solutions undesirable compared to shorter designs.

Selecting designs that favor *GCI* results in designs with less manipulability resulting in larger actuator velocities. It can be shown that maximizing the GMI increases the relative velocity transmission in the x- and y-directions at the expense of the relative velocity transmission in the z-direction. This can be seen in Fig. 5.9 where Fig. 5.9a show a design where the legs are perpendicular to the xy-plane and

Table 5.6: Single circle optimization results

Weight	ϕ_b	ϕ_p	r_b	r_p	h	l_{min}	l_{max}	GCI	GMI	GGI
0.0	9	9*	2.00*	2.00*	7.00*	5.44	8.60	3.03e-4	1.45e8	2.5433
0.1	5*	75	2.28	2.07	7.00*	5.53	8.74	0.1304	3.3399	0.1458
0.2	5*	75	2.84	2.58	7.00*	5.51	8.89	0.1631	1.7916	0.1447
0.3	5*	111*	2.35	2.00*	6.80	5.43	8.73	0.1913	1.1686	0.1478
0.4	5*	111*	2.61	2.00*	6.61	5.30	8.59	0.2195	0.8231	0.1523
0.5	5*	111*	2.90	2.00*	6.40	5.18	8.45	0.2516	0.5916	0.1573
0.6	5*	111*	3.25	2.00*	6.13	5.05	8.29	0.2936	0.4186	0.1641
0.7	5*	111*	3.50*	2.02	5.40	4.51	7.70	0.3568	0.2870	0.1857
0.8	5*	111*	3.50*	2.00*	4.54	3.80	6.92	0.4220	0.2221	0.2200
0.9	5*	111*	3.50*	2.00*	4.71	3.93	7.07	0.4076	0.2329	0.2126
1.0	5*	111*	3.50*	2.00*	4.48	3.75	6.87	0.4277	0.2183	0.2228

* Active constraint

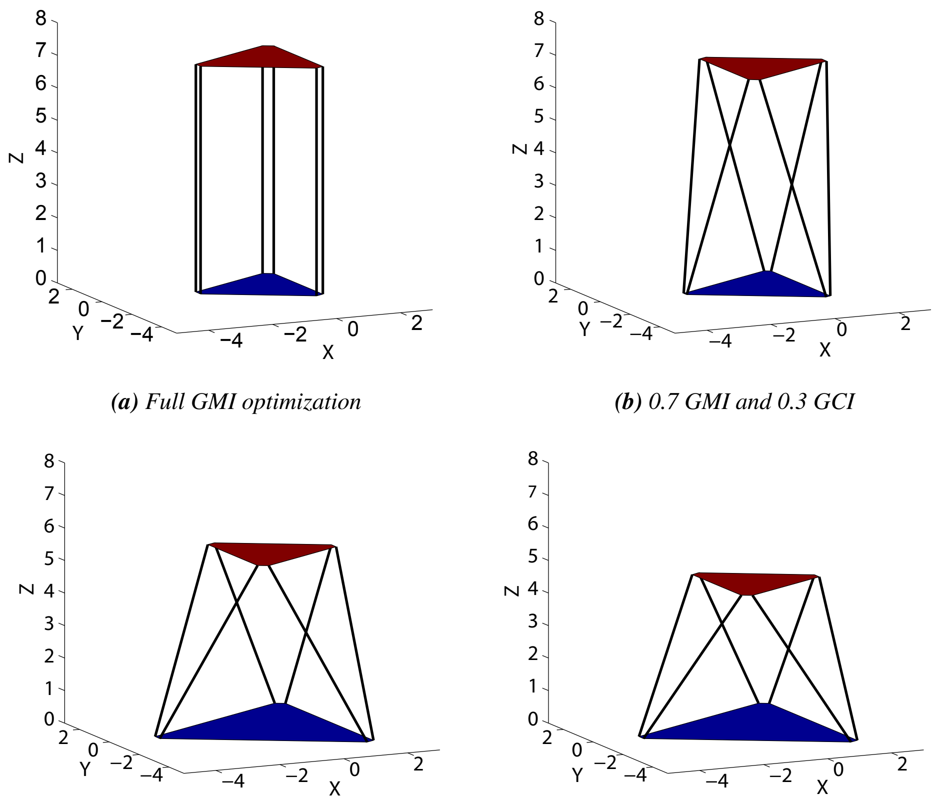

***(a)** Full GMI optimization*

***(b)** 0.7 GMI and 0.3 GCI*

***(c)** 0.3 GMI and 0.7 GCI*

***(d)** Full GCI optimization*

***Figure 5.9:** Results for weights 0.0, 0.3, 0.7, 1.0*

as tall as possible (constraint on h is 7 m). In this design small actuation velocities can generate fast tool center point velocities in the x- and y-directions relative to the z-direction. As more weight on *GCI* is introduced (Fig. 5.9b through 5.9d) the designs become more conical where the actuators are angled towards the xy-plane. This decrease the relative velocity transmission in the x- and y-direction and increase the transmission in the z-direction. This is expected as the *GCI* is improved which means force/velocity transmission is equalized.

Because the prescribed workspace is tall (z-direction) and relatively narrow (x- and y-direction) the best design must primarily generate tool center point velocities in the z-direction as the velocity transmission is most significant in the z-direction. According to the above discussion the best solution is the one with full emphasis on GCI (w=1.0). This solution is chosen as it ensures that forces can be generated in all directions within the wave compensation workspace (high *GCI*) and as the low *GMI* increase the velocity transmission capability in the z-direction compared to designs with larger *GMI*. For this reason the best single circle design for the wave compensation application is assessed to be the design with full emphasis on GCI (w=1.0). If the prescribed workspace were more uniform, designs with more emphasis on GMI would have been of significance in terms of reducing actuation velocities.

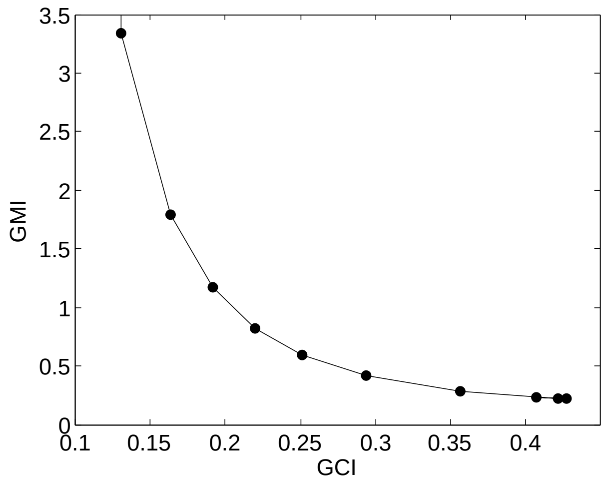

Figure 5.10: *Pareto front for GCI vs. GMI for single circle design.*

The design space bounds and the initial guess λ_0 for the best design and the final design variables λ_{final} are listed in Table 5.7. The initial guess for the optimization is required to initiate the optimization algorithm, and hence the final solution descents from this design. The scaled HYDAC Stewart platform design described in Section 5.3, see Fig. 5.11, is used as initial guess for the optimization.

Table 5.7: *Design space bounds, initial and final design of single circle configuration.*

Design variable	LB	UB	λ_0	λ_{final}	unit
ϕ_b	5	115	35	5*	[°]
ϕ_p	9	111	85	111*	[°]
r_b	2	3.5	2.5	3.50*	[m]
r_p	2	3.5	2.5	2.00*	[m]
h	3	7	4.2	4.48	[m]

* Active constraint

In the Table 5.7 it can be seen that the final design variables are not violating the lower and upper bound of the constraints, but that the constraints are active for ϕ_b, ϕ_p, r_b and ϕ_p as indicated with the asterisk. The final optimum kinematic design of the single circle Stewart platform is shown in Fig. 5.12.

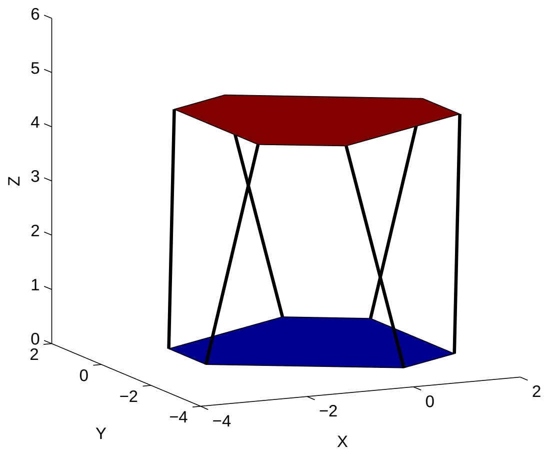

Figure 5.11: *Initial design λ_0 by HYDAC (scaled x5).*

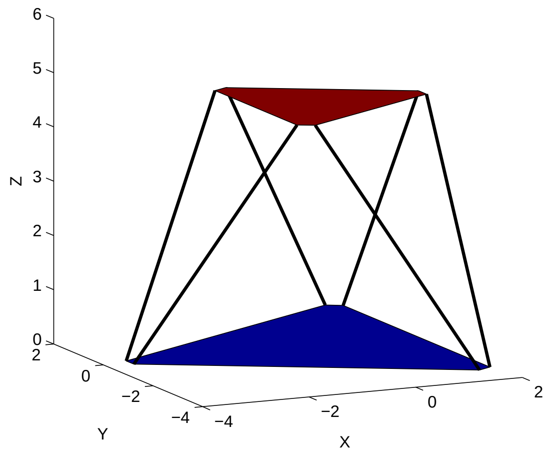

Figure 5.12: *Optimum kinematic configuration λ_{final} of single circle design.*

Comparing Fig. 5.11, Fig. 5.12 and the corresponding values in Table 5.7 the changes from the initial to the final design is seen. It can be seen that the spacing angles of the optimum design are 5° on the base and 111° on the platform and these angles position the mounting points as close as possible. This is in contrast to the initial design where the angles are 35° and 85°. In the initial design both base and platform have the same diameter, whereas the base and the platform in the optimum design is increased and decreased in diameter respectively. The base radius r_b reaches the upper bound of the design space and r_p decreases. In the optimum design the ratio between base and platform diameter is 0.6 whereas the ratio in the initial design is 1.

Designs with small leg separation angles and small platform diameters relative to the base, aligns the actuators closer to the xy-plane which increase force capability in the x- and y-directions relative to the z-direction and hence equalize these and increase the GCI.

The final design in Fig. 5.12 is reached because the leg spacing angles and platform diameters yield the most isotropic design that is possible for the given workspace and geometrical constraints according to 4.2.5, i.e. the force and velocity capabilities in all translational and rotational directions are as equal as possible.

Several different values of the initial guess has been tried in order to confirm that the SQP algorithm is not stock in a local minimum. All tried different initial guesses yields the same result confirming that the solution most likely is the global optimum. The SQP algorithm converged in 13 iterations as shown in the descent curve depicted in Fig. 5.13. The quick and robust convergence confirms that the SQP algorithm is a powerful optimization tool, see Section 5.6.2.

To confirm that the actuator penalty function P_{cyl}, cf. Section 5.5.1, is effective in ensuring that it is possible to recreate the legs as hydraulic actuators, the minimum and maximum required leg lengths for the entire workspace is tabulated in Table 5.8. As defined in Section 5.5.1 feasible hydraulic cylinders must have a ratio of at least 0.55 between the minimum and maximum length.

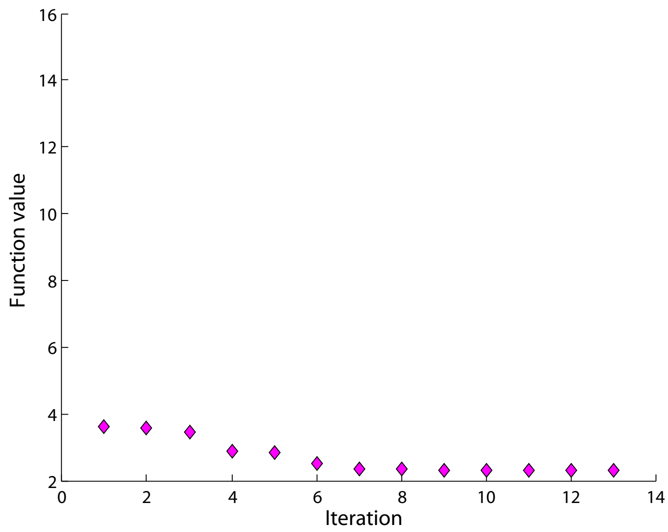

Figure 5.13: *Descent curve for single circle design optimization.*

Table 5.8: *Actuator length data for* λ_{final}.

	L_{min} [m]	L_{max} [m]	L_{stroke} [m]	L_{ratio}
cyl_1	3.89	6.69	2.80	0.58
cyl_2	3.75	6.87	3.11	0.55
cyl_3	3.75	6.86	3.11	0.55
cyl_4	3.75	6.86	3.11	0.55
cyl_5	3.75	6.87	3.11	0.55
cyl_6	3.89	6.69	2.80	0.58

5.7.2 Concentric Circle Design

The optimization of the concentric design is like the single circle design performed with different weights in the multi objective objective function. The objective function is repeated here for the sake of convenience:

$$\Phi_{CC} = \frac{1}{GCI} \cdot w + \frac{1}{GMI} \cdot (1-w) + P_{cyl} \cdot r_{CC1} + P_{col} \cdot r_{CC2}$$

The functionality of the weight are identical to the single circle optimization. The results of the optimization is listed in Table 5.9 where the weight also range from 0 to 1 with 0.1 increments.

Evaluating the results listed in Table 5.9 yields the same observations as for the single circle design. The Pareto front, Fig. 5.14 also show that the design objectives are conflicting and a comprise must be made between the performance indices. Again the height of the platform decrease as the weight favors GCI and the shape becomes more conical which increase force capacity in the x- and y-directions relative to the z-directions. The best solution for the wave compensation application is once again the design with full emphasis on GCI (w=1) due to the small height and velocity capacity in the z-direction.

The optimization parameters for the concentric circle design are summed up in Table 5.10, i.e. the design space bounds (LB and UB), the initial guess λ_0 and the optimum design configuration λ_{final}.

Table 5.9: *Concentric circle optimization results*

Weight	θ	ϕ	r_b	Δr_b	r_p	Δr_p	h	l_{min}	l_{max}	GCI	GMI	GGI
0.0	0	7	1.92	1.26	2.00*	1.33	7.00*	5.46	8.58	0.0023	1.55e5	0.2677
0.1	44	160	2.06	0.74	3.48	0.88	7.00*	5.57	9.61	0.1448	3.7677	0.1241
0.2	49	161	2.47	0.75	3.08	0.40	7.00*	5.64	9.84	0.1807	2.0326	0.1225
0.3	52	162	2.84	0.75	2.80	0.30*	7.00*	5.70	9.92	0.2117	1.3162	0.1202
0.4	52	163	3.24	0.75	2.71	0.30*	7.00*	5.81	10.06	0.2420	0.9263	0.1163
0.5	51	159	3.50*	0.74	2.54	0.30*	7.00*	5.87	10.09	0.2698	0.6983	0.1169
0.6	47	152	3.50*	0.70	2.00*	0.30*	6.47	5.42	9.28	0.3070	0.5044	0.1326
0.7	40	140	3.50*	0.66	2.00*	0.30*	6.15	5.03	8.97	0.3364	0.4097	0.1447
0.8	65	81	3.50*	0.55	2.00*	0.32	4.15	3.85	6.74	0.4693	0.1929	0.1585
0.9	62	78	3.50*	0.56	2.00*	0.32	3.80	3.55	6.40	0.4884	0.1832	0.1373
1.0	61	77	3.50*	0.57	2.00*	0.32	3.64	3.42	6.24	0.4946	0.1800	0.1256

* Active constraint

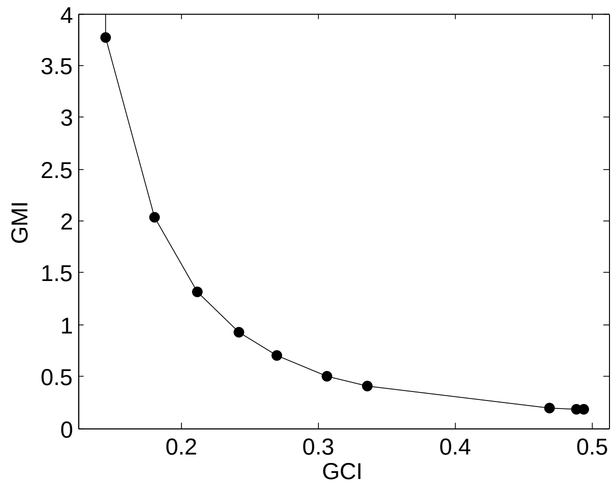

Figure 5.14: *Pareto front for GCI vs. GMI for concentric circle design.*

Table 5.10: *Design space bound, initial and final design of concentric circle configuration.*

Design variable	LB	UB	λ_0	λ_{final}	unit
θ	0	180	40	61	[°]
ϕ	0	180	90	77	[°]
r_b	2.00	3.50	2.50	3.50*	[m]
Δr_b	0.30	3.20	0.60	0.57	[m]
r_p	2.00	3.50	2.50	2.00*	[m]
Δr_p	0.30	3.20	0.60	0.32	[m]
h	3.00	7	6	3.64	[m]

* Active constraint

The constraints on the optimization problem are active on the optimum design for the base radius r_b and the platform radii defined by r_p and Δr_p as indicated by the asterisk. The optimum design of the

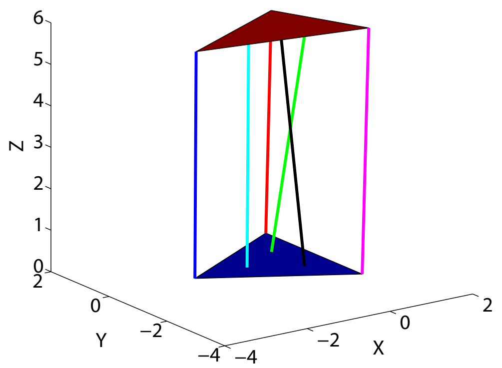

***(a)** Full GMI optimization.*

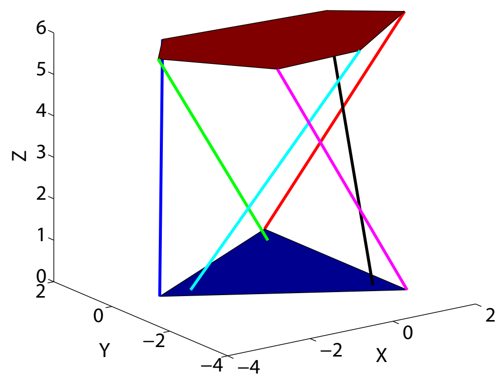

***(b)** 0.7 GMI and 0.3 GCI.*

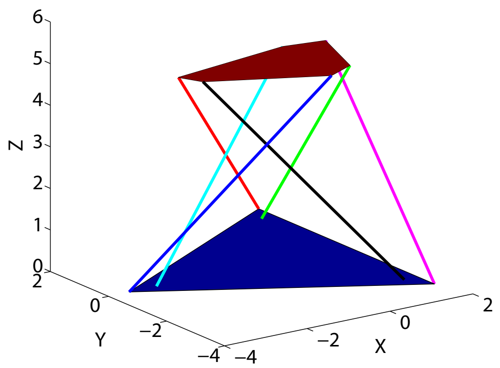

***(c)** 0.3 GMI and 0.7 GCI.*

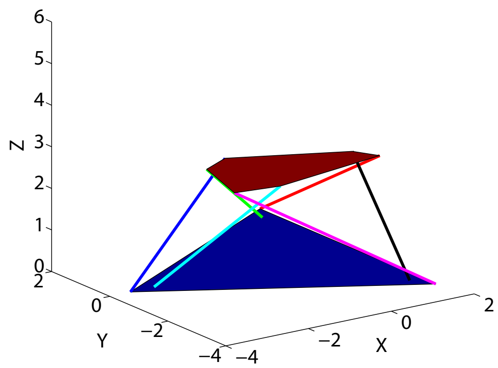

***(d)** Full GCI optimization.*

***Figure 5.15:** Results for weights 0.0, 0.3, 0.7, 1.0*

concentric circle Stewart platform is seen in Fig. 5.15d. Figure 5.15d and Table 5.10 shows that the ratio between base and platform diameters are as large as possible, as the lower constraint on the platform and the upper constraint on the base are active. Optimizations without the penalty function P_{col} (penalty function to preventing leg collision) have shown that Δr_b in the optimum design are restricted by the penalty, i.e. Δr_b activates the lower bound of its constraint, if the penalty function is omitted. Figure 5.15d also show that the legs are allowed to cross which is a characteristic for the concentric design. Similar optimized results with leg crossing are achieved by Stoughton and Arai [8].

The optimization converged in 17 iterations where the largest decrease in cost function value is obtained in the first 6 iterations. In the remaining iterations only minor decreases in the cost function are obtained. Table 5.11 confirms that the final design λ_{final} is feasible, as the requirements of leg length ratio L_{ratio} of at least 0.55 is fulfilled and the distance between the legs are at least 0.3 m. This indicate that both penalty terms are actively ensuring that the hydraulic actuators are produceable and that the actuators does not collide when working within the workspace.

Table 5.11: *Cylinder- and stroke lengths.*

	L_{min} [m]	L_{max} [m]	L_{stroke} [m]	L_{ratio}	L_{dist} [m]
cyl_1	3.50	6.09	2.59	0.57	0.34
cyl_2	3.51	6.10	2.59	0.57	0.36
cyl_3	3.42	6.24	2.82	0.55	0.34
cyl_4	3.43	6.18	2.75	0.56	0.34
cyl_5	3.46	6.18	2.72	0.56	0.36
cyl_6	3.42	6.12	2.70	0.56	0.36

5.8 Conclusion of the Kinematic Optimization

In this section the kinematic performance of the single circle design and concentric circle design is compared to select the best solution for the wave compensation application. The performance of the HYDAC Stewart platform is included to establish a frame of reference as the HYDAC platform is not optimized. The kinematic performance indices for the different designs are listed in Table 5.12.

Table 5.12: *Performance indices for HYDAC, SC. and CC. Stewart platforms.*

Performance index	HYDAC	SC	CC
Global Conditioning Index (GCI)	0.1739	0.4277	0.4946
Global Manipulability Index (GMI)	1.5571	0.2183	0.1800

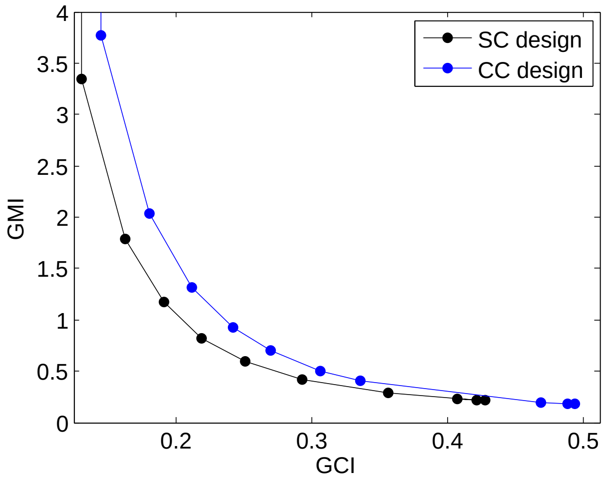

Figure 5.16: *Pareto front comparison.*

As mentioned earlier the GMI is not an significant performance indices for wave compensation due to the shape of the prescribed workspace. The results listed in Table 5.12 indicate that the the best design are the concentric circle design configuration. The GCI is improved 13.5% from the best single circle design to the best concentric circle design.

This is in contrast to the results obtained by Stoughton [8], who found that a 30 % improvement in GCI over a fixed centrally placed workspace, which dimensions are not specified, could be achieved using the concentric circle design compared to the single circle design. However, Stoughton does not account properly for the possibility of leg collision, as he only accounts for collision in the mounting points of the legs and not for collision of crossing actuators. The 30 % GCI improvement achieved by Stoughton is most likely obtained because his workpace is considerately smaller in relation to the manipulator, than the wave compensation workspace is and because of his insufficient avoidance of leg collision. Despite of this the concentric circle design is superior to the single circle design in the given application of wave compensation and the following chapter focus on development of the actuation system for this design.

In Fig. 5.16 the pareto front of both the SC and CC design is plotted together for comparison, which reveals that the CC pareto front is above the SC pareto front. This means greater manipulability is obtained using the CC design rather than the SC design provided that the dexterity must be equal.

CHAPTER 6

HYDRAULIC SYSTEM DESIGN

In this chapter a hydraulic system is designed that fits the optimum kinematic CC Stewart platform configuration, found in Chapter 5. In order to design a hydraulic system for the wave compensating Stewart platform, several factors should be taken into consideration. The hydraulic system must be able to operate at the most extreme load case, i.e in sea state 5 and with maximum load in order to comply with the demand regarding 95% workability, cf. 2.5. To design the hydraulic system for the Stewart platform to operate in sea state 5, it is required to determine the actuation forces, velocities and power accurately.

As the forces, velocities and power in the system are dependent on a combination of several non-linear equations, determining the conditions yielding the maximum forces, velocities and power are not intuitively straightforward. In this chapter the optimization algorithm described in Section 5.6.2 are used to accurately calculate the maximum values of these to determine the specifications of the most suitable hydraulic components for the system. To support the understanding of each optimization, a corresponding flowchart is included at the end of the section describing the optimization.

6.1 Overview and Synthesis of the Hydraulic System

To actuate the Stewart platform an electro-hydraulic position control servo system is chosen. The purpose of the system is to track a position reference that is opposite to that of the ship motion. The system consists of following components:

1. A constant pressure source - pump.
2. Hydraulic differential cylinders.
3. Servo valves with spool matched to the differential cylinders.
4. Position sensor.

5. A controller.

6. Hydraulic lines between valve and actuator.

7. Mechanical system - the Stewart platform.

The hydraulic system for the Stewart platform is illustrated in Fig. 6.1. Note the system is only illustrated for one of the hydraulic cylinders with one pump. The number and type of pumps in the complete system is not specified in this thesis and the pump pressure is considered constant. The pressure level of this system is chosen to be 300 bar. This is relatively large, but is chosen to limit the system flows as the actuation system has a large flow demand.

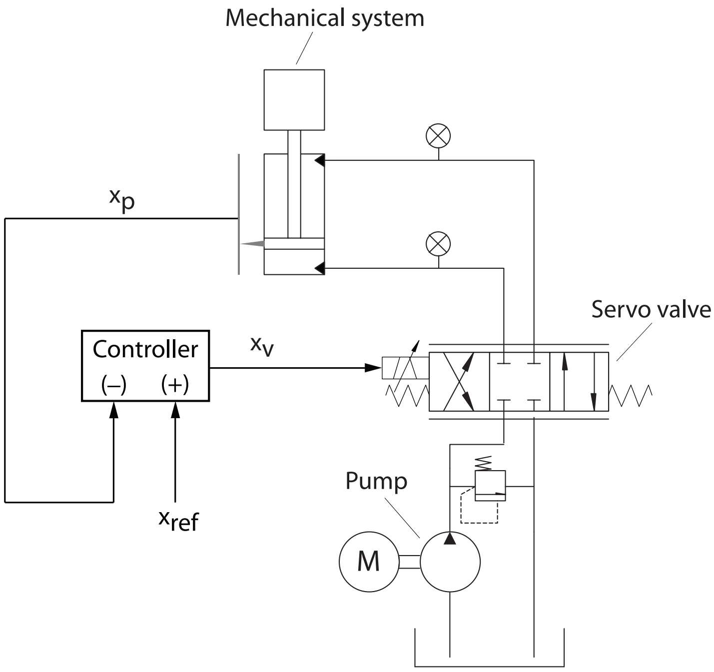

Figure 6.1: *Hydraulic System Layout.*

In order to dimension the hydraulic system the following steps are performed in this chapter:

1. Determine the Stewart platform operation cycle to determine the actuation forces and velocities required for the wave compensation application.

2. Determine the cylinder dimensions from the actuation forces and velocities in order to match the forces required.

3. Determine the system flows using the actuation velocities and the cylinder dimensions.

4. Determine the maximum power requirement in order to select a sufficient drive motor

5. Size volume of the hydraulic lines between the pump and valve to be as small as possible to maintain a high effective stiffness of the hydraulic fluid.

6.2 Motion and Load Modelling

In this section the motion (velocity and acceleration) of and load on the tool center point (TCP) of the Stewart platform is determined. The TCP loads and velocities are then used to calculate the forces and velocities of the Stewart platform actuators.

6.2.1 Motion Modeling

To counteract the wave induced ship motion, the Stewart platform must operate with the opposite motion pattern as the crane ship to keep the platform plate steady in space. As the exact motion pattern is dependent on the many different factors, as described in Section 3, and as exact wave and RAO data are not available, assumptions are made regarding the ship motion. To make a conservative estimation of the motion pattern, the motions in all directions are assumed to have maximum amplitude and equal frequency within the prescribed workspace. These assumptions are conservative as the motion of a ship operating at sea most likely would have different amplitudes and frequencies, as the direction of the ship in relation to the wave direction, influence the relation between the individual amplitudes and frequencies of all 6 DOF. For loading operations of a ship at sea, the bow (front) of the ship would most likely face the waves, damping the roll of the ship in relation to the pitch and heave, see Section 3.2.

In this thesis the ship motion is approximated by sinusoidal waveforms with the magnitudes of the workspace specifications given in Table 5.1 and in order to include some arbitrariness to the ship motion a phase is added to each dof. The motion point q in relation to the base is expressed as:

$$q(t) = \begin{bmatrix} x \\ y \\ z \\ \alpha \\ \beta \\ \gamma \end{bmatrix} = \begin{bmatrix} 0.23sin(\omega t + \xi(1)) \\ 0.48sin(\omega t + \xi(2)) \\ h + 1.22sin(\omega t + \xi(3)) \\ 0^\circ \\ 3^\circ sin(\omega t + \xi(4)) \\ 10^\circ sin(\omega t + \xi(5)) \end{bmatrix} \quad \text{where} \quad \xi(i) \in [0; 2\pi] \text{ for } i = 1..5 \tag{6.1}$$

where ξ is the phase shift between the individual 6 DOFs of the ship motion and h is the neutral height of the Stewart platform. The phase shift ξ is introduced in the motion equations, as it influence the forces and velocities exerted on the Stewart platform. The phase shift is dependent on the ship type (RAO data) and wave direction in relation to the ship. I.e. if RAO and wave data is available, the motion approximation is not necessary as the data would yield accurate time series of the ship motion, see Section 3.3. The velocities $\dot{q}$ and the accelerations $\ddot{q}$ of the platform is obtained by differentiation of the motion vector q with respect to time.

6.2.2 Load Modeling

A crane is mounted on the Stewart platform in the tool center point, cf. Section 2.1. This crane and its cargo is the load on the Stewart platform and exert both static and dynamic forces on the tool center point. The static forces come from the weight of the crane and cargo, and the dynamic forces occur, because the wave excited ship motion creates accelerations of the mass and inertia. The total forces and moments τ, applied to the end-effector in the tool center point q on the Stewart platform is described by:

$$\tau = M\ddot{q} + C\dot{q} + G \tag{6.2}$$

Where M is the mass and inertia matrix, C is the non-linear Coriolis/centripetal force matrix and G is the gravitational force matrix. The non-linear Coriolis/centripetal forces are neglected from the equation, because the Stewart platform is intended to keep the crane and load steady in space, and hence no or only small velocities $\dot{q}$ occur. The total forces and moments are then expressed by:

$$\tau = M\ddot{q} + G \tag{6.3}$$

The crane installed on the Stewart platform is a HMF 2430-K6 which has a mass of 2555 kg and can lift up to 4500 kg. The ship motion specifications given in Table 5.1 on page 28, specify that the Stewart platform must counteract rotational motions (and hence accelerations) around the x- (roll) and y-axis (pitch) as well as translational motion (and accelerations) in the x- (surge), y- (sway) and z-axis (heave) directions. To calculate the dynamics forces from these accelerations the moment of inertia of the crane is approximated using the simplified crane model in Fig. 6.2.

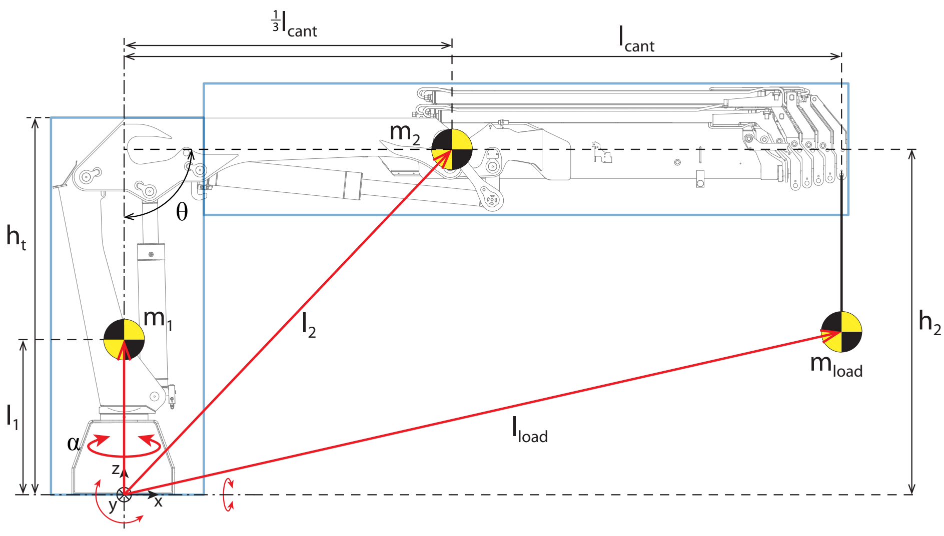

Figure 6.2: *Moment of inertia model. Crane by courtesy of HMF [24].*

In order to derive the inertia equations for the system, the mass of the crane is approximated by three point masses, one for each part of the crane as shown in Fig. 6.2. The point masses are denoted m_1, m_2 and m_{load} which are the masses of the tower, cantilever and load respectively and θ is the angle between the tower and the cantilever. The crane masses m_1 and m_2 are constant, and as a crane design and weight already include a foundation, the mass of the Stewart platform plate is assumed to be a part of this and hence neglected from the calculations. Opposed to the crane masses, the allowed magnitude of m_{load} change from extending or retracting the telescopic crane arm mechanism and/or changing the hoisting angle θ of the crane, see Fig. 6.3.

To express the largest value of m_{load} to a given length and angle of the cantilever, the load capacity of the crane is derived as 3 functions:

1. **Function 1** calculates the load capacity for region 1 (-10° $\leq \theta < 40°$) in Fig. 6.3. The load capacity is derived using an exponential interpolation between the load points for the horizontal crane position $\theta = 0$.

2. **Function 2** calculates the load capacity for region 2 ($40° \leq \theta < 60°$) in Fig. 6.3. The function is derived for the loadcapacity at $\theta = 45°$.

3. **Function 3** calculates the load capacity for region 3 ($60° \leq \theta \leq 70°$) in Fig. 6.3. This is derived from the loadcapacity at $\theta = 60$.

The functions are chosen as conservative estimates of the load capacity for the given regions as the functions are defined for the load capacity in the bottom of the regions and as the load lines in the figure curve inwards, which means that the actual load capacity decrease with increasing load angle θ.

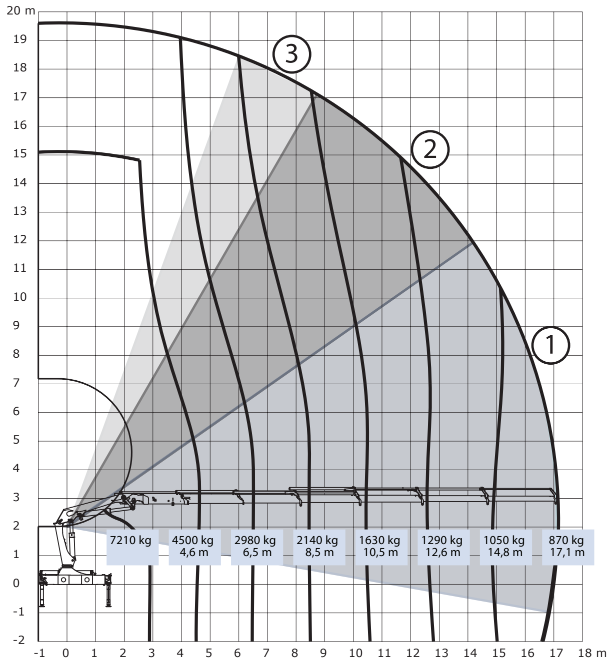

Figure 6.3: *Load curve for HMF 2430-K6 crane. By courtesy of HMF [24].*

In the simplified crane model, Fig. 6.2, the position of m_1 is stationary in relation the Stewart platform tool center point and hence the distance l_1 is fixed. Additionally l_2 and l_{load} is dependent on length of the cantilever l_{cant} and hoisting angle θ and hence the inertia are changing with changing cantilever length l_{cant} and hoisting angle θ. The lengths l_2, h_2 and l_{load} is given by Eq. (6.4), (6.5) and (6.6).

$$l_2(\theta, l_{cant}) = \sqrt{h_t^2 + (\tfrac{1}{3} l_{cant})^2 - 2h_t(\tfrac{1}{3} l_{cant}) cos(\theta)} \tag{6.4}$$

$$h_2(\theta, l_{cant}) = h_t + \tfrac{1}{3} l_{cant} sin(\theta - 90°) \tag{6.5}$$

$$l_{load}(\theta, l_{cant}) = \sqrt{(l_{cant} cos(\theta - 90°))^2 + (h_t + l_{cant} \cdot sin(\theta - 90°) - l_{wire})^2} \tag{6.6}$$

As the wave compensation does not require yaw motion the rotational inertia around the z-axis is irrelevant. The rotational inertia around x and y is given by:

$$I_x(\theta, l_{cant}) = m_1 l_1^2 + m_2 h_2^2 \tag{6.7}$$

$$I_y(\theta, l_{cant}) = m_1 l_1^2 + m_2 l_2^2 + m_{load} l_{load}^2 \tag{6.8}$$

Note the mass m_{load} does not contribute to the rotational inertia around the x-axis because the load is suspended by a flexible wire. In operation the crane is rotated α° around the z-axis and the rotational inertia around the y- and x-axis changes accordingly. To model this, the following relations are used:

$$I_{x\alpha}(\alpha, \theta, l_{cant}) = I_x cos(\alpha) + I_y sin(\alpha) \tag{6.9}$$

$$I_{y\alpha}(\alpha, \theta, l_{cant}) = I_y cos(\alpha) + I_x sin(\alpha) \tag{6.10}$$

From Eq. (6.9) and Eq. (6.10) it is seen that the inertia is a function of θ, l_{cant} and α. The total mass of the system is denoted m and hence the mass and inertia matrix M from eq. (6.3) yields:

$$M^T(\alpha, \theta, l_{cant}) = \begin{bmatrix} m & m & m & I_{x\alpha} & I_{y\alpha} & 0 \end{bmatrix}^T \tag{6.11}$$

The static force and moments G are like the inertias a function of the hoisting angle θ, the cantilever length l_{cant} and the rotation of the crane α. The gravitational force and moment matrix G is then defined in Eq. (6.12), where the moments around the x- and y-axis are also dependent of the rotation angle α of the crane, similar to the inertias in Eq. (6.9) and Eq. (6.10).

$$G(\alpha, \theta, l_{cant}) = \begin{bmatrix} F_x \\ F_y \\ F_z \\ M_x \\ M_y \\ M_z \end{bmatrix} = \begin{bmatrix} 0 \\ 0 \\ -mg \\ -g(m_{load} l_{cant} cos(\theta) + \frac{1}{3} m_2 l_{cant} cos(\theta)) sin(\alpha) \\ g(m_{load} l_{cant} cos(\theta) + \frac{1}{3} m_2 l_{cant} cos(\theta)) cos(\alpha) \\ 0 \end{bmatrix} \tag{6.12}$$

As seen from the above equations, the total forces and moments applied to the tool center point, as defined in Eq. (6.3), are dependent on four variables. The total forces and moments applied to the tool center point is hence given by vector τ:

$$\tau(\alpha, \theta, l_{cant}, \ddot{q}) = M\ddot{q} + G \tag{6.13}$$

6.3 Maximum Actuator Forces

In this section optimizations are performed to calculate the largest forces the Stewart platform will experience in sea state 5. Optimizations are performed to precisely calculate the forces in order to ensure that Stewart platform fully comply with the demand of 95% workability, see Section 2.5.

To calculate the forces applied to the actuators, the forces and moments τ on the tool center point (TCP) needs to be calculated as described in Section 6.2.2. The forces g applied to the actuators can then be calculated from the forces and moments τ, utilizing the Jacobian matrix J defined in Section 4.1.2. Thus the force vector g is given by the relation defined earlier in Eq. (4.10) and repeated here:

$$g(J,\tau) = J^T(q)^{-1}\tau(\alpha,\theta,l_{cant},\ddot{q})$$

The actuator forces g is a function of the Jacobian matrix J and the tool center point forces τ. As the forces τ, given by Eq. (6.13), is dependent on the load case and the Jacobian J is dependent on the pose, the actuator forces g are also dependent on the load case and pose. The load case is defined by the rotation of the crane α, the hoisting angle θ, the cantilever length l_{cant} and the accelerations $\ddot{q}$. Note that as the load case is a function of the accelerations, the load case is also a function of the motion defined in Section 6.2.1.

As the actuator forces accordingly are a function of multiple variables, determining the load case yielding maximum actuator force is not straightforward. Because of this, the SQP optimization algorithm described in Chapter 5 is used to determine the load case yielding maximum leg forces from Eq. (6.3) in the optimum Stewart platform design. Accordingly the load case variables are the optimization design variables, where the accelerations are substituted by a phase shift ξ for all motion directions. This substitution is made as the dynamic forces are a function of the accelerations and as the accelerations is assumed to have a constant amplitude the only change in the dynamic forces from the accelerations occur from a phase shift in the motion, see Section 6.2.1. The design variable vector λ for the force optimization is then given by:

$$\lambda = \begin{bmatrix} \alpha & \theta & l_{cant} & \xi_x & \xi_y & \xi_z & \xi_\beta & \xi_\gamma \end{bmatrix} \tag{6.14}$$

To locate the load case yielding the maximum force exerted on an actuators, g_{max}, two different optimizations are made. Optimization one determines the load case yielding the largest force compressing a cylinder during wave compensating motion and optimization two locates the load case yielding the largest tensile force exerted on a cylinder during wave compensating motion. The two objective functions are then defined in Eq. (6.15) and Eq. (6.16) respectively.

$$\Phi_{ten}(\alpha,\theta,l_{cant},\xi) = \frac{1}{g_{ten,max}} \tag{6.15}$$

$$\Phi_{comp}(\alpha,\theta,l_{cant},\xi) = \frac{1}{g_{comp,max}} \tag{6.16}$$

Minimizing Eq. (6.15) maximizes the largest force compressing any cylinder in the system and minimizing Eq. (6.16) equally maximizes the largest tensile force on any actuator. A flowchart for the optimization is seen in Fig. 6.4. The optimization yield the results in Table 6.1.

The maximum force excerpted on an actuator during one cycle of wave compensation in sea state 5 for the two given load cases are listed in Table 6.1. For compression it is seen that the static forces (normal force and moment) has a large effect on the force, as the crane is allowed to carry the heaviest load at 4.6 m. Additionally it is seen that the dynamic forces have the largest effect on the tension force, as the load inertia is greatest at $l_{cant} = 17.1$ m. Note that these load cases not necessarily are unique, as an equivalent force might be exerted on a different cylinder in a different load case. It is also significant to notice that the magnitude of phase shift is unimportant, as long as the relation between the magnitudes is constant.

Table 6.1: *Design space for and results of the maximum load case optimizations.*

Design variable	LB	UB	Compression	Tension	Unit
α	0	180	127	81	[°]
θ	-10	70	-10*	35	[°]
l_{cant}	4.6	17.1	4.7	17.1*	[m]
ξ_x	0	360	90	0*	[°]
ξ_y	0	360	180	180	[°]
ξ_z	0	360	0*	0*	[°]
ξ_β	0	360	1	0*	[°]
ξ_γ	0	360	2	180	[°]
Peak Force			94	78	[kN]
Peak Force cyl.			2	5	[-]

* Active constraint

The flowchart in Fig. 6.4 outline the flow of the optimization for maximum actuator forces.

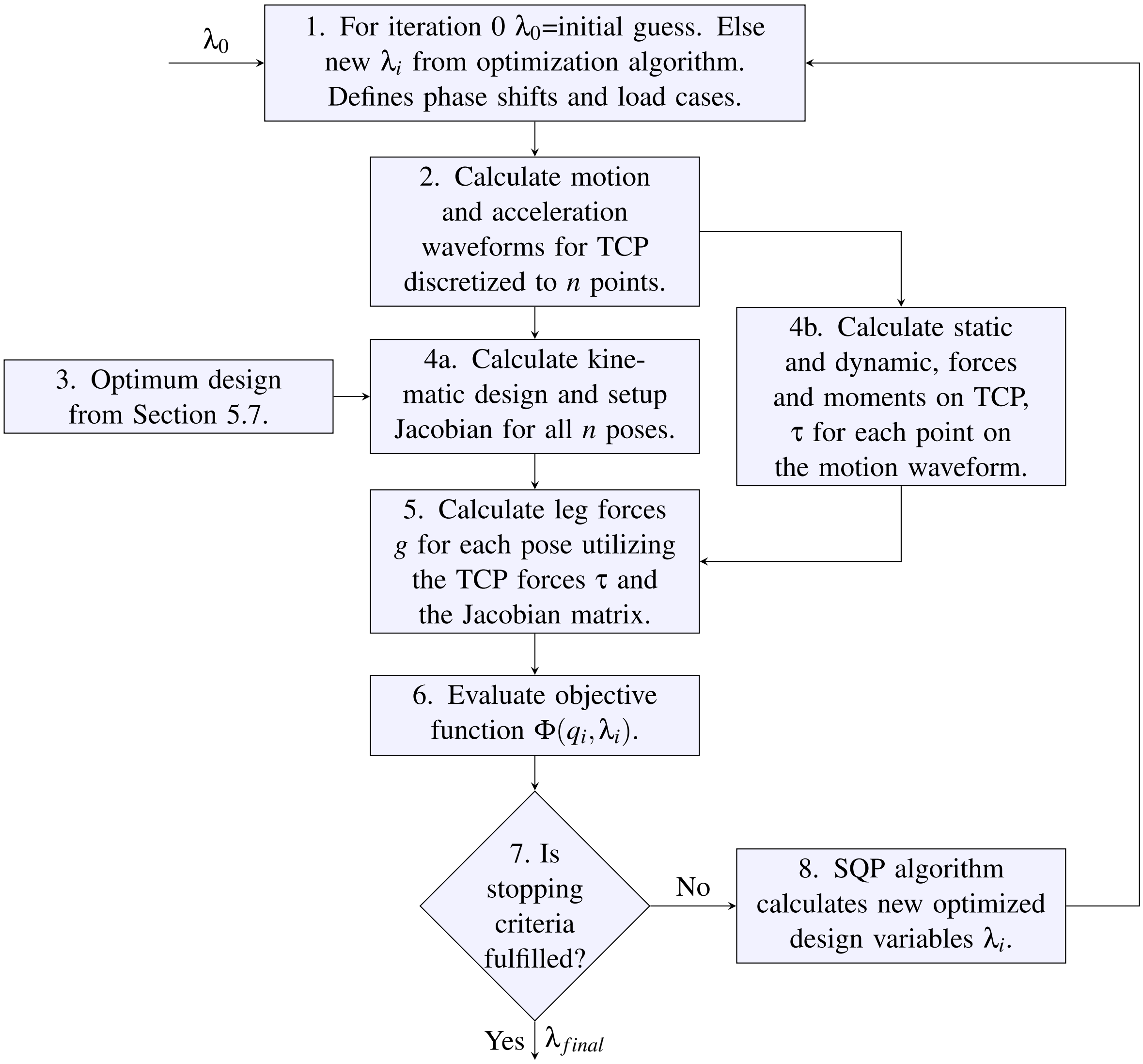

Figure 6.4: *Flowchart for the force optimization procedure.*

6.4 Hydraulic Actuator Sizing

In this section the hydraulic actuators for the Stewart platform is sized. First the initial actuator size is determined by calculation of the areas required to generate the forces needed. As the stroke length is relatively long the piston rod is sensitive to buckling and this becomes a significant factor in the sizing calculations. To reduce the actuator size and required system flow the rod diameter is minimized.

6.4.1 Initial Actuator Size

The dimensions of the hydraulic actuators are determined from the actuator forces calculated in Section 6.3. The hydraulic cylinders must be able to provide the actuation force and velocity required to operate the Stewart platform. The maximum force compressing the cylinder is $94kN$ and the maximum force tensioning the cylinder is $78kN$. Calculation of the minimum required areas to generate the actuation forces at maximum system pressure (300bar) yields:

$$A_p = \frac{94kN}{300bar} = 31.3cm^2 \tag{6.17}$$

$$A_r = \frac{78kN}{300bar} = 26.0cm^2 \tag{6.18}$$

These areas requires the smallest possible flow as flow Q_{cyl} is given by:

$$Q_{cyl} = A\dot{l} \tag{6.19}$$

where the $\dot{l}$ is the actuator velocity and A is the hydraulic area. The actuator velocity is fixed by the required motion and kinematics of the Stewart platform which indicate that the required actuator flow can only be reduced by minimizing the area A. Minimizing the flow makes it possible to reduce the size of the hydraulic components, costs and flow losses which is desired. The minimum piston area is calculated to be:

$$d_{piston} = \sqrt{\frac{4A_p}{\pi}} = 63mm \tag{6.20}$$

From the given piston diameter of 63 mm, the maximum allowed rod diameter d_r to obtain the required rod side area A_r is calculated:

$$d_{rod} = \sqrt{\frac{d_p^2\pi - A_r}{\pi}} = 56mm \tag{6.21}$$

To calculate if the rod size d_r pose a structural problem in terms of buckling Euler's formula for critical buckling load is used. The boundaries of the buckling problem dependents on whether the rod is inside the cylinder or outside as shown in Fig. 6.5 and 6.6.

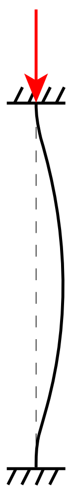

Figure 6.5: *Buckling boundary for rod inside cylinder.*

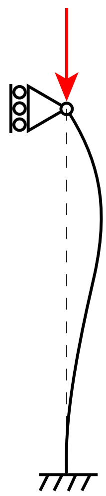

Figure 6.6: *Buckling boundary for rod outside cylinder.*

Buckling inside the cylinder is modeled as shown in Fig. 6.5 where the piston and cylinder head inhibit rotation at both ends of the rod and buckling outside the cylinder is modeled as shown in Fig. 6.6

where the cylinder head inhibits rotation close to the cylinder head and the joint at the other end allows rotation. A safety factor c_s of 2.5 must be used when dimensioning hydraulic cylinder against buckling [25]. The critical force for buckling inside and outside the cylinder is calculated in Eq. (6.22) and Eq. (6.23) respectively:

$$F_{in} = \frac{4\pi E I_{rod}}{L_{stroke}^2 c_s} = 66kN \tag{6.22}$$

$$F_{out} = \frac{2.046\pi E I_{rod}}{L_{stroke}^2 c_s} = 34kN \tag{6.23}$$

where the moment of inertia for a rod is given as:

$$I_{rod} = \frac{\pi d_{rod}^4}{64} \tag{6.24}$$

The moment of inertia of the rod is too small to withstand the maximum buckling force of $94kN$ which means that the rod diameter must be increased. A Calculation has shown that the rod diameter must be increased to 73 mm to resist the buckling force. The cylinder areas are therefore recalculated using a 73 mm rod:

$$d_{piston} = \sqrt{\frac{4A_r}{\pi} + d_{rod}^2} = 93mm \Rightarrow A_p = 67.9cm^2 \tag{6.25}$$

$$A_r = A_p - \frac{1}{4} d_{rod}^2 = 26cm^2 \tag{6.26}$$

The maximum actuation velocity is the same for extension and retraction of the cylinders and is calculated to be $0.89\frac{m}{s}$ in Section 6.5. The system flows are calculated using the maximum actuation velocity and the cylinder areas. The system pressures are calculated the using the actuation forces and the cylinder areas. The results are listed in Table 6.2.

Table 6.2: *Initial cylinder data.*

Description	value	unit
d_{piston}	93	[mm]
d_{rod}	73	[mm]
p_{piston}	139	[bar]
p_{rod}	300	[bar]
Q_{piston}	362	[L/min]
Q_{rod}	139	[L/min]

In Table 6.2 it can be seen that the rod side pressure p_{rod} is equal to the maximum system pressure whereas the piston side pressure p_{piston} is small compared to the maximum pressure. The flow rate to the piston side Q_{piston} is large compared to Q_{rod}. The flow to the piston side can potentially be reduced if the rod diameter could be reduced, which may be possible as the largest buckling force may not be applied to the cylinder in the most vulnerable position of the cylinder stroke (fully extended), i.e this is investigated.

6.4.2 Optimization of the Actuator Rod Dimension

To investigate if the calculated rod diameter can be reduced an optimization problem that accurately calculates the minimum required rod diameter necessary to prevent buckling is formulated. The optimization calculates the minimum required diameter for all six actuator rods in all poses within the prescribed workspace.

To calculate the minimum required rod diameter for a given pose in the optimization, it is required to know how much of the rod that is inside the cylinder and how much that is outside. To calculate this it is utilized at the cylinder length properties are known for the optimized design, see Table 5.11. From the minimum cylinder length l_{cylmin}, the stroke length $l_{strokemax}$ and the cylinder length for the given pose, the lengths can be calculated:

$$l_{out} = l_{cyl} - l_{cylmin} \tag{6.27}$$

$$l_{in} = l_{strokemax} - l_{out} \tag{6.28}$$

The equations for critical buckling load, Eq. (6.22) and Eq. (6.24) are then rewritten to expressions for the critical rod diameters $d_{crit,in}$ and $d_{crit,out}$. The critical diameters for all six actuator rods are then calculated as a function of the current loading on the actuators (instead of the critical load) and for the current rod length, Eq. (6.27) and Eq. (6.28). The expressions for the critical rod diameter inside and outside the cylinder respectively, are then given by:

$$d_{crit,out}(l_{out}, F_{cyl}) = \sqrt[4]{\frac{64 l_{out}^2 c_s F_{cyl}}{2.046 \pi^3 EI}} \tag{6.29}$$

$$d_{crit,in}(l_{in}, F_{cyl}) = \sqrt[4]{\frac{64 l_{in}^2 c_s F_{cyl}}{4 \pi^3 EI}} \tag{6.30}$$

As the lengths l_{in} and l_{out} change for every pose, they are a function of the Stewart platform motion and hence the waveform phase ξ. Additionally the forces F_{cyl} change for every pose and F_{cyl} is a function of the load case (α, θ, l_{cant} and ξ). Therefore the optimization is a function of these variables and the design variables are then given by:

$$\lambda = \begin{bmatrix} \alpha & \theta & l_{cant} & \xi_x & \xi_y & \xi_z & \xi_\beta & \xi_\gamma \end{bmatrix} \tag{6.31}$$

Using the design variables given in Eq. (6.31) the forces in all cylinders and the corresponding lengths l_{in} and l_{out} can be found within the entire workspace and thus the corresponding critical rod diameter. The largest of the minimized functions d_{out} and d_{in} is the critical rod diameter and is labeled d_{req}, i.e. the optimization cost function becomes:

$$\Phi(\alpha, \theta, l_{cant}, \xi) = \frac{1}{d_{req}} \tag{6.32}$$

As the SQP minimize the cost function, the reciprocal of d_{req} is used to find the largest required rod diameter. The optimization is described by the flowchart in Fig. 6.7.

The optimization yields a minimum allowable rod diameter of 65 mm, which in smaller than the required rod diameter of 73 mm given in Table 6.2. This indicate that the largest compression force is

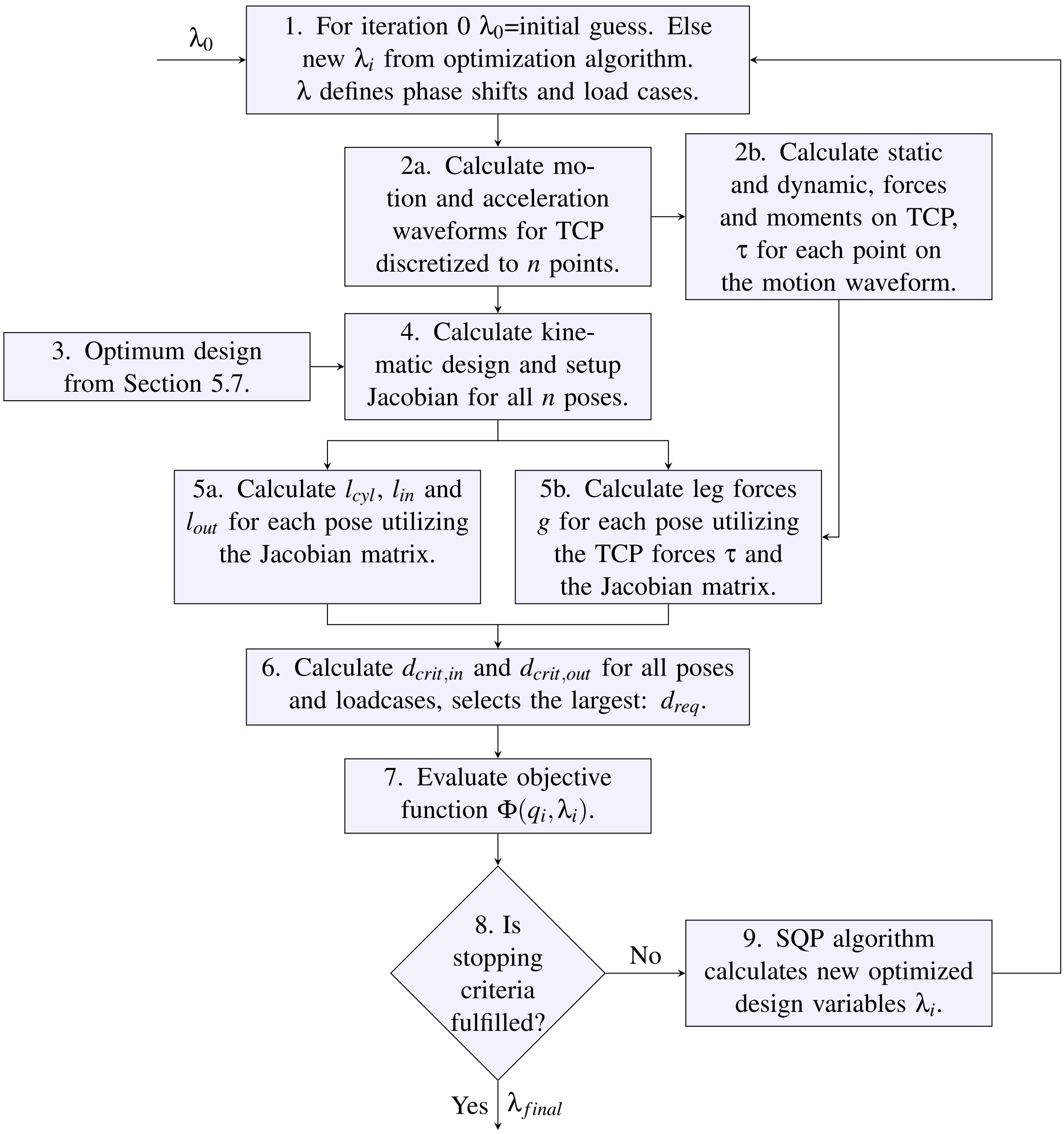

Figure 6.7: *Flowchart for the diameter optimization procedure.*

not exerted on the cylinder when it is fully extended, which is confirmed by Fig. 6.8. In the figure it is seen that the largest compression force on the cylinders, occur when the cylinder is fully retracted, and that the smallest force in this case is defining for the critical diameter.

6.4.3 Conclusion of the Actuator Sizing

In order to evaluate the potential of reducing the rod diameter and hence the actuator size can be seen in Table 6.3. It is seen that the rod diameter d_{rod} can be reduced from 73 mm to 65 mm without any risk of buckling. The reduction is possible because the largest compressive force are not applied to the rod

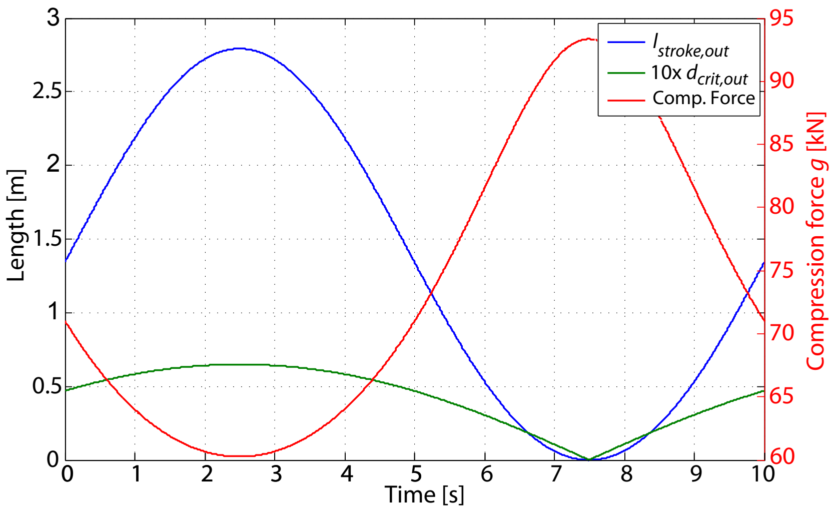

Figure 6.8: *Stroke length, compression force and required minimum diameter of the dimensioning cylinder.*

when fully extended as this is the most buckling sensitive position. The reduction of rod diameter render it possible to reduce the piston diameter d_{piston} from 93 mm to 87 mm.

This has the advantage that the largest system flow Q_{piston} is reduced from 362 $\frac{L}{min}$ to 316 $\frac{L}{min}$ which is a reduction of 47 $\frac{L}{min}$. The reduction lower the flow losses and allow smaller and cheaper components to be used in the hydraulic circuit. The calculations are based on the peak actuation velocity of 0.89$\frac{m}{s}$ but as a smaller cylinders are used flow is reduced independent of actuation velocity.

Table 6.3: *Comparison of optimized and not optimized cylinder data.*

Description	not optimized	optimized	difference	unit
d_{piston}	93	87	-5	[mm]
d_{rod}	73	65	-8	[mm]
p_{piston}	139	159	+20	[bar]
p_{rod}	300	300	0	[bar]
Q_{piston}	362	316	-47	[L/min]
Q_{rod}	139	139	0	[L/min]

The ratio between the rod side area and the piston side area is 1:2.26, and servo valves with a spool matched to exactly this area ratio may not be commercially available. A spool with the ratio of 1:2 on metering areas may be used instead as this ratio is close and the valve is not to operate around the neutral position, as the wave motion require the cylinders to move forward and backwards with relatively long strokes. The diameters of the cylinder tubing and rod may also not be commercially available. In this thesis it is assumed that the sizes are available, and if the system are to be realized the method of sizing the cylinders are still valid, if the cylinder and rod diameter are rounded to the nearest available size. Knowing the dimensions of the cylinders the components for the remaining hydraulic system can be selected. The data necessary to select the remaining hydraulic components are the system pressure and system flow which is listed in Table 6.4 along the final cylinder dimensions.

Table 6.4: *Final cylinder data.*

Description	data	unit
p_{max}	300	[bar]
d_{piston}	87	[mm]
d_{rod}	65	[mm]
l_{min}	3.42	[m]
l_{max}	6.24	[m]
l_{stroke}	2.82	[m]

6.5 Maximum System Flow and Velocity

In this section optimizations are performed to calculate the largest system flow and actuator velocities required by the Stewart platform actuators in sea state 5. Optimizations are performed to precisely calculate the flow requirements in order to ensure that Stewart platform fully comply with the demand of 95% workability, see Section 2.5.

The maximum combination of actuator velocities are required to calculate the maximum required system flow to all cylinders in order to size the hydraulic pump to match the demand. The maximum flow to the individual cylinders is required to select suitable hydraulic valves. The velocity is also needed to select cylinders that can withstand the velocity without damaging seals.

Hydraulic differential cylinders are used on the Stewart platform which means that the flow rate required for extension and retraction is dependent on the area ratio. The area ratio is found to be 1:2.26, see Section 6.4.3, which means that twice the flow rate is required to extend the cylinder than to retract it. In order to calculate the system flow, the flow to each cylinder is calculated from the following loop:

$$\begin{aligned}
if \quad & \dot{l}_i \geq 0 \qquad \text{for } i = [1;6] \\
& Q_{(i)} = A_p \dot{l}_i \\
else\,if \quad & \dot{l}_i < 0 \qquad \text{for } i = [1;6] \\
& Q_i = A_r \dot{l}_i
\end{aligned}$$

where $i = [1;6]$ as there are six cylinders on the platform, which is summed for each pose to calculate the system flow:

$$Q_{system} = \sum_{i=1}^{6} Q_i \tag{6.33}$$

To determine the the largest required system flow, the flow must be maximized. In Section 6.2.1 the motion of the tool center point is given, from which the velocity is obtain by differentiation of the motion vector q with respect to time. Using the kinematic equation defined in Eq. (4.4), the velocities of the actuators are calculated. The equation is repeated here for convenience:

$$\dot{l} = J\dot{q} \tag{6.34}$$

The actuator velocities and flows are dependent on the tool center point motion, which is dependent on the phase shift between the wave motions in all d.o.f. on the TCP. Hence an optimization problem is formulated in a similar manner as the maximum force optimization, to find the the phase shift yielding the largest leg velocity and largest system flow. The design variable vector λ for the maximum velocity optimization is then given by:

$$\lambda = \begin{bmatrix} \xi_x & \xi_y & \xi_z & \xi_\beta & \xi_\gamma \end{bmatrix} \tag{6.35}$$

The objective functions are then expressed in Eq. (6.36) for maximum system flow and Eq. (6.37) for the largest velocity. A flowchart for the optimization is depicted in Fig. 6.9.

$$\Phi_{flow}(\xi) = \frac{1}{Q_{system}} \tag{6.36}$$

$$\Phi_{vel}(\xi) \quad = \frac{1}{max(\dot{l})} \tag{6.37}$$

The largest flow and actuator velocity from the optimization are listed in Table 6.5 with the respective phase shift. The design space for ξ in the optimization, are for all phase shifts constraint in an interval from 0 to 360°.

Table 6.5: *The maximum velocity, system flow and the respective phase shifts of the motion.*

Design variable	Velocity	System Flow	Unit
ξ_x	14	39	[°]
ξ_y	2	219	[°]
ξ_z	0	0	[°]
ξ_β	2	217	[°]
ξ_γ	2	215	[°]
Max. Sys. Flow	-	1300	[$\frac{\mathrm{L}}{\mathrm{min}}$]
Max. vel.	0.89	-	[$\frac{\mathrm{m}}{\mathrm{s}}$]
Max. vel. cyl.	3	-	[-]

From Table 6.5 it is seen that the actuators must be able to operate with a maximum velocity of 0.89 $\frac{\mathrm{m}}{\mathrm{s}}$. For the given set of phase shifts ξ in Table 6.5 it is only cylinder 3 that operates with the maximum velocity, but other phase shifts will render the same velocity in other cylinders, i.e. this is the required maximum velocity for all cylinders. Additionally it is seen in Table 6.5 that the maximum required system flow (to all cylinders simultaneously) is $1300\frac{\mathrm{L}}{\mathrm{min}}$. The maximum system flow is obtain in the optimization for the given set of phase shifts ξ in Table 6.5, but the set of phase shifts ξ is not unique as the maximum system flow occurs for other sets of phase shifts. It is not the magnitudes of the phase shifts that are important to obtain the results, as the same results is obtained as long as the intervals between phase shift are constant.

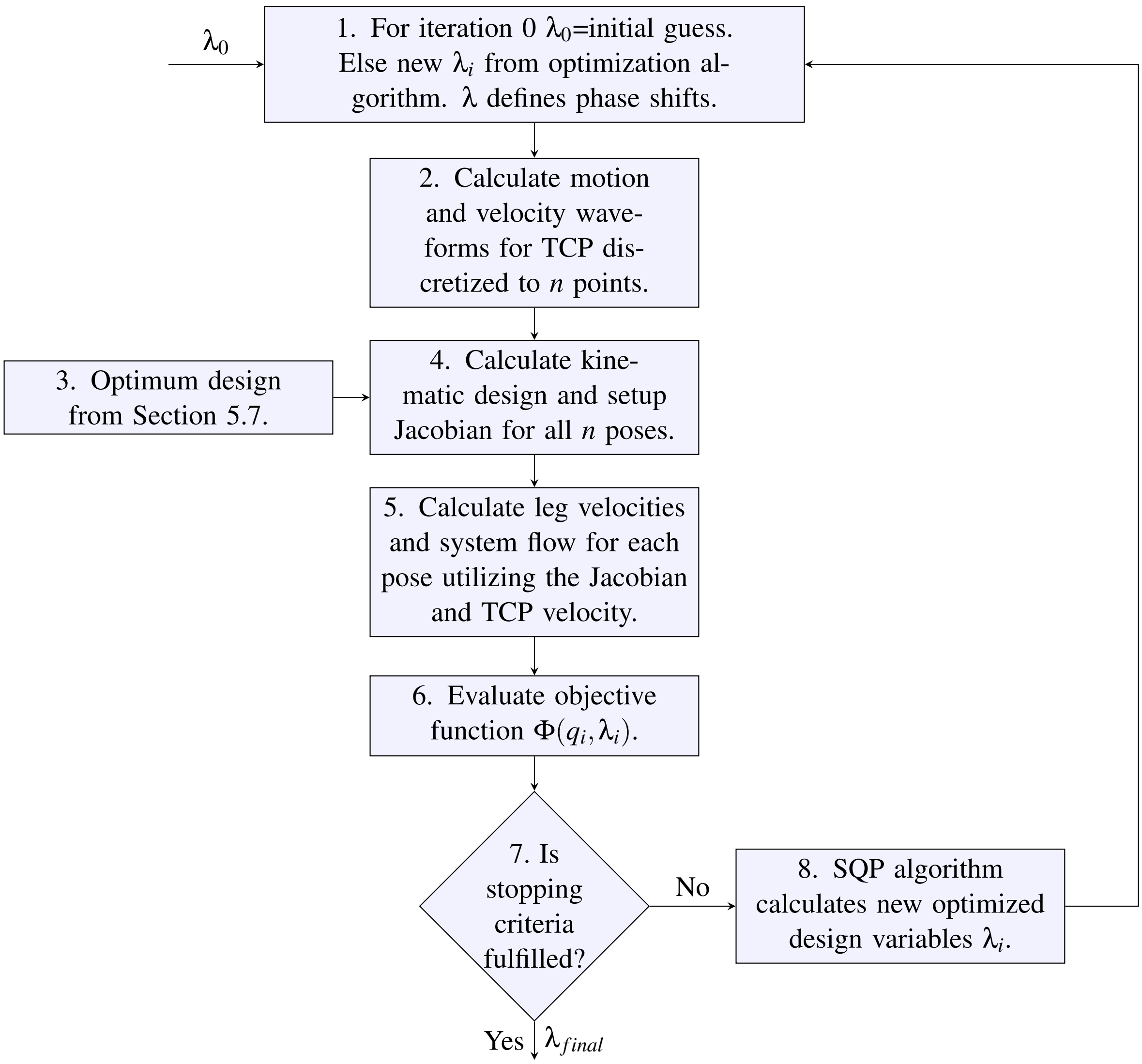

Figure 6.9: *Flowchart for the velocity and flow optimization procedure.*

6.6 Power Requirements

As the hydraulic system must be able to actuate the Stewart platform in sea state 5 with a 95% workability, the maximum power requirement must be calculated to ensure that the drive motor is capable of providing the power required. In order to select the smallest and hence cheapest possible drive motor for the hydraulic system, determining the maximum power requirement accurately is paramount. The power requirement of the system can be derived by combining Eq. (6.3) and Eq. (6.34):

$$P = g\dot{l} \tag{6.38}$$

The maximum required power does not necessarily equals maximum force times maximum velocity as these might not occur simultaneously in the system. To locate the largest power requirement the optimization procedures utilized in sections 6.3 and 6.5 are combined to locate the load case yielding the largest power consumption. The maximum power requirement occurs where the product of the actuation force and velocity is greatest. To locate the load case yielding this, a design variable vector λ for the optimization is defined:

$$\lambda = \begin{bmatrix} \alpha & \theta & l_{cant} & \xi_x & \xi_y & \xi_z & \xi_\beta & \xi_\gamma \end{bmatrix} \tag{6.39}$$

The design variable vector is equal to the one defined in Eq. (6.14) for maximum force optimization and hence the design space are also similar. The bounds of the design space for the optimization is tabulated in Table 6.6. From Eq. (6.38) the objective function is defined as follows:

$$\Phi_{power}(\alpha, \theta, l_{cant}, \xi) = \frac{1}{max(\sum_{i=1}^{6} |g_i||\dot{l}_i|)} \tag{6.40}$$

The flow of the optimization can be seen from the flowchart in Fig. 6.10. The largest system power requirement for the Stewart platform calculated by the optimization, in addition with the load case causing the power requirement is listed in Table 6.6.

Table 6.6: *Design space for and results of the maximum power optimizations.*

Design variable	LB	UB	λ	Unit
α	0	180	68	[°]
θ	-10	70	35	[°]
l_{cant}	4.6	17.1	17.1*	[m]
ξ_x	0	360	221	[°]
ξ_y	0	360	214	[°]
ξ_z	0	360	8	[°]
ξ_β	0	360	0	[°]
ξ_γ	0	360	126	[°]
Max. Power			155	[kW]
Mean Power			88	[kW]

* Active constraint

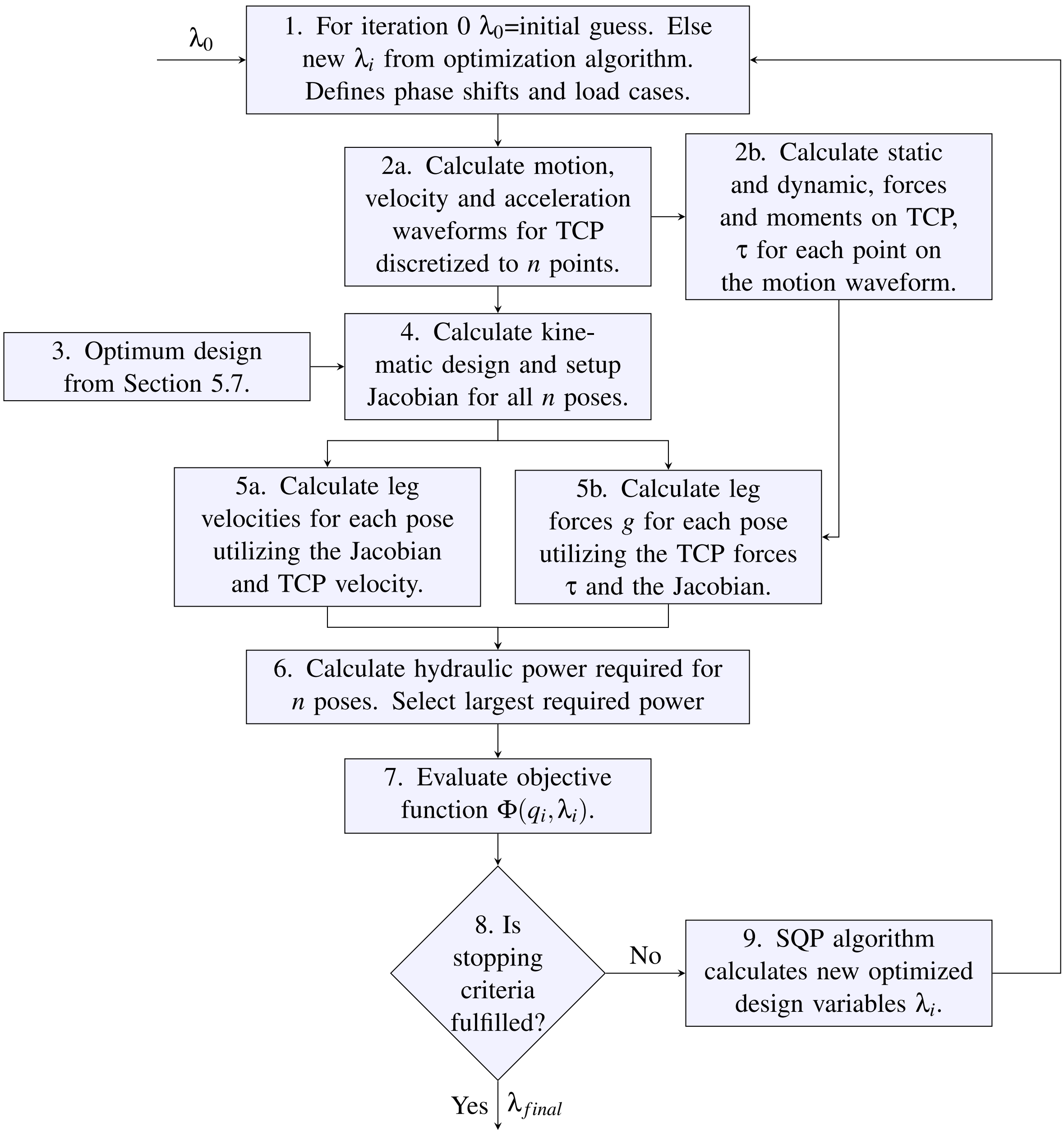

Figure 6.10: *Flowchart for the hydraulic power optimization procedure.*

6.7 Hydraulic Pipe Sizing

In order to obtain a low response time of the hydraulic servo system, the volumes of the hydraulic pipes between the valve and cylinder should be as small as possible, to obtain as high an effective stiffness of the hydraulic fluid as possible. Reducing the volumes increases the fluid velocity in the pipes, and the maximum velocity of the fluid in a servo system is allowed to be as high as 30 $\frac{m}{s}$ [26]. The hydraulic pipes between valve and cylinder must be steel pipes instead of hydraulic rubber hoses to additionally increase the stiffness of the system. This means that the valves must be mounted on the cylinders because steel pipes are not flexible, as the cylinders moves relative to all other possible mounting locations for the valves. This is also beneficial as this limit the length of the pipes and hence the pipe volumes are additionally reduced.

The valves are mounted on side of the cylinder close the bottom which defines the length of the pipes to be approximately 0.34 m and 3.08 m for piston and rod side respectively. The maximum flow rates Q_{piston} and Q_{rod} is 316 $\frac{L}{min}$ and 139 $\frac{L}{min}$ respectively and for these flow rates the maximum flow velocity in the pipes are 30 $\frac{m}{s}$. For simplicity the diameter of both hydraulic lines are decided to be the same. To calculate the minimum diameter pipe required the largest flow rate is dimensioning:

$$d_{hose} = \sqrt{\frac{4Q_{piston}}{\pi v_{fluid}}} \approx 15mm \tag{6.41}$$

The pressure drop in the pipes are calculated using a fluid viscosity of 60cSt and the results is tabulated in Table 6.7 along with the volumes of the pipes.

Table 6.7: *Hydraulic hose data.*

Description	data	unit
l_{hose1}	0.34	[m]
l_{hose2}	3.08	[L]
V_{hose1}	0.06	[L]
V_{hose2}	0.54	[L]
Δp_{hose1}	1.26	[bar]
Δp_{hose2}	2.20	[bar]

6.8 Hydraulic Valve Selection

To select a suitable servo valve for the hydraulic system is it is necessary to determine the minimum required effective bandwidth ω_v, and the minimum rated flow, $Q_{n,min}$ of the valve.

The valves required to control the Stewart platform must be faster than the hydraulic-mechanical system, which means that the valves must be able to operate at higher frequencies, than the lowest eigenfrequency ω_n of the hydraulic-mechanical system in order to control the system. A rule of thumb denotes that the operation frequency of the valves that corresponds to a 90° phase lag, should be three times larger than the system eigenfrequency ω_n [27]. This frequency is defining the effective bandwidth ω_v of the valve. The eigenfrequency of the mechanical system is later found in Section 6.10 be to 12.5 Hz or 79 $\frac{\text{rad}}{\text{s}}$, and thus, the effective valve bandwidth ω_v should correspond to:

$$\omega_v \geq 3\omega_n \quad \Rightarrow \quad \omega_v \geq 237 \ \frac{\text{rad}}{\text{s}} \tag{6.42}$$

To calculate the minimum required rated flow $Q_{r,min}$, it is necessary to determine the required supply pressure. The largest required pressure in the cylinders are p_{max}=300 bar (Table 6.4), and the pressure losses in the lines are determined be to 2.2 bar in Table 6.7, and a rated 35 bar pressure drop Δp_n across the servo valve gives the minimum supply pressure:

$$p_s = p_{max} + \Delta p_n + \Delta p_{hose2} = 338 \text{ bar} \tag{6.43}$$

p_s is the minimum supply pressure required at the valves for an ideal system and therefore pump pressure should be set at higher value when choosing a pump for the real system.

Knowing the supply pressure and the maximum load pressure p_{max}, it is possible to determine minimum rated flow $Q_{n,min}$. The maximum flow through the servo valves in the system is given by:

$$Q_{max} = Q_{n,min}\sqrt{\frac{p_s - p_{max}}{\Delta p_n}} \tag{6.44}$$

Equation (6.44) can be rearranged and the minimum rated flow can be calculated. The maximum required flow to the cylinder is defined in Table 6.3 as $Q_{max} = 316\ \frac{\text{L}}{\text{min}}$. A safety factor of 1.1 must be included in the minimum rated valve flow [28], and thus the minimum rated flow for the valves are given by:

$$Q_{n,min} = 1.1 \cdot \frac{Q_{max}}{\sqrt{\frac{p_s - p_{max}}{\Delta p_n}}} = 334\ \frac{\text{L}}{\text{min}} \tag{6.45}$$

From this the valve requirements are specified in Table 6.8. A valve should thus be selected to have $\Delta p_n = 35$ bar and an eigenfrequency and rated flow of an equivalent or higher magnitude than the one specified in the table.

Table 6.8: *Valve specification.*

Description	data	unit
Δp_n	35	[bar]
$Q_{n,min}$	334	$[\frac{\text{L}}{\text{min}}]$
ω_v	237	$[\frac{\text{rad}}{\text{s}}]$

6.9 System Modeling

In this section it is presented how a mathematical simulation model of both the hydraulic and mechanical system is derived. The combined model of is used to calculate the eigenfrequency of the system in order to select an appropriate servo valve in Section 6.8. The models in this chapter can additionally be used to develop controllers for the system, but controller design for the Stewart platform is beyond the scope of this project.

6.9.1 Model of the Hydraulic System

In this section a non-linear model of the hydraulic actuation system is derived to determine the hydraulic forces acting on the piston as a function of valve command x_v and the exteral load. The forces are the input to the mechanical model described later in this section. The actuators used on the Stewart platform is double acting hydraulic cylinders. The cylinders are connected to servo valves and the position control of the piston is obtained by controlling the oil flow in and out of the cylinder chambers. A shematic diagram of the servo valve and cylinder can be seen in Fig. 6.11.

As seen in Fig. 6.11 the system consists of two orifices and two volumes. The volumes are modelled using the continuity equation:

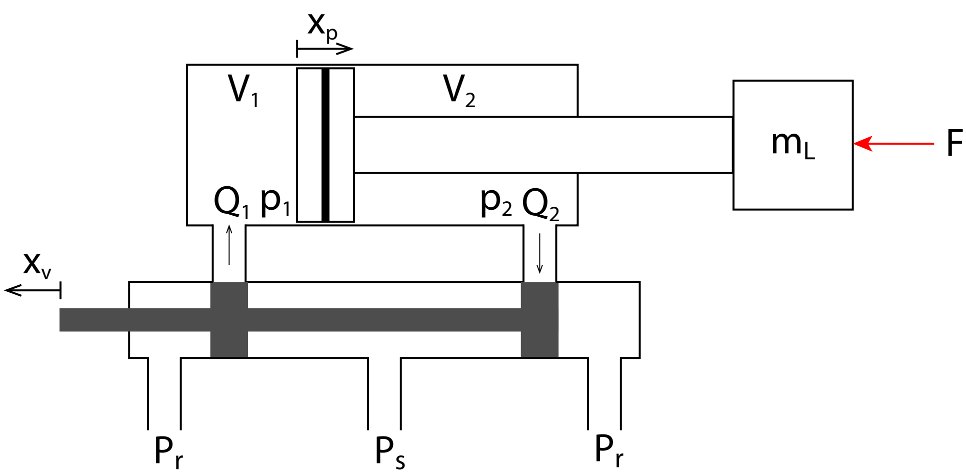

Figure 6.11: *Shematics of valve and hydraulic cylinder.*

$$\frac{dp_1}{dt} = \frac{\beta_F}{V_1}(Q_1 - A_1\dot{x}_p) \tag{6.46}$$

$$\frac{dp_2}{dt} = \frac{\beta_F}{V_2}(A_2\dot{x}_p - Q_2) \tag{6.47}$$

Equation 6.46 and 6.47 are derived for motion in the positive direction indicated in Fig. 6.11. The equations are also valid for downward motion if the sign convension for flow and direction of motion is kept.

The volumes V_1 and V_2 includes the volume of piston and rod side chamber respectively and the volumes of the hydraulic hoses between the cylinder and valve. As the position changes the volumes change accordingly and this variation must be included in the non-linear model of the system. The volumes V_1 and V_2 is given by:

$$V_1 = V_{hose1} + A_p x_p \tag{6.48}$$

$$V_2 = V_{hose2} + A_r x_p (L_{stroke} - x_p) \tag{6.49}$$

The flow through the servo valves is modeled with the orifice equation. In the data sheet for servo valves following flow equation is found:

$$Q = Q_N \sqrt{\frac{\Delta p}{p_N}} \tag{6.50}$$

where Q_N is the rated flow and Δp_N is the rated pressure drop per metering orifice, which means that pressure drop of across the metering orifice of Δp_N yeilds an output flow of Q_N. There is a linear relation between spool positon x_v and output flow Q provided that pressure drop across the metering spool is constant. The equations for the output flows Q to both volumes is dependent on direction of the spool position x_v. The flows for the positive direction (extension of cylinder) are given by:

$$Q_1 = Q_N \sqrt{\frac{p_s - p_1}{\Delta p_n}} x_v \qquad\qquad Q_2 = Q_N \sqrt{\frac{p_2 - p_r}{\Delta p_n}} x_v \tag{6.51}$$

and the flows for the negative direction (retracting of cylinder) are given by:

$$Q_1 = Q_N \sqrt{\frac{p_1 - p_r}{\Delta p_n}} x_v \qquad\qquad Q_2 = Q_N \sqrt{\frac{p_s - p_2}{\Delta p_n}} x_v \tag{6.52}$$

In order to keep the sign convension of the flows the spool position x_v must be negative for retracting the cylinder. The relation between the spool position and the valve input signal u_{ref} can be considered as a second order system. The transfer function is given as:

$$\frac{x_v(s)}{u_{ref}} = \frac{K\omega_n^2}{s^2 + 2\zeta\omega_n s + \omega_n^2} \tag{6.53}$$

The bode diagram provided in servo valve datasheets is used to determine the coefficients to obtain the transfer function. The governing equations are used to construct a non-linear simulation model in Simulink. The blockdiagram can be seen in Fig. 6.12. The input to the model is a voltage signal to the valve and the output is resulting actuation force. The actuation force is input the mechanical model described in the next section. Velocity and position are inputs to the hydraulic model and these are obtained in the mechanical model.

6.9.2 Model of the Mechanical System

The mechanical system model of the Stewart platform is created in MATLAB using the Simscape based SimMechanics. Simscape is a platform product for Simulink allowing physical system modelling of rigid body machinery and their motions, to investigate system dynamics, forces and torques according to physical principles [29]. The mechanical SimMechanics model of the Stewart platform is seen in Fig. 6.13. Note that signals are shown by arrows and that physical connections are shown by "circle-" to "square" or "circle-" to"circle"-icon connections.

The mechanical Stewart platform model is created to investigate how well the hydraulic system, modeled in Section 6.9.1, performs on the actual Stewart platform setup. Additionally the mechanical model makes evaluation of a controller design possible, as it gives the tool center point position for the given cylinder lengths without having to solve the manipulator forward kinematic problem, recall that this has to be solved numerically see Section 4.1, and hence the position error of TCP can be calculated.

The Stewart platform, Fig. 6.13 consist of a rigid body platform plate, denoted *platform* in the figure, a rigid base plate (ground) and six independent hydraulic cylinders connecting the platform with the base. The platform body is modeled to have the mass and inertia of the modeled load from the crane (the load case), see Section 6.2.2, and the position of the center of gravity of the body is likewise adapted to the load case (position of the crane and load carried).

Each hydraulic cylinder consists of two rigid bodies: *cylinder* and *rod*, which is the lower and the upper part of the hydraulic actuator respectively. Each of these bodies has dimensions as specified in Section 6.4 and the respective mass and inertia, which for simplicity are calculated as if the elements

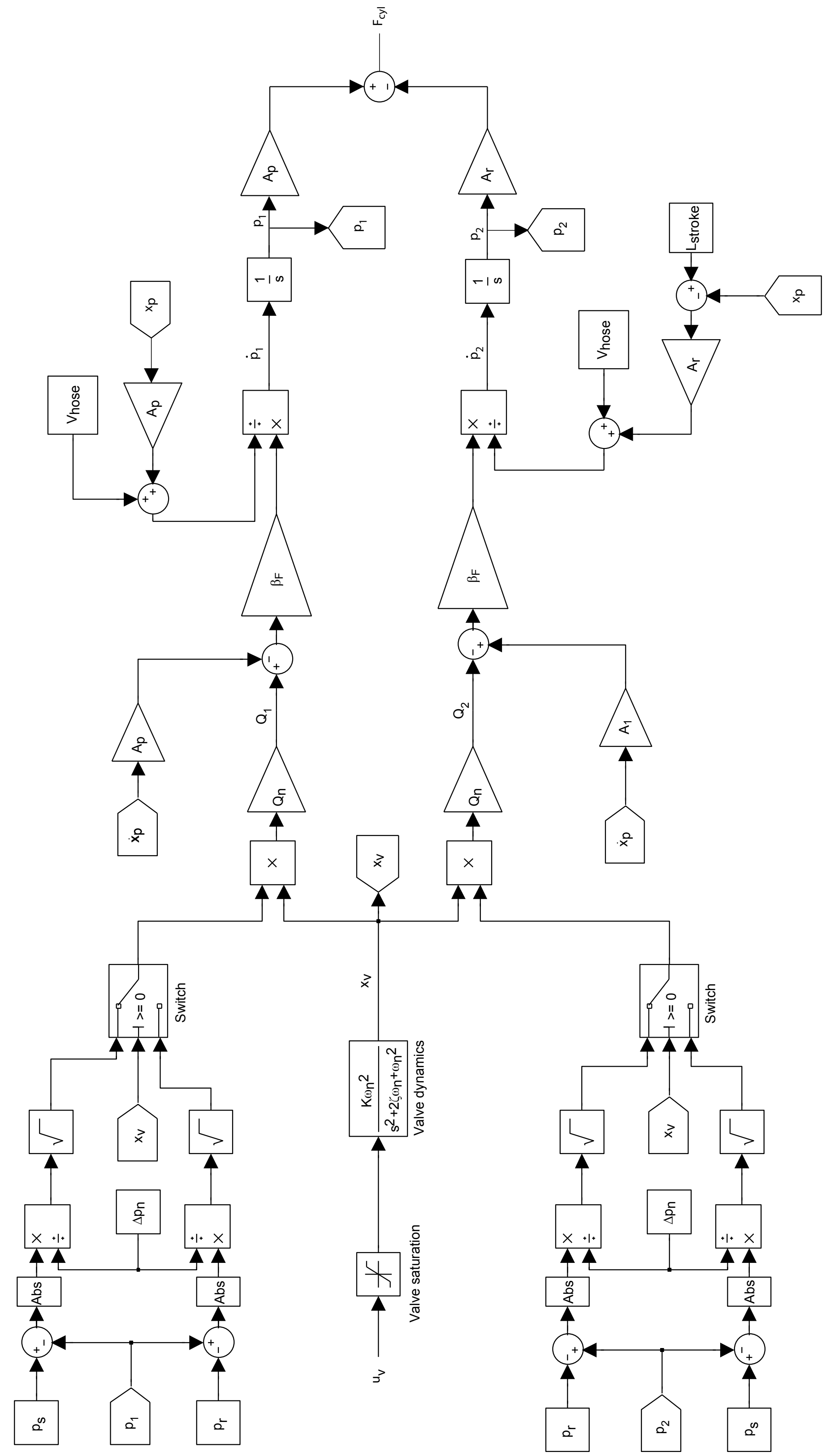

Figure 6.12: *Block diagram of hydraulic system*

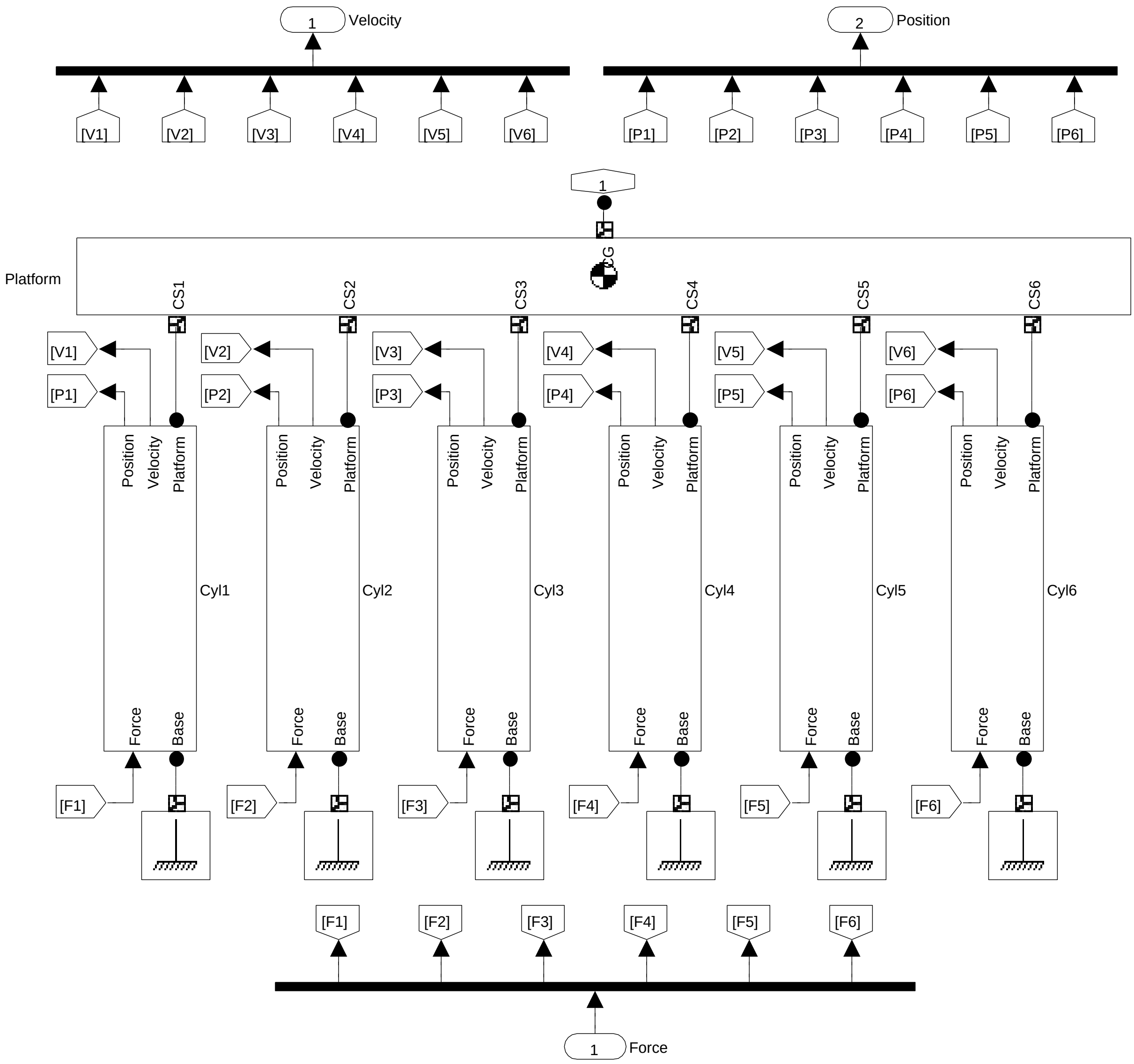

Figure 6.13: *SimMechanics model of the Stewart platform mechanical system.*

were cylindrical elements of massive steel. Additionally an universal joint is mounted at the base of the cylinder, a prismatic joint creates the connection between the cylinder and rod, and finally a spherical joint is placed at the top of the rod, connecting the rod to the platform body. Each rod is actuated by a force input created by the pressures in the upper and lower chamber of the hydraulic cylinder in the hydraulic model, see Section 6.9.1. The mechanical model of a cylinder is seen in Fig. 6.14.

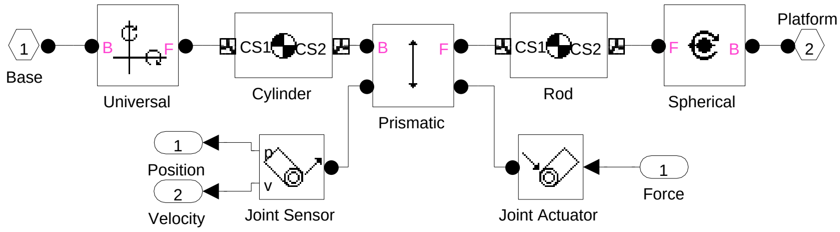

Figure 6.14: *SimMechanics model of a hydraulic cylinder mechanical system.*

6.10 Determination of System Eigenfrequency

To simplify the hydraulic and mechanical system of the Stewart platform into a linear model of every cylinder, the corresponding equivalent mass m_{eq} must be known. This makes it possible to determine the hydraulic-mechanical system eigenfrequency in order to select a servo valve with appropriate bandwidth to control the system.

For translational and simple rotational 2D systems it is often possible to determine the equivalent mass as the equivalent mass can be calculated with relative ease. But as the Stewart platform is a 6 DOF system performing both translational and rotational motions by activating several or all of the actuators, calculating the equivalent mass for every cylinder is complex. Instead the mechanical system model in Section 6.9.2 and the hydraulic model in Section 6.9.1 is combined into complete system model and the eigenfrequency of the hydraulic-mechanical system is found by given the model a step input and monitoring the frequency of the response.

The eigenfrequency is dependent on the pose of the actuator as the pose both determine the inertia and the volumes in the cylinders. The neutral position $q = [0,0,h,0,0,0]$ is chosen as linearization point in the calculation of the eigenfrequency, as this point is the origin for all motions.

The linearization load case selected is where the crane is placed in $\alpha = 0°$ (along the x-axis), with the cantilever in an angle of 10° and extended to 10 m with a load of 1780 kg cargo load. The eigenfrequency is then found by giving the system a step input on the valve opening and measuring the oscillations in the system pressures. A plot of the system pressures in given in Fig. 6.15.

From the system pressures in Fig. 6.15 the eigenfrequency ω_n is determined to 12.5 Hz or 79 $\frac{\text{rad}}{\text{s}}$. The pressures in the figure is from cylinder 1 in the Stewart platform, but the oscillation frequency does not change significantly to the other cylinders.

When the hydraulic-mechanical eigenfrequency is known, this can be utilized to determine the equivalent mass on each cylinder from the formula for linearized eigenfrequency:

$$\omega_n = \sqrt{\frac{A_1^2\beta_F}{m_{eq}V_{10}} + \frac{A_2^2\beta_F}{m_{eq}V_{20}}} \tag{6.54}$$

where V_{10} and V_{20} are the linearized volumes of the cylinder. The linearized volumes are defined by the linearization point, where the pistons are in the middle of the cylinder and the volumes are defined by the respective areas and $\frac{1}{2}L_{stroke}$. Equation 6.54 assumes that the structural stiffness is infinite, which

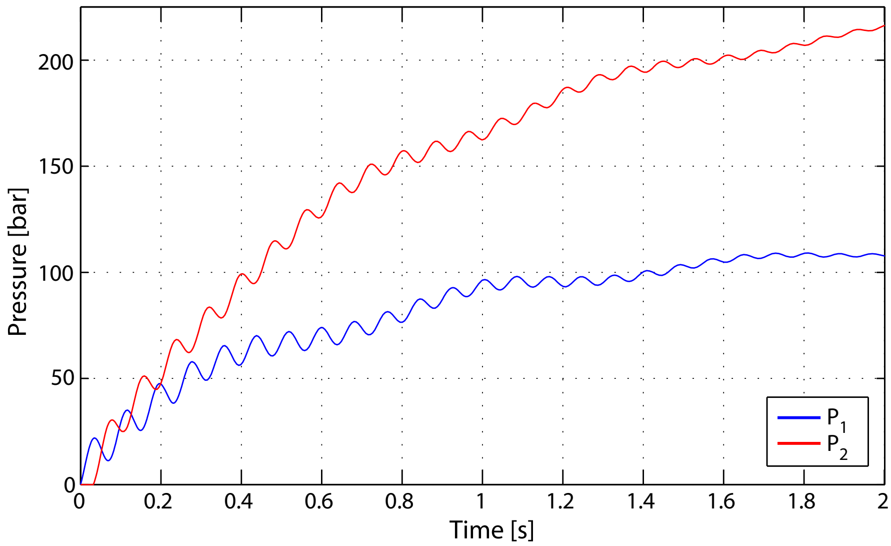

Figure 6.15: *Pressure oscillations in cylinder chamber 1 (blue) and 2 (red).*

indicate that the actual natural eigenfrequency is lower than calculated. However the structure of a Stewart platform in general is known to be very stiff. Equation (6.54) is then rearranged to calculate the equivalent mass m_{eq} for each cylinder:

$$m_{eq} = \frac{A_1^2 \beta_F}{\omega_n^2 V_{10}} + \frac{A_2^2 \beta_F}{\omega_n^2 V_{20}} \tag{6.55}$$

From Eq. (6.55) the equivalent mass for one cylinder is calculated to $m_{eq} = 660$ kg. As this equation originates from Eq. (6.54) which assumes infinite structural stiffness, the actual equivalent mass may be a larger. The eigenfrequency and equivalent mass are listed in Table 6.9

Table 6.9: *Eigenfrequency and eqvivalent mass.*

Description	data	unit
ω_n	79	$[\frac{\text{rad}}{\text{s}}]$
m_{eq}	660	[kg]

The total load on the Stewart platform, in the eigenfrequency calculation, is the 1780 kg load and the weight of the crane which yields 4325 kg. As the cylinders are close to vertical in space it can be presumed that the load is directly acting on the cylinders in the neutral position. This indicate that a feasible equivalent mass can be calculated simply be dividing the total load by 6, which yields 721 kg. Compared to the calculated value in Table 6.9 confirms the accuracy of equivalent mass of 660 kg and the precision of both the hydraulic and mechanical model.

6.11 Additional Components

In order to design a complete hydraulic system additional components must be included in the hydraulic circuit. Hydraulic servo systems has significant energy losses which is dissipated into the hydraulic fluid as heat, and to ensure that the hydraulic fluid continuously lubricates all moving parts, a radiator must be installed remove the excess heat.

The high precision parts of the hydraulic system are sensitive to fluid contamination and filters must be inserted into the circuit to clear the fluid from the contaminants. Adding appropriate filters into the circuit increases the lifespan significantly.

Hydraulic accumulator tanks may be necessary to install close the hydraulic valves in order to stabilize the pump pressure and yield extra power when needed.

CHAPTER 7

CONCLUSION

The work in thesis is intended to give a deeper understanding of the 6 DOF parallel manipulator known as the Stewart platform, and the possibility of using a Stewart platform for compensation of ship mounted cranes. The Stewart platform for wave compensation is intended to be used as a mounting platform for ship cranes and act as a stable foundation on the moving ship and thus minimize crane cargo pendulation. The Stewart platform is suitable for the wave compensation application because it has 6 degrees of freedom which is equivalent the motion of a ship, and thus it can counteract all motions of the ship within a certain range. Additionally, the Stewart platform has a high strength to size ratio as 6 hydraulic actuators are carrying the same load and a high positioning accuracy as actuator positioning errors does not amplify each other.

In order to be a feasible solution to the wave compensation problem the Stewart platform must be able to counteract ship motion for up to 95 % of the waves in sea state 5 on the Pierson-Moskowitz Sea Spectrum. To evaluate the ship motion for this sea state an approach to determine the ship motion is described in Chapter 3. As no ship or location is specified in this thesis for the wave compensation application, a generalized set of parameters for ship motion patterns are defined

The kinematics and kinematic properties of the Stewart platform are thoroughly investigated in Chapter 3 and it is found that it is important to evaluate and design the Stewart platform accordingly to the wave compensation application. For the wave compensation application dexterity and manipulability are important performance indices, as dexterity describes the platforms ability to generate velocities and exert forces in all directions and manipulability describes the transmission ratio of force and velocity.

Designing a Stewart platform yields several challenges that are impossible to accomplish by hand. Designing the kinematics to yield good kinematic performance requires the use of mathematical formulations and an optimization algorithm to solve the problem. In this thesis detailed explanations are given regarding the formulation of kinematic performance problem. Additionally methods are developed that ensure feasible actuator proportions and avoidance of actuator collision. The methods are directly incorporated into the solution process of the kinematic performance problems. The methods have proven to be very efficient as good designs are easily generated.

A single circle and a concentric circle Stewart platform design are chosen to be optimized for the wave compensation application. Multi objective cost functions are formulated to include kinematic performance indices and the insurance of feasible actuator proportions and avoidance of leg collisions. To solve the problems Sequential Quadratic Programming (SQP) is utilized to generate 10 optimum designs using different weights on the design objectives.

From the weighted designs it is concluded that the dexterity is the primary objective for wave compensation and the best design of each type of Stewart platform with full weight on dexterity is chosen. The single circle design yields a maximum GCI of 0.4277 and the concentric circle design a maximum GCI of 0.4946. It is seen that the concentric circle Stewart platform offer a 13.5 % improvement in dexterity compared to the single circle design, why this design is chosen for the wave compensation application.

A hydraulic servo system is designed and sized for the optimum concentric circle Stewart platform design. To determine the requirements for the hydraulic components, additional optimizations are performed with the SQP algorithm. This is done as the forces on the actuators, the required actuator velocity and the system power are dependent of multiple factors and hence determining these not intuitively straightforward. From the optimizations it is concluded that the dimensioning factor on the actuators are buckling and that the actuators should not be sized to prevent buckling from the largest compression load, meaning the cylinder dimensions can be downsized.

Finally simulation models of the hydraulic and mechanical systems are made, and the models are used to determine the eigenfrequency of the hydraulic-mechanical system, for the valve selection. Additionally the models can be used for further works and controller design for the system.

From the previous it can be concluded, that the optimized concentric circle Stewart platform design fulfills the requirements given in Chapter 2. First of all the manipulator can physically operate 95 % of the waves up to sea state 5, as the kinematic design allow good dexterity within the prescribed workspace. Additionally the kinematic design ensures that no leg collisions occur and that the actuators proportions are physically realizable as they fulfill the length ratio of 0.55. The forces required of the actuators are also within a reasonable range (maximum of 94 kN) and the optimized design does not violate the 7 m size constraint. Finally it is concluded that optimizing the dexterity of the HYDAC prototype yield a 59 % inprovement in dexterity to the single circle design, and a further 13.5 % improvement in dexterity can be achived utilizing the concentric circle Stewart platform design instead of the single circle design with regard to wave compensation.

BIBLIOGRAPHY

[1] H. Schaub. Rate-based ship-mounted crane payload pendulation control system. *Control Engineering Practice*, 16(1):132–145, 2008.

[2] T. Vaughers. Joint logistics over the shore operations. *Naval Engineers Journal*, 1994.

[3] P. J. Rawston and G. J. Blight. Prediction of weather downtime for derrick barges. *Proceedings of the 10th Annual Offshore Techn. Conf.*, 1978.

[4] Jørn Andresen, Tech. Dept. Gen. Manager. *Dampskibsselskabet NORDEN A/S*. d. 29-02-2012. Telefonsamtale.

[5] V. E. Gough. Automobile stability, control and tyre performance. *Automobile Div., Inst. Mech. Eng.*, 1956.

[6] D. Stewart. A platform with six degrees of freedom. *PROCEEDINGS OF THE INST. OF MECH. ENG. PART C-J. OF MECH. ENG. SCIENCE*, 223(17):266–273, 1965.

[7] J. C. Faugére and D. Lazard. Combinatorial classes of parallel manipulators. *Mech. Mach Theory*, 30(6):765–776, 1995.

[8] R. Stoughton and T. Arai. Design and kinematic optimixation of parallel manipulators. *Bulletin of Mechanical Engineering Laboratory, Japan*, 1992.

[9] I. R. Young. *Wind generated Ocean Waves*. Elsevier Science & Technology, 1999.

[10] Orcina Ltd. *Vessel Theory: RAOs and Phases*. Used: 15-05-2012. URL: `http://http://www.orcina.com`.

[11] TMC Marine Consultants Ltd. *Seakeeping Analysis*. Used: 15-05-2012. URL: `http://http://http://www.tmcmarine.co.uk/`.

[12] J. Angeles. *Fundamentals of Robotics Mechanical Systems*. Springer, 3 edition, 2007.

[13] John Craig. *Introduction to robotics - Mechanics and control*. Pearson Prentice Hall, 3 edition, 2005.

[14] D. C. Lay. *Linear Algebra and its applications*. Pearson Prentice Hall, 3 edition, 2006.

[15] W. Khalil and E. Dombre. *Modeling, Identification & Control of Robots*. Hermes Penton Science, 1 edition, 2002.

[16] I. Fassi, G. Legnani, and D. Tosi. Geometrical conditions for the design of partial or full isotropic hexapods. *J. of Robotic systems*, 22(10):507–518, 2005.

[17] A. Fattah and A.M. Ghasemi. Isotropic design of spatial parallel manipulators. *Int. J. of Robotic Research*, 21(9):811–824, 2002.

[18] L. Mollnari-Tosattia, I. Fassia, G. Legnanib, and F. Jovane. Kineto-static optimisation of PKMs. *CIRP Annals - Manufacturing Techonology*, 52(1):337–341, 2003.

[19] J. P. Merlet. Jacobian, manipulability, condition number, and accuracy of parallel robots. *J. of Mechanical Design*, 128:199–206, 2006.

[20] F.A. Lara-Molina, J. M. Rosario, and D. Dumur. Multi-objective optimization of stewart-gough manipulator using global indices. *IEEE/ASME Int. Conf. on Adv. Int. Mechatronics*, pages 79–85, 2011.

[21] R. Kurtz and V. Hayward. Multiple-goal kinematic optimization of a parallel spherical mechanism with actuator redundancy. *IEEE Transactions on Robotics and Automation*, 8(5):644–651, 1992.

[22] J. S. Arora. *Introduction to Optimum Design*. Elsevier Academic Press, 2 edition, 2004.

[23] K. Schittkowski and Ya xiang Yuan. Sequential quadratic programming methods. 2010.

[24] HMF. *HMF Knækarmskran 2430-K*. Used: 12-03-2012. URL: `http://www.hmf.dk/default.aspx?id=4195`.

[25] P. W. Rasmussen et. al. *Hydraulik Ståbi*. Nyt Teknisk Forlag, 1 edition, 1996.

[26] T. O Andersen and M. R. Hansen. *System Design and Analysis*. Aalborg University, 3 edition, 2007.

[27] T. O. Andersen and M. R. Hansen. *Fluid Power Circuits - System Design and Analysis*. Aalborg University, 3 edition, 2003.

[28] MOOG. Electrohydraulic valves... a technical look.

[29] MATLAB. *R2011b Documentation*. Used: 29-02-2012. URL: `http://www.mathworks.se/help/releases/R2011b/`.